Adaptive Digital Predistortion with Applications for LMDS Systems

by
Daniel Eric Johnson

Thesis submitted to the Faculty of the
Virginia Polytechnic Institute and State University
in partial fulfillment of the requirements for the degree of

Master of Science
in
Electrical Engineering

Charles W. Bostian, Chair
Jeffery H. Reed
Dennis G. Sweeney

August 25, 2000
Blacksburg, VA

Keywords: Measurement, Simulation, Nonlinear Amplification, AM-AM, AM-PM, Broadband

Adaptive Digital Predistortion with Applications for LMDS Systems

Daniel Eric Johnson

(ABSTRACT)

A limiting factor in the widespread deployment of LMDS systems is the limited distance of current systems. Rain attenuation and limited transmitter power are the primary causes of the limited distance. Adaptive digital predistortion is presented as a method of increasing effective transmitter power.

A background on LMDS link design, non-linear amplification, and predistortion is presented to assist the reader. A developed simulation uses AM-AM and AM-PM characteristics obtained from laboratory measurements of a 28 GHz amplifier to determine the effect of several predistortion implementation options and to confirm the feasibility of the proposed architecture.

The potential impact of this predistortion architecture on LMDS system design is considered. The presented multi-stage predistortion architecture is found to be capable of implementation at Msymbol/second rates utilizing a FPGA or custom IC and a moderate speed digital signal processor.

Acknowledgements

I would like to thank Dr. Bostian for being my advisor throughout my graduate school career. His experience with advising students made my stay enjoyable, and his comments and suggestions greatly improved this thesis. I am grateful that he is an advisor that always provided options rather than decisions. I would also like to thank my other committee members. Dr. Sweeney provided invaluable assistance in performing the amplifier measurements. Dr. Reed exposed me to the topic of adaptive digital predistortion during his class and suggested the topic during the initial phases of my research.

I would like to thank Dr. Sanjay Raman for use of the network analyzer and Chris Haskins for his assistance with the operation and setup of the network analyzer. Barry Taylor of Agilent Technologies provided the millimeter-wave amplifiers for measurement. The measurements would not have been possible without these people.

I would also like to thank CWT, Virginia Tech's Communication Network Services, and WavTrace for their financial support and opportunities during my stay at Virginia Tech.

I would like to thank the faculty, staff, and students of CWT for their assistance during my stay at Virginia Tech. I am grateful to Cortney Martin, John Nichols, and Tim Callahan and the many other people at CNS for their assistance and friendship.

Finally, I would like to thank my friends and family that supported my decision to return to graduate school.

Table of Contents

Table of Figures

Chapter 1. Introduction

A limiting factor of current LMDS systems is the restricted distance over which they can operate reliably. Increasing the output power of the transmit amplifier can increase the range or reliability, but the cost per dBm increases greatly after the output power exceeds what is possible with a single solid-state device.

The current limit for a single semiconductor device operating at 28 GHz is approximately 30 dBm. Increasing the amplifier power above this limit requires combining multiple semiconductor devices or using vacuum tube in place of a solid-state device. Both options are expensive and greatly increase the cost per dBm.

This high cost motivates the LMDS equipment designer to find ways to increase the performance of the system without requiring a higher power amplifier. Two possibilities are increasing the antenna gain or implementing predistortion.

Typical LMDS systems use QAM (Quadrature Amplitude Modulation), which is sensitive to non-linear distortions. QAM is sensitive to non-linear distortions because the signal has a non-constant envelope power. As the number of symbols increases, the sensitivity to the distortion also increases because the symbols become more like each other. The multiple amplitude nature of QAM allows it to achieve excellent bandwidth efficiency but makes QAM susceptible to non-linear distortions.

The amplifier might capable of producing signals at higher powers, but the distortions become more severe at higher powers. If a predistorter adapts to be the inverse of the amplifier distortion function, the amplifier can become an ideal limiting amplifier.

Previous implementations of predistortion are for low bit rate (2400 bps) systems. LMDS presents the challenge of having symbol rates of near 10 Msymbols/second. The proposed mixture of digital logic and a digital signal processor is capable of achieving predistortion at mega-symbol per second speeds.

Chapter 2 details background on link design for LMDS systems, non-linear amplifiers, and predistortion concepts. Chapter 3 details the results and procedure used to measure a

28 GHz amplifier for several different operating conditions. A simulation of a digital communications system in Chapter 4 uses these measurements in a non-linear amplifier model. The major contributions of Chapter 4 are a determination of potential gain from implementing predistortion with the measured amplifier and the effect of various parameters. Chapter 5 details a proposed predistortion system suitable for operation near 10 Msymbols per second and the implications of predistortion for LMDS system design.

Chapter 2. Theory

2.1 Link Margin

2.1.1 Introduction

One of the most important aspects of designing a LMDS system or any other wireless communication system is the link margin. It would not be wise to design a system that is on the verge of failure. Therefore, all communication systems are over designed. In a LMDS system the amount of margin or over design required is determined by the desired link reliability.

2.1.2 Percent Reliability

LMDS links are generally designed to deliver a certain probability of outage due to rain. This however does not take into account outages from other sources such as equipment failure and power outages. Nevertheless, when taking into account link reliability, a dominant cause of an outage in an LMDS link is rain attenuation.

The microwave link designer determines from customer requirements what level of reliability is required for the link. The reliability is usually specified in a percent availability. Some typical availability values are 99.9, 99.99%, and 99.995%. When spoken these percent reliabilities might be called ‘three-nines’, ‘four-nines’, and ‘four-nines and a five’ respectively. Reliability can also be specified in percent outage, which is 100% minus the percent availability.

2.1.3 Clear Weather Margin

The clear weather margin is the amount by which the received signal strength exceeds the receive threshold during clear weather conditions. The clear weather margin and link distance allow the link reliability to be determined. When given the link reliability the maximum link distance can be determined by iteration.

2.1.4 Receiver Sensitivity

This specification is needed to calculate the link margin. The receiver sensitivity is the minimum signal required to obtain a particular bit error rate. This is usually measured for

a pre-FEC (pre-forward-error-correction) BER (bit error rate) of 10^{-6}. With FEC, a near error free link is still achievable at this BER.

Different modulations schemes require different signal to noise ratios to achieve the same BER. For QAM (quadrature amplitude modulation) and PSK (phase shift keying) the required signal to noise ratio for the same BER increases and the spectral efficiency increases as the number of modulation levels increases.

Example LMDS receiver sensitivities for different modulations are shown in table 2.1 along with the corresponding theoretical E_b/N_0. The receiver sensitivity changes for different modulation schemes. This change is due to the increase in signal-to-noise ratio required to keep the same bit error rate at the modulation level increases.

Table 2.1: Harris SpectraPoint Receiver Sensitivity and Theoretical E_b/N_0

Modulation	Sensitivity for pre-FEC BER of 10^{-6} [1]	E_b/N_0 for pre-FEC BER of 10^{-6} [2]
QPSK or 4-QAM	-85 dBm	10.5 dB
16-QAM	-79 dBm	18.5 dB
64-QAM	-71 dBm	28.5 dB

2.1.5 Antenna Gain vs. Beamwidth

In point-to-multipoint systems the antenna located at a subscriber site is typically a narrow beam parabolic dish antenna. The antenna located at a multi-point base station is generally a horn that allows coverage of a sector. The hub horn antenna can have different beamwidths in the horizontal and vertical directions. The horizontal beamwidths are typically 30, 45, or 90 degrees. The beamwidth in the vertical plane is typically much smaller as it is assumed that subscribers in the coverage area have similar elevations and anything radiated above building tops is wasted radiation. Typical values for the vertical beamwidth are 3 to 5 degrees.

The selection of the beamwidth is inversely proportional to the antenna gain and is an important selection in overall system design. Beamwidth selection becomes a tradeoff between the number of transmitters required to cover 360 degrees and the maximum link distance that can be achieved.

The vertical beamwidth geometry can limit both the maximum and minimum distances from the transmitter. The minimum and maximum distances can be found by simple trigonometry if the height (h) above the receiving antenna, the distance (R) from the base station, and the vertical beamwidth (vbw) are known. The downtilt angle (t) is typically specified as the angle below the level line to the horizon.

$$R_{\min} = \frac{h}{\tan(t + \frac{1}{2} \cdot vbw)} \qquad \text{(Eq. 2.1)}$$

$$R_{\max} = \frac{h}{\tan(t - \frac{1}{2} \cdot vbw)} \qquad \text{(Eq. 2.2)}$$

The beamwidth of the antenna is inversely related to the maximum gain of the antenna. The beamwidth can be varied in either the horizontal or the vertical dimension and the gain will vary inversely when either beamwidth is altered. For example, an antenna with a 30 degree beamwidth in the horizontal plane and a 3 degree beamwidth in the vertical plane has roughly the twice the gain when compared to an antenna with a 60 degree beamwidth in the horizontal plane and a 3 degree beamwidth in the vertical plane.

The following equation can be used to estimate antenna gain when given the horizontal and vertical beamwidths in degrees. The G is the antenna gain as a ratio, and the HP_{E° and HP_{H° are the half power bandwidths of the horizontal and vertical beamwidths.

$$G = \frac{26000}{HP_{E^\circ} \cdot HP_{H^\circ}} \qquad \text{(Eq. 2.3) [4]}$$

Using a reference horn antenna we estimate its gain. The reference antenna with a measured gain of 22 dBi is specified to have a horizontal beamwidth of 30 degrees and a vertical beamwidth of 3 degrees. The estimated gain using this equation results in a gain of approximately 288.89 or 24.6 dB. It can also be seen that decreasing the beamwidth in a single dimension increases the gain by the same factor. Using the equation again we can find that an antenna with a 15 degree horizontal beamwidth and the same vertical beamwidth would have a gain of approximately 27.6 dB or twice the calculated gain of

the reference antenna. This relationship results in a tradeoff between the antenna gain and the number of sectors required to cover 360 degrees.

Table 2.2: Beamwidth Selection Tradeoffs

Reference Beamwidth (degrees)	30	30	30	30	30	30	30	30
Reference Gain (dB)	22	22	22	22	22	22	22	22
Desired Beamwidth (degrees)	10	15	20	30	45	60	90	180
Sectors required for full coverage	36	24	18	12	8	6	4	2
Gain (dB)	26.77	25.01	23.76	22.00	20.24	18.99	17.23	14.22
Change in Gain (dB)	4.77	3.01	1.76	0.00	-1.76	-3.01	-4.77	-7.78
Relative number of sectors	3.00	2.00	1.50	1.00	0.67	0.50	0.33	0.17

2.1.6 Free Space Loss

As a radio signal travels through space the signal strength decreases at a rate of the square of the increase in distance. The equation to predict the power (P_r) at the receiver is based upon the transmitted power (P_t), wavelength of the signal (λ), distance (d) between the transmitter and receiver, and the isotropic antenna gains of both the transmitter (G_t) and receiver (G_r).

$$P_r(d) = \frac{P_t G_t G_r \lambda^2}{(4\pi)^2 d^2} \qquad \text{(Eq. 2.4) [2]}$$

Since the received power and antenna gain are commonly specified in decibels, this equation can be rearranged using logarithmic properties to the following more convenient equation.

$$P_{r(dBm)}(d) = P_{t(dBm)} + G_{t(dB)} + G_{r(dB)} + 20 \cdot \log_{10} \lambda - 20 \cdot \log_{10} 4\pi - 20 \cdot \log_{10}(d) \qquad \text{(Eq. 2.5)}$$

The free space loss component of the above equation represented by the following equation.

$$F_{(dB)} = 20 \cdot \log_{10} \lambda - 20 \cdot \log_{10} 4\pi - 20 \cdot \log_{10}(d) \qquad \text{(Eq. 2.6)}$$

The figure 2.1 shows the free space loss (F) at 28 GHz for distances applicable to LMDS.

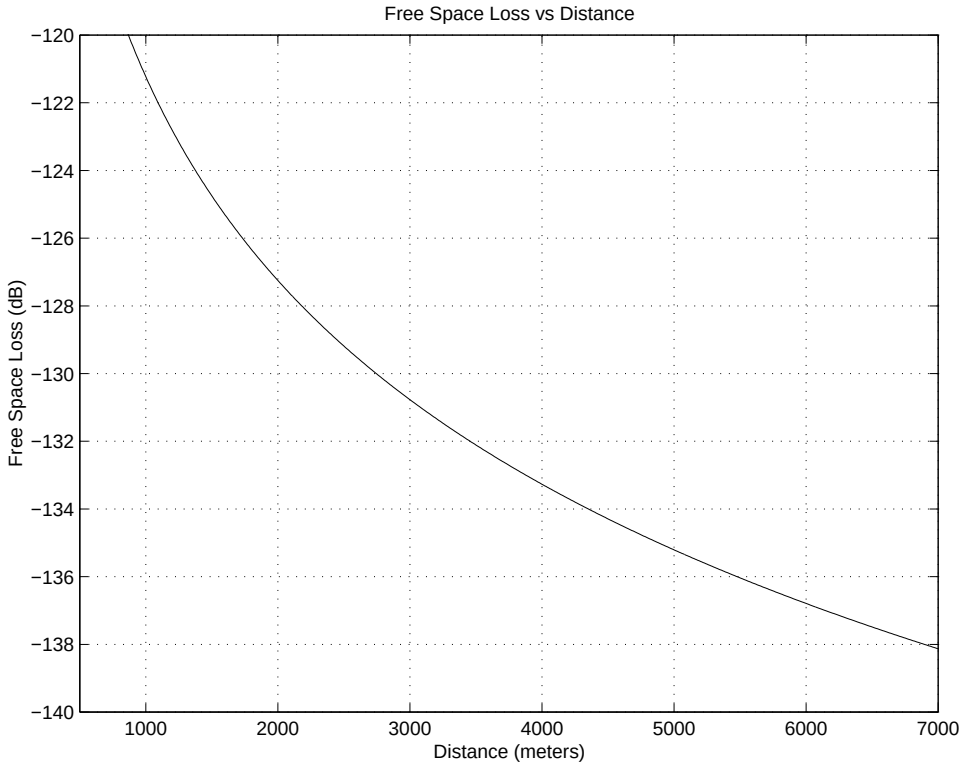

Figure 2.1: Free Space Loss vs. Distance for a 28 GHz Signal for Distances Typical in a LMDS System

2.1.7 Rain Attenuation

Organizations such as the ITU publish the amount of time a year that a particular rain rate is exceeded in a particular region [3]. This is the basis of calculating the needed margin when given the desired reliability.

This published rain rate data can then be turned into a probability distribution function that can show the probability of exceeding a particular rainfall rate during the entire year at a particular location. The link should be designed with enough link margin to continue to operate during this rain rate. The following equation can be used to calculate the amount of attenuation for a particular distance in kilometers. The *A* is the attenuation per kilometer due to rain and *r* is the rain rate in millimeters per hour.

$$A_{(\frac{dB}{km})} = \alpha \cdot r_{(\frac{mm}{hr})}^{\beta} \qquad \text{(Eq. 2.7)}$$

For a 30 GHz signal with horizontal polarization $\alpha = 0.187$ and $\beta=1.02$.

Table 2.3: ITU Predicted reliability, rain rates, and attenuation for a 28 GHz signal in Blacksburg, VA

Percent Outage	Percent Available	Minutes unavailable/year	Rain rate (mm/hr) [3]	Attenuation (dB/km)
0.001	99.999	5.3	108.0	22.18
0.002	99.998	10.5	89.0	18.21
0.005	99.995	26.3	64.5	13.11
0.010	99.990	52.6	49.0	9.90
0.020	99.980	105.1	35.0	7.03
0.050	99.950	262.8	22.0	4.38
0.100	99.900	525.6	14.5	2.86
0.200	99.800	1051.2	9.5	1.86
0.500	99.500	2628.0	5.2	1.00
1.000	99.000	5256.0	3.0	0.57
2.000	98.000	10512.0	1.5	0.28
5.000	95.000	26280.0	0.0	0.00

Once the desired link reliability is chosen, data from rain measurements are used to determine the corresponding rain rate that is not exceeded for the same percentage of the time as the link reliability. This rain rate is converted into attenuation per kilometer using equation 2.7. The attenuation per kilometer is then multiplied by the effective link distance in kilometers to determine to attenuation due to rain at that rate. Links with a longer distance therefore require a higher margin to operate at the same reliability. The assumption that the effective link distance is equal to the actual link distance is used here. This assumption is valid for short links such as those considered here.

2.1.8 Maximum Link Distance

Once the desired reliability is known, it can be converted into a minimum required margin per kilometer. The transmitter power, receiver antenna gain, transmitter antenna gain, and receiver sensitivity can be used to iterate the maximum distance for the link to maintain that reliability. When rain margins are considered, the increase in radius gained from an increase in transmitter power is not as great. This is because as the link distance increases, the required margin also increases.

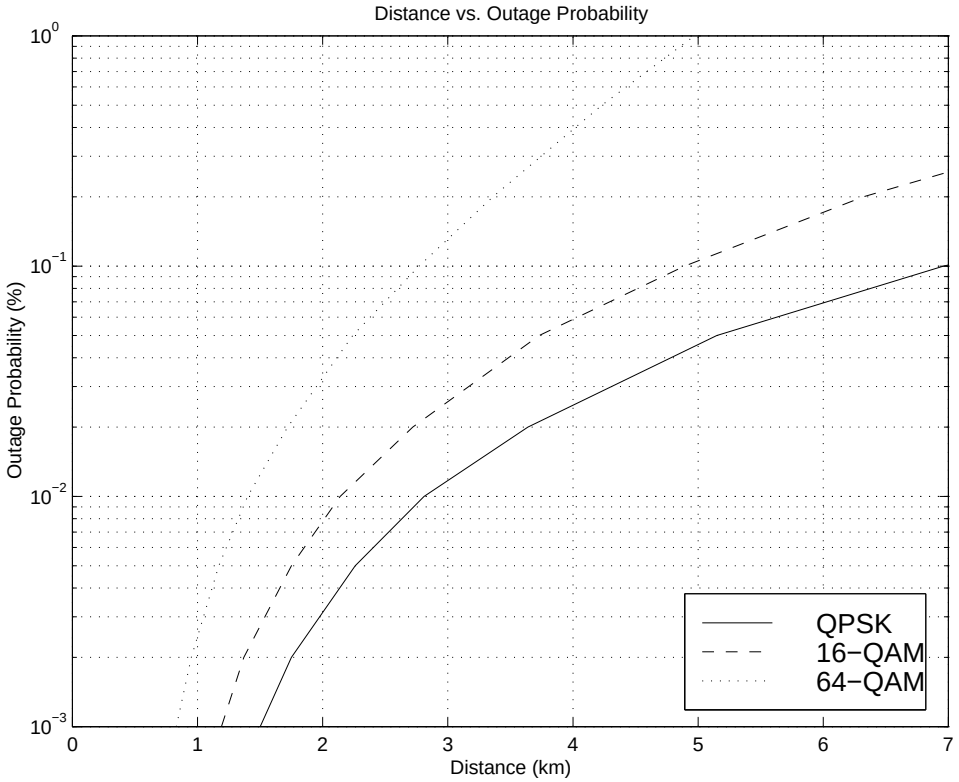

Figure 2.2: Link Outage Probability vs. Distance for a Sample LMDS System

Figure 2.2 shows the maximum link distance of a realistic LMDS system for various probabilities of outages and was created by solving for the distance where the clear weather margin equaled the necessary rain margin for the desired link distance.

Predicting link availability in this way takes into account only the total time the link will be available for an entire year. This does not consider the distribution of the times the link will not be useable. For example, a single 20-minute outage in a single year is likely to have a different impact than when compared to twenty 1-minute outages evenly spaced throughout the year, but both will have the same reliability. Which is worse depends on the application.

Table 2.4: Sample Link Budget Analysis

Link	Site 1	Site 2	Site 3
Modulation	64 QAM	16 QAM	16 QAM
Frequency (GHz)	27.504	27.504	27.529
Wavelength (m)	1.09E-02	1.09E-02	1.09E-02
Distance (m)	924	823	2575
Free space (dB)	-120.5	-119.5	-129.4
TX Power (dBm)	7.0	10.0	10.0
TX Gain (dBi)	22.0	22.0	22.0
RX Gain (dBi)	38.0	38.0	38.0
Free space (dB)	-120.5	-119.5	-129.4
Estimated RX (dBm)	-53.5	-49.5	-59.4
Rx Threshold (dBm)	-71.0	-79.0	-79.0
Estimated RX (dBm)	-53.5	-49.5	-59.4
Estimated Margin (dB)	17.5	29.5	19.6
Distance (m)	924	823	2575
Estimated Margin (dB)	17.5	29.5	19.6
Relative Reliability Factor (Maximum dB of rainfade possible / km)	18.91	35.82	7.59

Even with this uncertainty, calculating the link margin per unit distance can be used to compare the relative reliability of links in the same region and can be done even if the rain rate data is unknown for the region. Using table 2.4 as an example it can be determined that during rainfall that Site 3 would drop out first followed by Site 1 and then Site 2.

2.2 Amplifier Theory

2.2.1 Non-linear Effects of Typical Power Amplifier

Transistors are governed by non-linear equations, but used in linear power amplifiers. If the input signal is kept small, it is possible to make the transistor appear to be a linear amplifier. The non-linear distortions become more prominent as the input power is increased. All real amplifiers have limits to their output power. As this limit is approached the distortions increase faster than any benefits gained by increasing the power.

2.2.2 Amplifier Class

Amplifiers are divided into several different classes. Different classes have different bias networks, linearity, and efficiencies. A Class A amplifier offers the most linear response of the amplifiers considered below. However, this high linearity comes at the price of power efficiency. The power efficiency or η can be considered to be defined by the equation below.

$$\eta = \frac{\text{load power } (P_L)}{\text{supply power } (P_s)} \qquad \text{[5] (Eq. 2.8)}$$

The transistors in a Class A amplifier are always biased to obtain high linearity. The theoretical maximum power efficiency of 25% is obtained when the transistor is at the edge of saturation. The transistor shows non-linear effects before reaching the saturation point and the practical efficiencies obtained are around 10% to 20%. [5]

The Class B amplifier trades linearity for a higher power efficiency (η) than the Class A. The transistors are not turned on unless a signal exceeds a threshold in either the negative or positive direction. This causes what is called crossover distortion or a 'dead band'. The theoretical maximum power efficiency (η) for a class B amplifier with a sinusoidal input is 78.5%. [5]

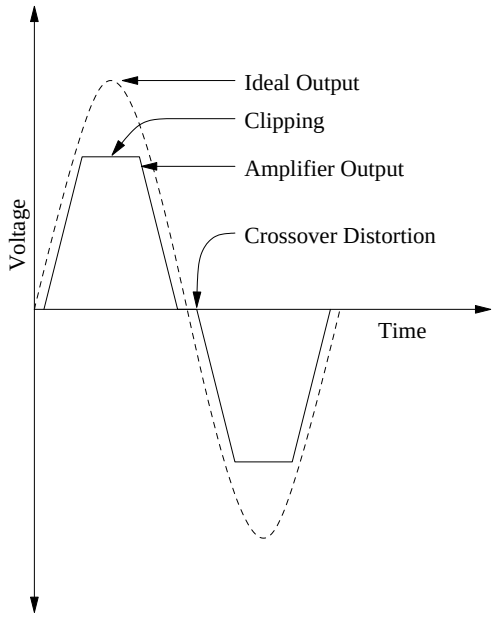

Figure 2.3: Example of Crossover Distortion and Clipping

The Class AB amplifier is a compromise between the Class A and Class B amplifiers. The transistors are slightly forward biased when no signal is applied to eliminate crossover distortion but without the efficiency penalties of the Class A biasing scheme. The effectiveness of this biasing network though is subject to aging, temperature, and device variations.

The Class C amplifier has increased efficiency at the expense of linearity. Class C amplifiers are not generally considered for use with modulations that require a linear response because of their non-linearity and are more suitable for use with FM or FSK modulations where non-linear amplification is acceptable.

Table 2.5: Common Amplifier Efficiencies and Linearity

Class	Efficiency	Linearity
Class A	25% maximum	Best
Class B	78.5% maximum	Crossover distortion
Class AB	<78.5%	Less crossover distortion than Class B
Class C	>78.5%	Poor

2.2.3 Backoff

As the input power is increased, the output power approaches a maximum or saturation. The distance in decibels between the average input power and the saturated input power is called the 'backoff'. As backoff is reduced, a point is reached were any additional increase in input power does not result in improved link error performance. The location of this point is dependent upon amplifier characteristics and the characteristics of the modulation.

The input backoff is defined by [6] to be the ratio of the input power required to achieve saturation to the average input power.

$$IBO = 10\log_{10}\frac{P_{inSat}}{\overline{P_{in}}} \qquad \text{[6] (Eq. 2.9)}$$

Two things happen when the QAM modulation index increases. The transmitted signal becomes more sensitive to distortions in the transmitter and a higher E_b/N_0 is required at the receiver to maintain the same BER performance. As a result, increasing the modulation index will require an increase in backoff. The link margin of a higher modulation index is therefore reduced by both the higher E_b/N_0 requirement as expected and by the decrease in average input power or increase in backoff [7].

2.2.4 Traditional Amplifier Characterizations

2.2.4.1 Third Order Intercept Point (IP3)

Third order intermodulation products are of interest in characterizing amplifier performance because third order products are very close in frequency to the desired signal. The 3rd order intercept point is a figure of merit associated with 3rd order intermodulation products and is the point at which third-order products overtake the desired first order component. The IP3 can be specified by either the input power at which the 3rd order products equal the desired signal or the output power at which the 3rd order products are equal to the desired signal. It is possible that this point is beyond the maximum output power of the amplifier. In this case the point is located at the intersection of input vs. output power gain curves. If referenced from the output power

this is called the OIP3 and IIP3 if referenced from the input power. Intermodulation products with odd orders such as the 3rd and 5th order products are considered because they can create interference within the bandwidth of the desired signal. [8]

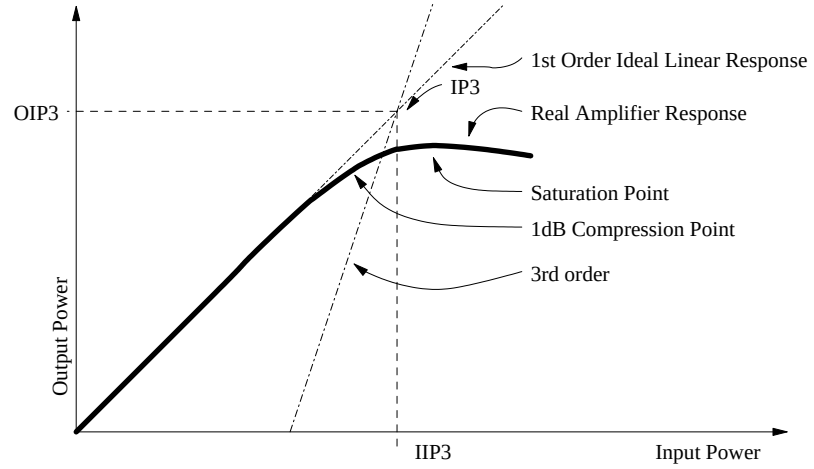

Figure 2.4: Intermodulation, Compression, and Saturation Points

2.2.4.2 1 dB Gain Compression Point

The 1 dB compression point is defined as the point at which the output of an amplifier has dropped 1 dB below the idea linear output. Compression points might be specified for particular amounts of compression. Other commonly specified points are 3 dB and 0.1 dB below ideal gain. The AM-AM distortion curve can be used to determine these points.

2.2.4.3 Saturation Point

Saturation occurs when the maximum input power is exceeded. At this point the output is 'clipped' to a maximum voltage, and gain compression results until a maximum power is achieved. Saturation also causes phase modulation of the signal by the power amplifier [9].

2.2.5 Distortion Characterizations

Additional amplifier characterizations can give a more accurate representation of non-linear distortions in an amplifier. When a signal is sent through a near linear amplifier

the amplifier gain and phase shift are functions of the input amplitude. The following equation represents the input to the amplifier where *R* is the amplitude of the input signal.

$$x(t) = R_x(t) \cdot \cos\left[w_o t + \theta_x(t)\right] \quad \text{[10] (Eq. 2.10)}$$

The output of the amplifier (*y*) can be expressed as the following, where *G* is the amplitude distortion as a function of the input amplitude and Ψ is the phase distortion as a function of the input amplitude R_x.

$$y(t) = G\left[R_x(t)\right] \cdot \cos\left\{w_o t + \theta_x(t) + \Psi\left[R_x(t)\right]\right\} \quad \text{[10] (Eq. 2.11)}$$

Although the output is shown in a polar form here, implementations typically use I and Q signals.

2.2.5.1 AM-AM Distortion

The ideal amplifier has constant gain across all input powers. A practical amplifier has a maximum output power, which will limit the output power to a particular value. In reality as this limit is approached gradually as the apparent gain of an amplifier decreases with increasing input. The AM-AM distortion is created by this variation in the gain of the amplifier across different input powers. The AM-AM distortion graph can be used to determine the gain compression for any input power.

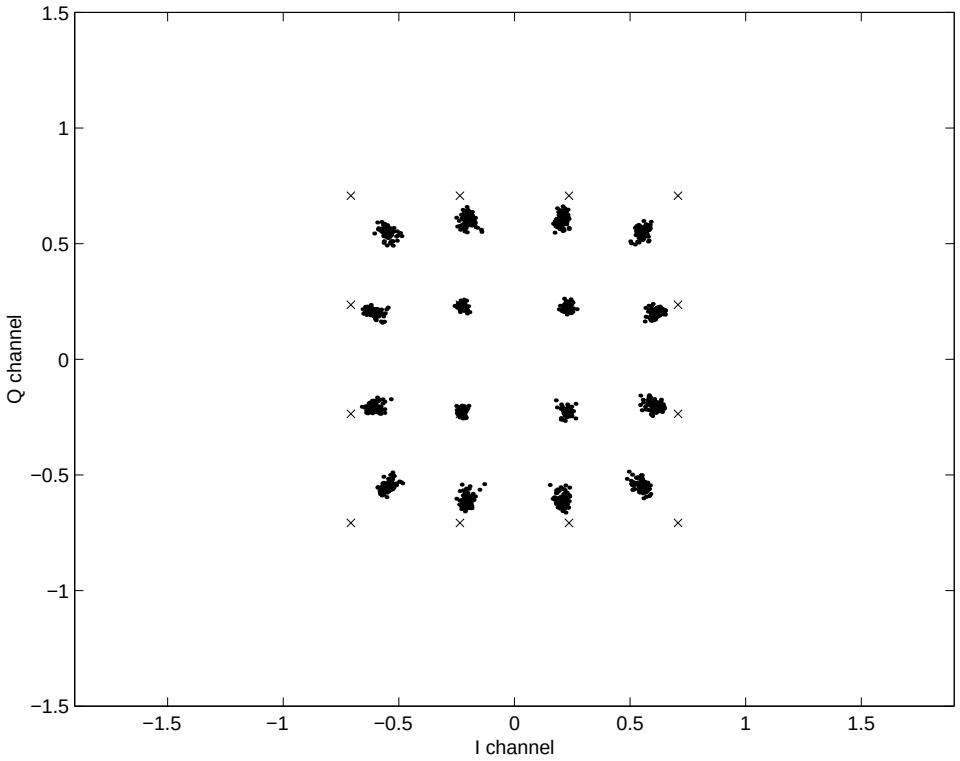

Figure 2.5: Simulated 16-QAM constellation with AM-AM distortion

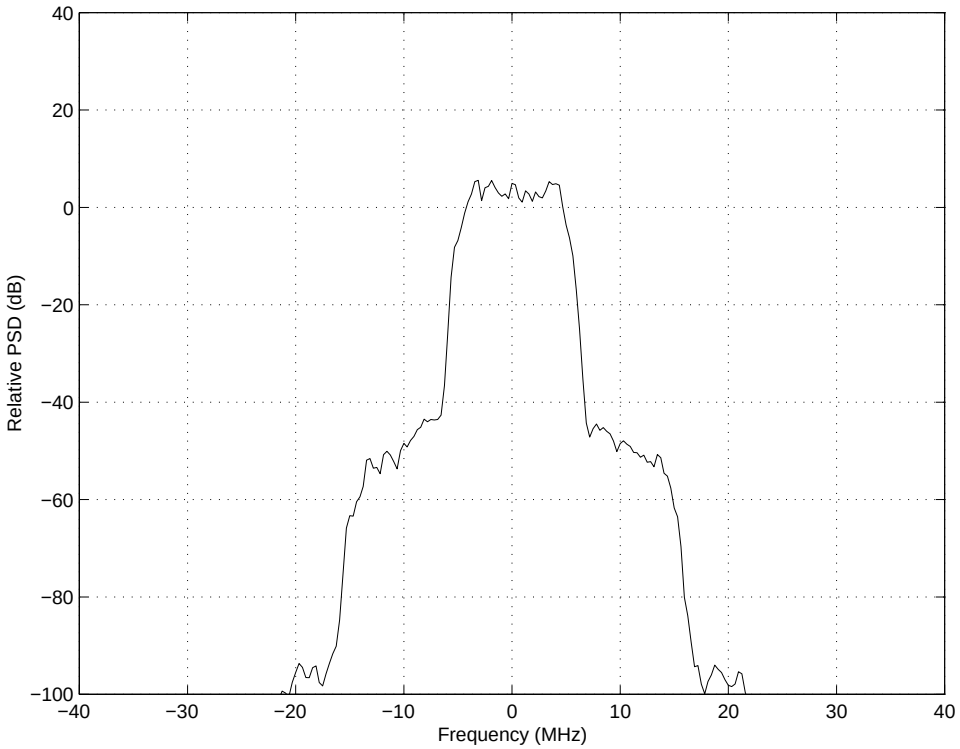

Figure 2.6: Simulated 16-QAM spectrum with AM-AM distortion

The constellation and spectrum of a severely AM-AM distorted 16-QAM signal is show in the previous figures. The distortion gives the constellation compressed spacing at its outer points. The dispersion in the constellation is not due to noise, as this signal contained no noise. The dispersion is induced by the root raised cosine filter and is described in more detail later. The 'X' shows the desired constellation point location. The inner four points are dispersed around the ideal point while the outer points are being 'compressed' with the corner points showing the most compression.

2.2.5.2 AM-PM Distortion

AM-PM distortion is a change in the phase between the input and output signal of the amplifier. If seen in a plot of the demodulated signal constellation, this distortion tends to skew or twist the constellation through angles that depend on the distance from the center of the constellation or the magnitude of the signal. The average phase shift is not as important as is the range over which the phase varies. Amplifiers of different classes have dramatically different AM-PM distortions [11].

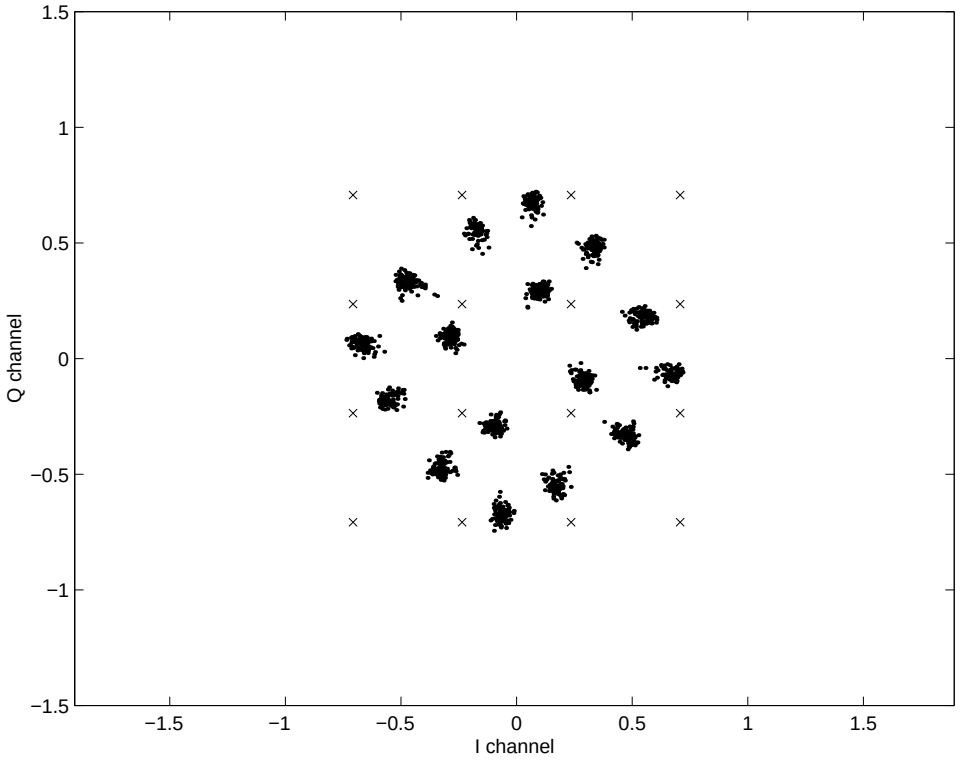

Figure 2.7: Simulated 16-QAM constellation with AM-AM and AM-PM distortion

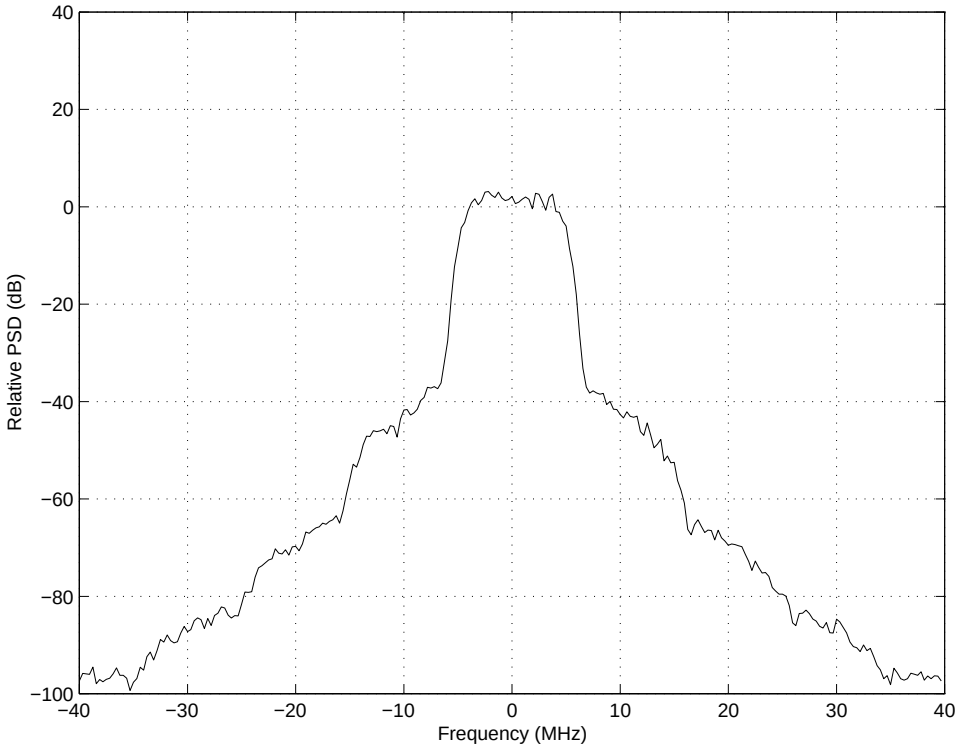

Figure 2.8: Simulated 16-QAM spectrum with AM-AM and AM-PM distortion

2.2.5.3 Memory Effects

If a non-linear amplifier introduces a phase distortion then memory is present. However if the time constants of the memory are smaller than the maximum envelope frequency, the system can be considered a quasi-memoryless system. [12]

Memory effects are usually caused by time constants in the biasing circuit or are due to an impedance mismatch with the amplifier [13]. The AM-AM and AM-PM characteristics vary for different symbol rates if the time constants of the memory are larger that the inverse of the maximum envelope frequency [12].

Two network analyzers were used in [12] determine the dynamic AM-AM and AM-PM characteristics for different offsets between the carriers. It is possible that a resonance can be found at a particular offset. This would cause certain modulation frequencies to possibly have drastically lower performance than predicted from AM-AM and AM-PM plots.

2.2.5.4 Adjacent Channel Power Ratio (ACPR)

The adjacent channel power ration or ACPR is defined by [13] to be the power contained within the upper and lower adjacent channels divided by the power in the main channel. The division of the power in either the upper or lower channel by the main channel power is represented by $ACPR_{UPPER}$ or $ACPR_{LOWER}$. Variations in the definition are possible by defining different frequencies for the start and stop of the adjacent channel. Other names for ACPR include adjacent channel interference ratio (ACIR) [14] and signal to intermodulation power ratio (SIMR) [7].

The increase in ACPR after an amplifier with non-linear effects amplifies a signal is called spectral regrowth [13]. This increase 'steals' power that could otherwise be used for the desired signal while potentially interfering with adjacent signals or inefficiently using spectrum [15].

It is difficult to relate IP3 and ACPR because IP3 is measured with a relatively simple two-tone measurement while ACPR is measured as a result of complex linear modulations and cannot be represented by a finite number of tones [13].

2.3 Predistortion Theory

2.3.1 Advantages of Linearization

The advantages of amplifier linearization include a reduction in adjacent channel interference or out-of-band distortion, a reduction of in-band distortion, and an increase in power efficiency. Out-of band distortion is undesirable because it robs power from the desired signal as well as interferes with the adjacent channels. A reduction of the in-band distortion will result in an increase in effective transmitter power. Linearization can also enable the use of less linear but more power efficient amplifiers.

2.3.2 Linearization Techniques

2.3.2.1 Addition of a Non-Linear Component

For this method, a non-linear component such as a diode corrects the non-linear characteristics of the power amplifier. The ideal diode for this purpose has near opposite AM-AM and AM-PM characteristics of the amplifier. The method has the advantage of

being easy to implement but it may not completely correct the non-linear effects of the amplifier. [16]

2.3.2.2 Feedforward

The feedforward method generates an error signal by subtracting the signal at the input of the amplifier from an attenuated version of the amplifier output. Analog methods are used to amplify the error signal and subtract it from the output of the amplifier. The result of the subtraction is the amplified desired signal. Disadvantages of this method include requiring a powerful error-signal amplifier to cancel the distortion after the amplifier, complexity, and adjustment.[10] Imperfections in the error-amplifier also degrade the performance of the feedforward method. [16]

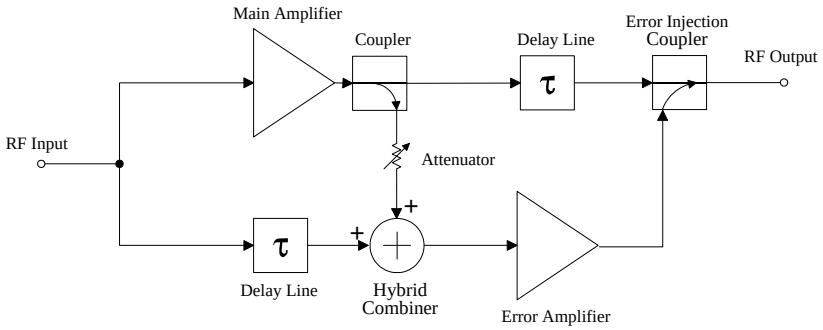

Figure 2.9 Feedforward Transmitter [16]

2.3.2.3 Cartesian Loop Feedback

The Cartesian loop feedback method is similar to feed-forward but the error signal is combined with the input to the amplifier rather than the output of the amplifier. A sample of the amplifier output is quadrature downconverted to analog baseband signals. The sampled amplifier output is subtracted from the desired signal and the result is used to predistort the input the amplifier [B7]. The delay of the signal traveling through the amplifier and frequency conversions limits the bandwidth of this scheme [18].

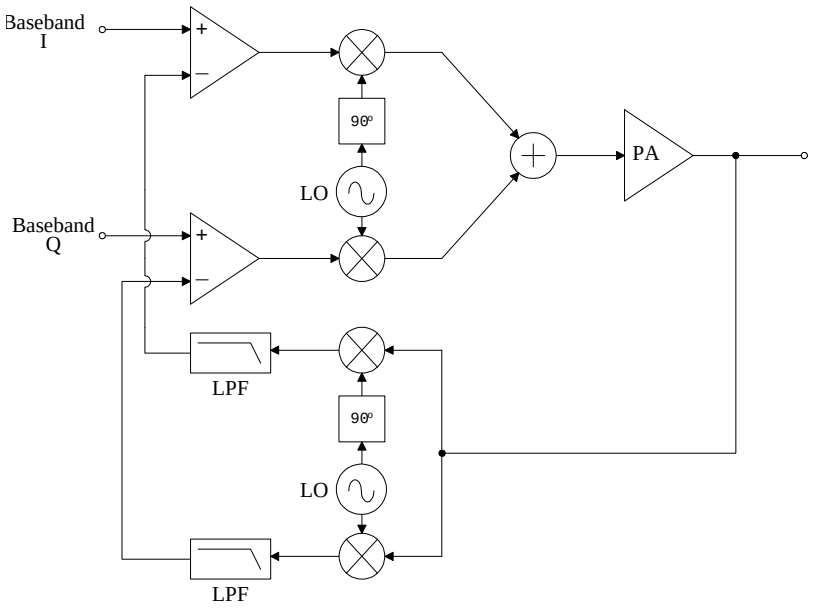

Figure 2.10 Cartesian Loop Feedback [16]

2.3.2.4 LINC / CALLUM

The LINC (Linear amplification with Non-linear Components) method uses two matched non-linear power amplifiers to create a linear signal. A combiner sums the output of both amplifiers and enables the creation of any amplitude and any phase signal. This method reduces non-linear distortions in non-linear amplifiers because the amplitudes of both sine waves remain both constant. The phase between the two equal amplitude sine waves is varied to produce the desired phase and amplitude at the output of the combiner.

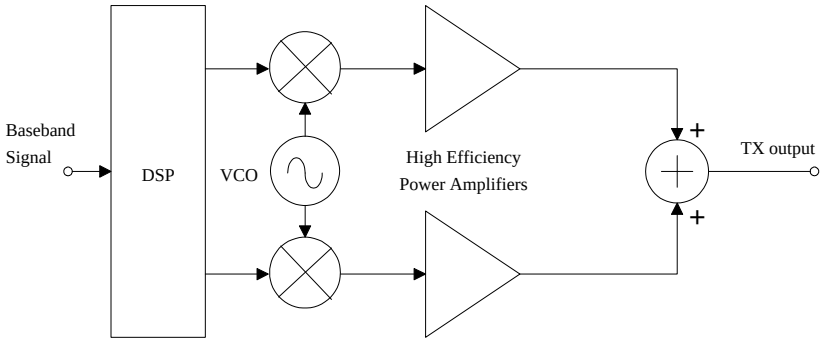

Figure 2.11 LINC Transmitter [16]

The CALLUM (Combined Analog Locked Loop Universal Modulator) method is a closed-loop extension of the LINC method, which is open-loop. CALLUM adds feedback to help solve the problem of obtaining matched amplifiers. The disadvantage with both of these methods is the need for a power-combining network and the requirement of two amplifiers. The CALLUM method is also susceptible to instability when the vector magnitude becomes zero. [17]

2.3.2.5 Digital Predistortion

Digital predistortion is similar to Cartesian feedback in that the correction is applied ahead of the amplifier input. The digital predistortion predicts the needed correction using past knowledge about the characteristics of the non-linear distortions rather than using feedback from the current signal. The predistortion prediction adjusts much like an equalizer to minimize the error between the amplified signal and the input to the predistorter. This prediction makes digital predistortion immune to the loop delay limitations associated with Cartesian feedback [18].

2.3.3 Adaptive Digital Predistortion

There are many variations of digital predistortion systems but all have the same basic principle. A lookup table or computation is used to determine the quadrature output of the predistortion block. Since the amplifier distortion is a function of amplitude, the lookup table is indexed by amplitude of the quadrature input. If the system is adaptive as many digital predistortion systems are, the transmitted signal from the output of the

power amplifier is downconverted and turned into quadrature samples of the signal. This sample is then compared to the desired signal and an adaptation algorithm is used to adjust the predistortion block in such a way that the predistortion block becomes the inverse to the amplifier distortion and the output of the amplifier will match the desired signal.

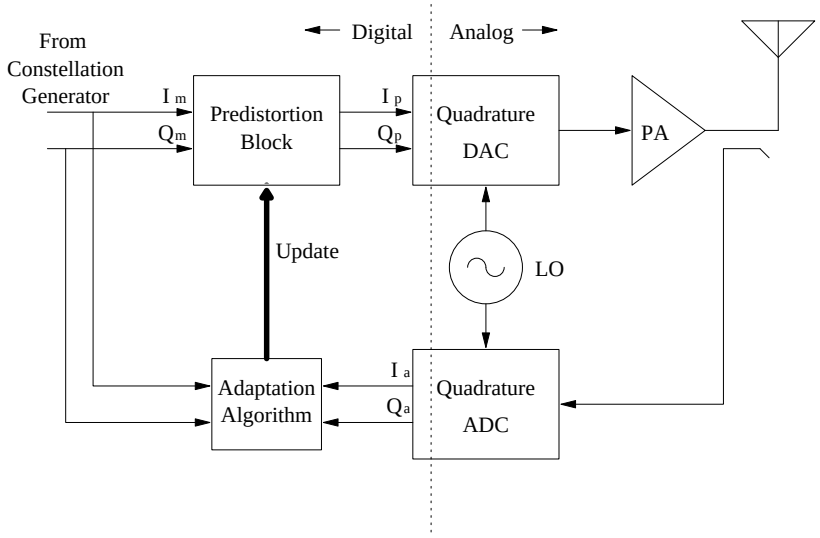

Figure 2.12: Block Diagram for a Inverse Modeling Adaptive Digital Predistortion System [19]

2.3.3.1 Implementation Types

2.3.3.1.1 Lookup Table

The lookup table uses RAM to store outputs for corresponding inputs and can be either a two-dimensional table or a one-dimensional table.

The 2-D table method builds a table that is indexed by the I and Q inputs of the predistorter and stores the appropriate predistorter output. The disadvantage of 2D tables is their large memory requirement and large number of samples required before the table is full. A table entry is required for each possible input to the amplifier, making the table size the square of the number of quantization levels of the in-phase and quadrature

samples. The advantage of the 2-D table is that no polar-to-rectangular or rectangular-to-polar conversions are necessary.

$$I_P = F_I(I_m, Q_m) \quad \text{[20] (Eq. 2.12)}$$

$$Q_P = F_Q(I_m, Q_m) \quad \text{[20] (Eq. 2.13)}$$

Another method uses two 1-D tables to correct for amplitude and phase distortion. The following equations demonstrate how the 1-D polar table might be implemented. R_P represents the magnitude of the predistorter output, F_R represents the AM-AM function of the predistorter, F_ϕ represents the AM-PM function of the predistorter, R_M represents the magnitude of the predistorter input, ϕ_P represents the phase of the signal at the output of the predistorter, and ϕ_M represents the phase of the signal at the input of the predistorter.

$$R_P = F_R(R_M) \quad \text{[21] (Eq. 2.14)}$$

$$\phi_P = \phi_M + F_\phi(R_P) \quad \text{[21] (Eq. 2.15)}$$

The above equation shows the phase offset (F_ϕ) as a function of the output of the predistorter (R_P) rather than the input magnitude (R_M). This implementation is called the cascade implementation and has the desirable effect of separating the convergence of the phase and magnitude characteristics [21]. Enhancements to the 1-D tables include using interpolation methods to reduce the number of entries required. A disadvantage of the 1-D table is that it requires conversions between rectangular and polar representations.

2.3.3.1.1.1 Lookup Table Size

An implementation can have a table entry for every possible digital value. If the number of bits used to quantize the signal is represented by *n*, a full two dimensional table memory requires $(2^n)^2$ entries while a one dimensional table requires a two tables of 2^n values. The use of interpolation can be used to decrease the number of points required in the look up table [22].

Table size has an inverse relationship with adjacent channel interference [18]. Each doubling of the table size decreases the ACPR by 6 dB up to a limit after which

increasing the table size no longer reduces the adjacent channel interference. The specific case in [22] shows a 6dB decrease in adjacent channel interference for every doubling of the look up table size up to 256 entries using interpolation.

2.3.3.1.1.2 Table Indexing

The spacing between table entries must be considered if a table entry does not exist for every possible quantized value. The typical options for index spacing are optimal indexing, equal amplitude indexing, and equal power indexing. The optimal index spacing can be found by applying a method detailed in [23] that is similar to the Lloyd-Max algorithm for picking optimal points for quantization. This calculation depends on amplifier distortion, the probability density function of the modulation, and the level of backoff. [23]

The equal power spacing has the worst spacing scheme for class AB amplifiers. The equal power spacing concentrates more points in the saturation region rather than in the low power region where crossover distortion lies. Nevertheless, equal power indexing has a computational advantage because the predistortion is a function of power eliminating the requirement for calculating the square root. [23]

The equal amplitude spaced method is a compromise of simplicity and performance. The method has intermodulation powers of 4 dB to 10 dB better than the equal power spacing method and is 1 dB to 4 dB worse than optimal spacing. [23]

2.3.3.1.1.3 Table Load Time

[14] has derived the time required to trace every path. Where T is the total time required to trace all paths, N is the number of symbols, W is the symbol rate, and L is number of symbols stored in the raised-cosine filter.

$$T = \frac{N^L}{W} \qquad \text{[14] (Eq. 2.16)}$$

The time to load the table is most important in low symbol rate systems where it can take 10 seconds to trace all possible points.

2.3.3.1.2 Calculation

An alternative to using a lookup table is to use a computation to calculate the output signal as a function of the input signal. This method is favorable because of the elimination of large banks of RAM required by the table look-up method.

A polynomial function is one way to perform a calculation predistorter. As polynomial order is increased the model becomes closer to the amplifier distortions but computational load is increased. It was noted in [24] that a 16^{th} order polynomial with nine even terms was sufficient to model the AM-PM distortions. Similarly, a ninth order polynomial with five odd terms was sufficient to model the AM-AM distortions.

2.3.3.1.2.1 Adaptation Algorithms

If a calculation such as interpolation or a polynomial is used to predistidort, then an adaptation algorithms are necessary to adjust the function or table values that control the predistorter. Adaptation algorithms or optimization methods are divided into two basic categories. Direct methods provide the exact answer within a predetermined number of calculations and are the preferred method for orders less that 100 [25]. Iteration or gradient methods approach a solution gradually. Methods such as LMS, RLS, RASCAL [35], Secant [11, 18] have all been proposed for optimizing predistoter functions and lookup tables.

2.3.3.2 Multi-stage Predistortion

In the multi-state predistortion proposed in [19], the forward model of the power amplifier is determined by comparing samples from the predistorter output to the samples downconverted and digitized from the power amplifier output. This multi-stage method then uses the forward model to generate the inverse model needed in the predistortion block. Synthetic data formulated to speed convergence of the model can then be used to determine the predistorter without interrupting the data being sent by the transmitter. This method eliminates the delays of waiting for a symbol to propagate through the analog chain or the delay of waiting for the input sample to change. [19]

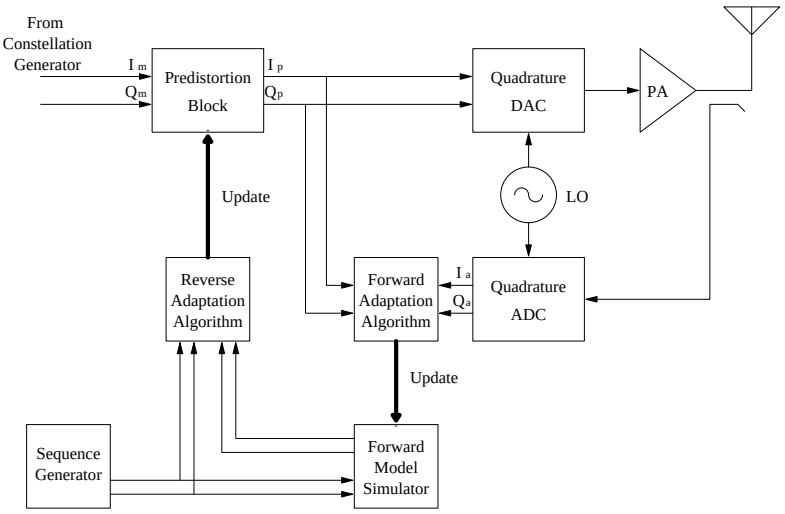

Figure 2.13: Block Diagram for a Multi-stage Predistortion System [19]

The multi-stage predistortion techniques differentiate themselves from inverse modeling predistortion techniques by comparing the output of the amplifier to the input of the amplifier rather than comparing to the input to the predistorter. The predistortion then becomes an open loop that closes only during predistorter updates.

Both models can be created using tables as in [11]; the models can be based upon calculations as in [19], or a mixture of a table model and a calculation model can be used.

Four advantages of multi-stage modeling over inverse modeling are presented in [19]. First, the multi-stage modeling is less sensitive than inverse modeling to measurement noise. Second, adaptation of the predistorter at high amplitudes is important but high amplitudes occur infrequently. The multi-stage method can use synthetic data with high amplitudes to derive the reverse model from the forward model. Third, the gradient needed for inverse modeling must be estimated and is available when using forward modeling. Adaptation while using inverse modeling is delayed by these errors in estimation. Finally, The inverse modeling adaptation rate is limited because of analog delays in the feedback path. After an initial delay, each sample obtains data which can be used to improve the forward model. With inverse modeling, each step toward adaptation requires a sample pass through the delay.

2.3.3.3 Signal or Data Predistortion

The digital predistorter can predistort individual samples of the signal just before the digital to analog conversion or predistort individual symbols. Data predistortion is equivalent to adjusting the location of the constellation points in the signal-space. While data predistortion is easy to implement, the distorter only reduces distortion at the symbol sampling time and does not reduce out-of-band distortions. [10]

Signal predistortion adjusts individual samples as the last step before digital to analog conversion. This allows the amplifier to appear as a near ideal amplifier up to the saturation point [10] and allows correction of both in-band and out-of-band distortions.

2.3.3.4 Delay Estimation

A variable delay is present between the digital output of the predistortion block and the samples taken from the amplifier output [35]. This delay is not constant and must be estimated to derive the correct predistorter. The delay must be estimated within $1/64^{th}$ of a symbol period for less than –60 dB ACPR. The delay may be estimated by comparing the slope of the magnitude of the two signals and adjusting the delay in the appropriate direction if the sign of the slope is different. [14] A typical delay can be 20 μs to 100 μs [19] and can be quite significant for high sample rates.

2.3.3.5 Update Rate

Adaptive digital predistortion has the ability to adapt to changing characteristics caused by aging, temperature, and output matching variations. While it is possible to perform digital predistortion in a static manner without adjusting the predistortion block, this would be unable to take into account variations in amplifier characteristics. However, [26] acknowledges that the amplifier characteristics change slowly and it is not necessary to continuously update the predistorter.

2.3.3.6 Sample Rate

The required sample rate will be larger than the Nyquist sampling rate for the desired signal. How much larger will depend on the degree of distortion and the desired

reduction in ACPR. The sample rate of the feedback must be at least twice as wide as the bandwidth of the distortion to be eliminated [14].

2.3.3.7 Raised Cosine Filtering

Raised cosine pulse shaping is used in transmitters to limit bandwidth and intersymbol interference. This is typically implemented as a filter with a square-root raised-cosine frequency response in both the transmitter and receiver. The resulting frequency response of the cascaded filters is the desired raised-cosine frequency response. Because a square-root raised-cosine filter is used in the transmitter, the signal contains inter-symbol interference that can be removed by the filter in the receiver, but the non-linear distortion in the amplifier between these filters has the effect of spreading the constellation points after filtering in the receiver.

The rolloff parameter of the raised cosine filter has an effect on the required backoff of the transmitted signal according to [7]. It was found by [7] found that performance for rolloffs of 35% to 50% was constant but that a 20% rolloff required an additional 1dB of backoff.

2.3.3.8 Implementation Errors

If a reduction in the adjacent channel interference is desired, then the dominant noise must not be due to quantization. A quantization of at least 10 bits is necessary to obtain a -60dB ACPR [14]. The maximum signal (P_s) to quantization noise (N_q) ratio is expressed by the following equation where b is the number of bits [27].

$$\left(\frac{P_s}{N_q}\right)_{dB} = 1.76 + 6.02b \qquad \text{[27] (Eq. 2.17)}$$

The quadrature conversion is susceptible to gain imbalance, phase imbalance, and carrier or local oscillator (LO) feedthrough [11]. The reduction in ACPR is in reality limited by quantization and LO carrier feed through [35].

Chapter 3. Measurement

3.1 Measurement Motivation

Previous studies of predistortion have included AM-AM and AM-PM characteristics of amplifiers in cellular and PCS bands. Since this study concentrated on the use of predistortion for LMDS, it was beneficial to measure the characteristics of an amplifier in the LMDS bands.

Other predistortion studies consider a static amplifier characteristic and only note that the characteristics change with conditions. This set of measurements shows the change in characteristics with changes in frequency, voltage, current, and temperature. It is perhaps impossible to predict the amplifier's response with so many variables, but these measurements show the significance of these variations.

The AM-AM and AM-PM distortions obtained in the measurements are used in the next chapter as non-linear distortion models in a simulation of a digital communication system with a non-linear amplifier. Although each amplifier is different, these measurements provide the simulation with real data of a 28 GHz amplifier distortion characteristic.

3.2 Measurement Procedure

The Agilent-HMMC-5033 is a class A amplifier [28] that is suitable for use at LMDS frequencies and both the input and output terminate to 50 ohms. The Agilent-HMMC-5040 is a similar amplifier designed to drive the Agilent-HMMC-5033. Agilent Technologies recommends a backoff of at least 10 dB below the 1 dB compression point for their HMMC-5040/HMMC-5033 amplifier chain to keep distortions acceptable when using complex modulations [28].

Both amplifiers are supplied as chips with connections made via gold bond wires. Agilent assembled the tested amplifiers into test packages with the power connections brought to pins and the RF input and RF output of the amplifiers to 2.4 mm female connectors.

Table 3.1: Amplifier Specifications

	HP-HMMC-5040 [29]	HP-HMMC-5033 [30]	Combined Amplifier
Frequency	20 – 40 GHz	17.7 – 32 GHz	20 – 32 GHz
Description	Driver	Final Amplifier	Combined Amplifier
Saturated Output Power	21 dBm	28 dBm	28 dBm
Estimated Input Saturation Power (based on typical gain)	3 dBm	10 dBm	-13 dBm
Output Power at 1 dB Gain Compression	18 dBm	26 dBm	26 dBm
Estimated Input Power 1dB Gain Compression (based on typical gain)	-5 dBm	8 dBm	-15 dBm
Typical Gain @ 28 GHz	23 dB	18 dB	41 dB
Max Input Power	21 dBm	23 dBm	21 dBm
Minimum Drain Voltage	2 V	-	
Typical Drain Voltage	4.5 V	V_{D1} 3.5 V, V_{D2} 5.0V	
Maximum Drain Voltage	5 V	V_{D1} 5.0 V, V_{D2} 5.0V	
Typical Gate Voltage	-0.6V	-0.8V	
Absolute Max Drain Voltage	5.2 V	V_{D1},2 5.2 V	5.2 V
Absolute Max Gate Voltage	0.5 V	V_{G1},V_{GG} 0.5 V	0.5 V
Absolute Min Gate Voltage	-3.0 V	V_{G1},V_{GG} −3.0 V	-3.0 V
Nominal VDD current	225 – 300 mA	V_{D1} 180 mA, V_{D2} 400 mA	805 – 880 mA
Operational Temperature	-55°C to +75°C	-55°C to +85°C	-55°C to +75°C

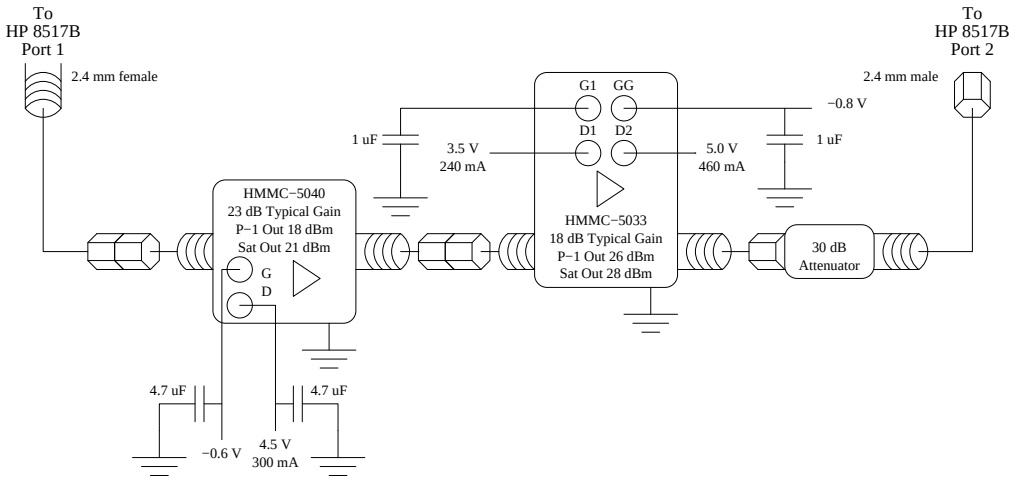

Figure 3.1 Amplifier Test Configuration

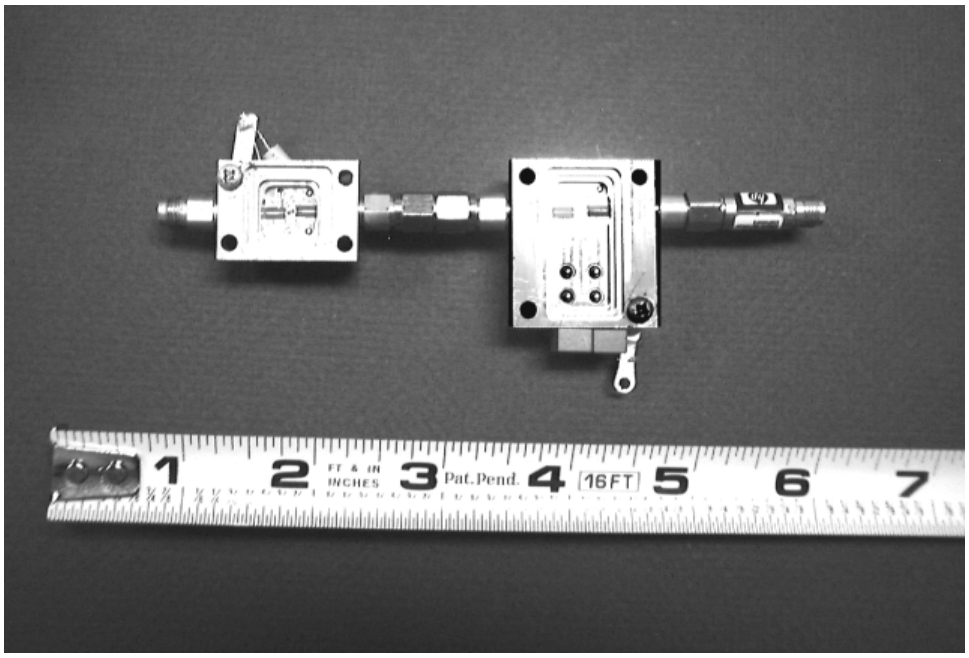

Figure 3.2 Amplifier under Test with Attenuator and Joining Adapter

Figure 3.3 Agilent 8510C Measurement System

Measurements were taken using an Agilent HP 8510C analyzer configured to use a HP 8517 S-parameter deck and HP 85621B source. Other equipment used is summarized in the following table. The analyzer was placed into step mode which steps through each frequency or power and takes the data after the analyzer has achieved phase lock on the signal from the device under test. The analyzer was also set to average the last 16 sweeps to reduce measurement noise. The averaging factor of 16 was used for all measurements. Four hundred and one data points were taken for each frequency sweep. These points were equally spaced in frequency. Similarly, four hundred and one data points were taken for each power sweep. These points were equally spaced in decibels.

Table 3.2 Equipment Summary

	Model	Serial
Driver Amplifer	Agilent HMMC-5040	TC906#9
Power Amplifier	Agilent HMMC-5033	TC915#1
30 dB fixed attenuator	Agilent HP 8490D	00785
Power Meter	Agilent HP E4418B	US39251642
Power Sensor	Agilent 8487A	3318A03286
Network Analyzer	Agilent HP 8510C/HP85106D E25	3031A09808
S-Parameter Test Set	Agilent HP 8517B	3602A00724
Signal Generator	Agilent HP 83651B	3844A00457
Signal Generator	Agilent HP 83620B	3844A00870
Power Supply for 5040		
Power Supply for 5033	Agilent HP E3631A	KR92921103
Digital Multi-meter	Agilent HP 34401A	US36086291
Temperature Sensor	Peet Brothers Ultimeter 800	

It was found that the input power to the amplifier from the analyzer was nearly 20 dB lower than the power specified in the setup. The output power specified in the analyzer setup is the output from the signal generator and does not take into account losses in cables and the S-parameter deck. A power flatness calibration was performed to correct this problem.

The power meter HP-IB interface was connected to the system bus of the 8510. This allows the HP 8510 to read the power meter during the power flatness calibration. The power meter was configured for the 8487A power sensor and the frequency was set to 28

GHz. The power meter was then zeroed and then calibrated to the RF source on the front panel of the power meter. The power of the Port 1 source was set to 10 dBm. Port 1 of the HP 8517 was connected to the HP 8487A power sensor and a power flatness calibration was performed. More information on the procedure can be found in Agilent product note 8510-16 entitled "Controlling Test Port Output Power Flatness" [31].

The output power was confirmed after power calibration for several output powers at 28.0 GHz. The results are shown in the table below.

Table 3.3 Recorded Output Power after Flatness Correction

Set Power	Measured Power
-12 dBm	-12.01 dBm
-20 dBm	-20.05 dBm
-25 dBm	-25.16 dBm
-30 dBm	-30.65 dBm

A full 2-port calibration procedure was attempted with the 30 dB fixed attenuator considered as part of the test set-up. The resulting measurements contained increased noise because of the noise captured during the calibration with the 30 dB fixed attenuator. It was decided to remove the 30 dB fixed attenuator from the measurement setup during calibration. The 30 dB fixed attenuator was then characterized so its effect could be removed from the measurements later.

A full 2-port calibration without the attenuator was made after the power was leveled. The male-to-female adapter from the 2.4 mm calibration kit was placed on the Port 1 cable during calibration. Although not required to complete the calibration, the insertion of this connector during calibration compensates for the insertion of the male-to-male adapter required at the input of the HMMC-5040 driver amplifier during measurements.

The HMMC-5033 can be biased in one of two ways. The power connections for the device consist of two drain ($V_{D1,}$ V_{D2}) and two gate connections (V_{G1},V_{GG}). The first method of biasing consists of 3 supply voltages of 3.5 V at V_{D1}, 5 V at V_{D2}, and –0.8 V at V_{GG} with no connection to V_{G1}. V_{G1} is biased internally from V_{GG} to give the desired ratio of current between I_{D1} and I_{D2}. The second biasing configuration connects the V_{D1} and V_{D2} to the same 5.0 V supply and connects V_{G1} and V_{GG} to the same –0.8 V supply.

This configuration provides equal I_{D1} and I_{D2}. All measurements were performed with the first bias configuration.

Four measurements were taken for each variation when applicable. Frequency sweeps were performed between 27.5 GHz and 28.5 GHz for powers of –12 dBm and –20 dBm. This was performed to see the variations in the saturation power with frequency. The maximum calibrated 28 GHz output power of the analyzer at the input of the amplifier was found to be -12 dBm. The lowest power possible in a single sweep was -30 dBm. For power sweeps, the S_{21} or forward gain of the amplifier was measured with varying input powers from -30 dBm to -12 dBm or just where the final amplifier HMMC-5033 began to approach saturation. An additional sweep not presented here was made from -40 dBm to -22 dBm to confirm that the amplifier exhibited a linear response at an input power of -30 dBm.

Table 3.4 Measurement Types

Type	Sweep Type	Range	Constant
1	Frequency	27.5 GHz – 28.5 GHz	-20 dBm
2	Frequency	27.5 GHz – 28.5 GHz	-12 dBm
4	Power	-30 dBm to -12 dBm	28 GHz
5	Power	-40 dBm to -22 dBm	28 GHz

Measurements were taken on both HP-HMMC-5040 alone and the combined amplifier made from the HP-HMMC-5040 and HP-HMMC-5033. The combined amplifier was tested with several different variations in frequency, drain current, drain voltage, and device temperature. The bias conditions for each measurement variation are summarized. An ‘X’ denotes bias conditions such as the gate current that are not important or not applicable. The following table summarizes the variations.

Table 3.5 Measurement Variation Summary

Variation	Conditions
12	Ideal bias, No cooling
13	Ideal bias, No cooling, Power sweeps at 27.5 GHz and 27.6 GHz
14	V_{D1} and V_{D2} on 5033 lowered 10% on 5033, No cooling
15	V_{G2} on 5033 changed to drop I_D by 10%, No cooling
17	V_{G2} on 5033 changed to drop I_D by 10%, Cooled to 51° F

The ideal bias and no cooling measurement is used as a reference for comparison with the other variation in amplifier conditions. Power sweeps were made at different frequencies to determine the effect of changing of frequency on the AM-AM and AM-PM characteristics of the amplifier. Variations 14 and 15 were performed to determine the effects of non-ideal biasing on the AM-AM and AM-PM characteristics of the amplifier. The temperature of the amplifier was cooled using a Peltier effect device. The case temperature of the HMMC-5040 amplifier was measured using the Peet Brothers Ultimeter 800 temperature sensor.

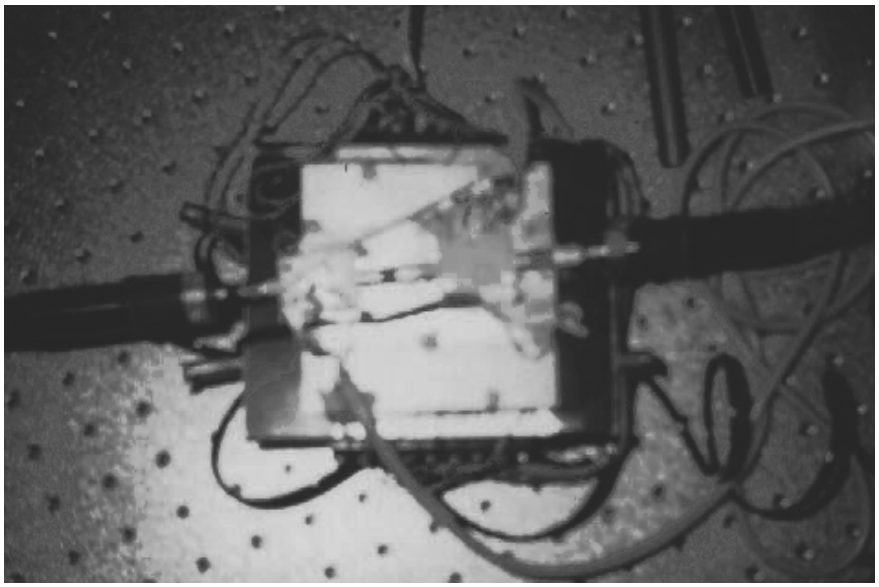

Figure 3.4 Amplifiers on Peltier Devices while Testing

3.3 Measurement Results

The data from the measurements was saved to a floppy disk using the save data feature of the 8510C Network Analyzer. A Matlab program was written to read this data into Matlab arrays for plotting and for later use in simulations. Each measurement is shown below with the conditions for the measurement.

3.3.1 Fixed 30 dB Attenuator

These measurements confirm that the attenuator does not introduce any non-linear effects and has a constant gain across frequency and power and a constant phase across swept power. As a result of these measurements future measurements are corrected for a constant attenuation of 30.75 dB.

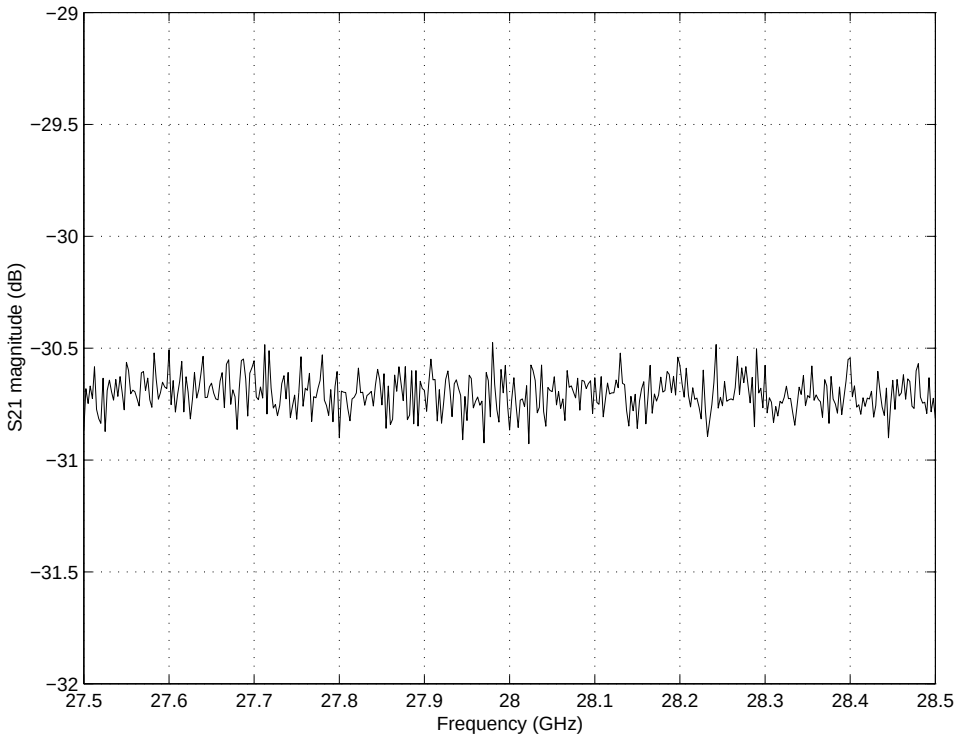

Figure 3.5 30 dB Fixed Attenuator Frequency Sweep S21 Magnitude

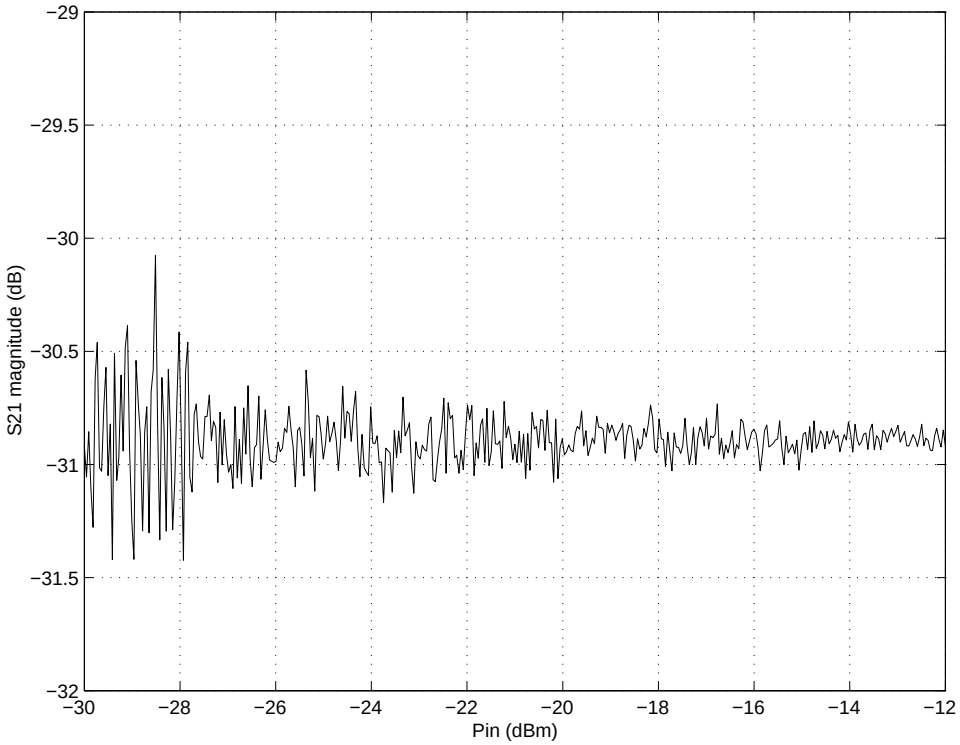

Figure 3.6 30 dB Fixed Attenuator Power Sweep S21 Magnitude

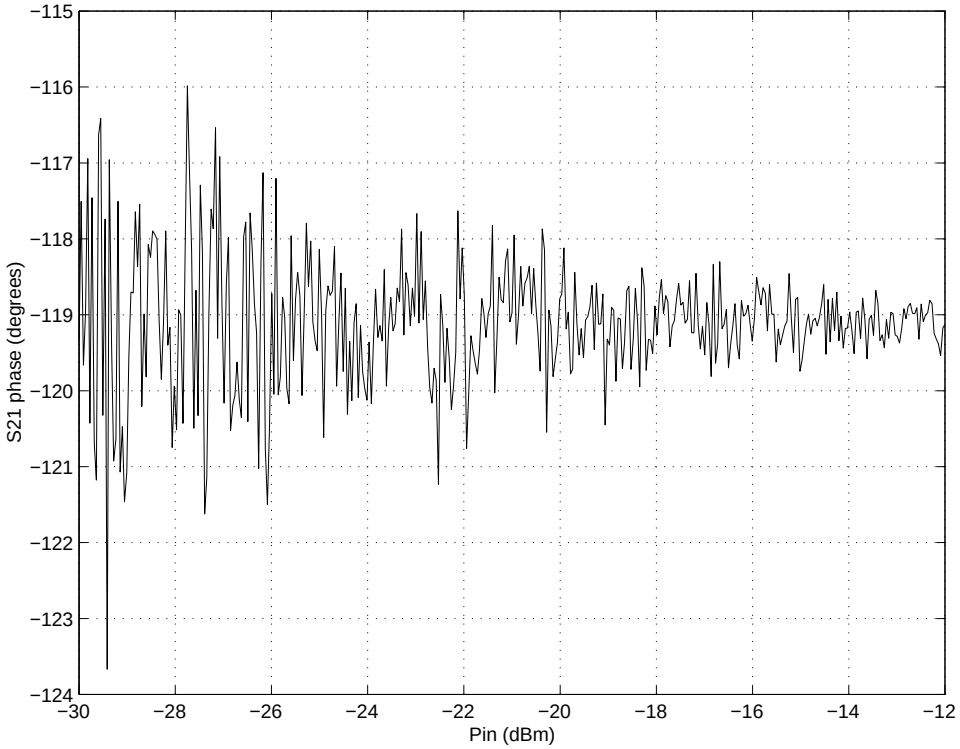

Figure 3.7 30 dB Fixed Attenuator Power Sweep S21 Phase

3.3.2 HMMC-5040 Amplifier

Table 3.6 HMMC-5040 Amplifier Conditions

HMMC-5040 Driver	Set Voltage	Measured Voltage	Minimum Measured Voltage at Peak Input	Current with no RF Input	Peak Current at Peak Input
V_D	4.5 V	4.454 V	4.454 V	250 mA	250 mA
V_G	-0.6 V	-0.657 V	-0.657 V	-	-

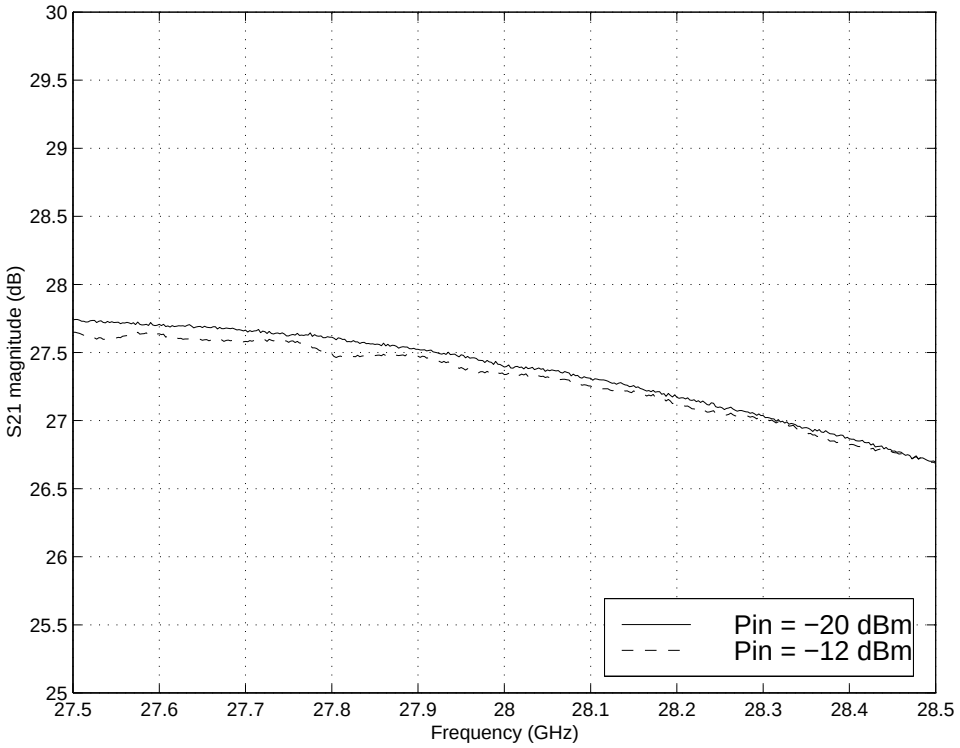

Figure 3.8 HMMC-5040 Frequency Swept S21

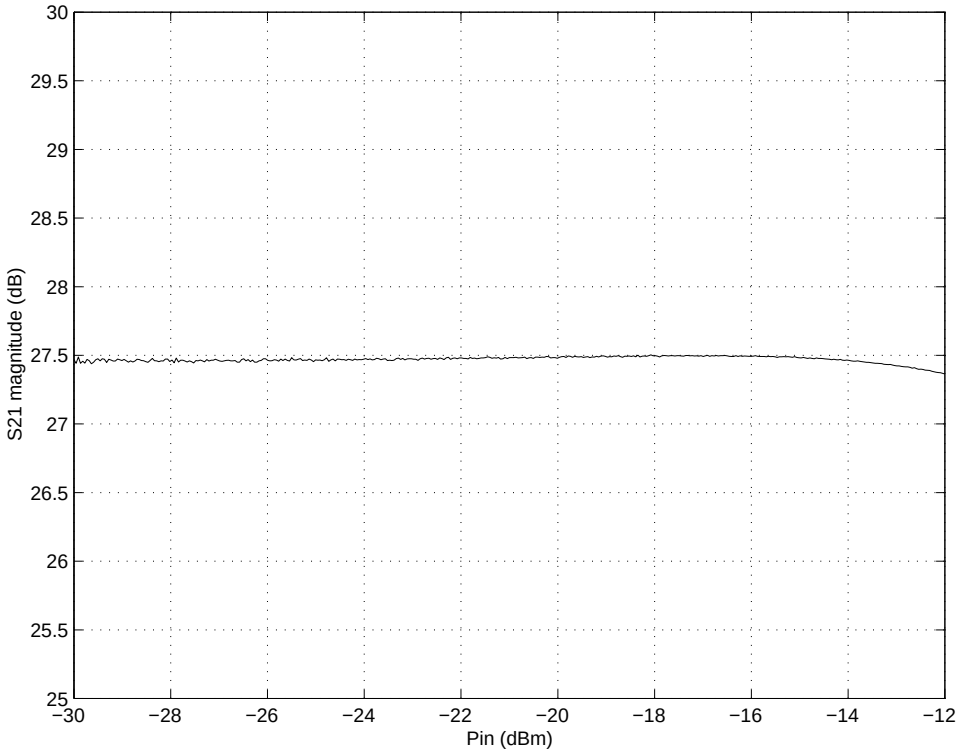

Figure 3.9 HMMC-5040 Power Swept S21 Magnitude

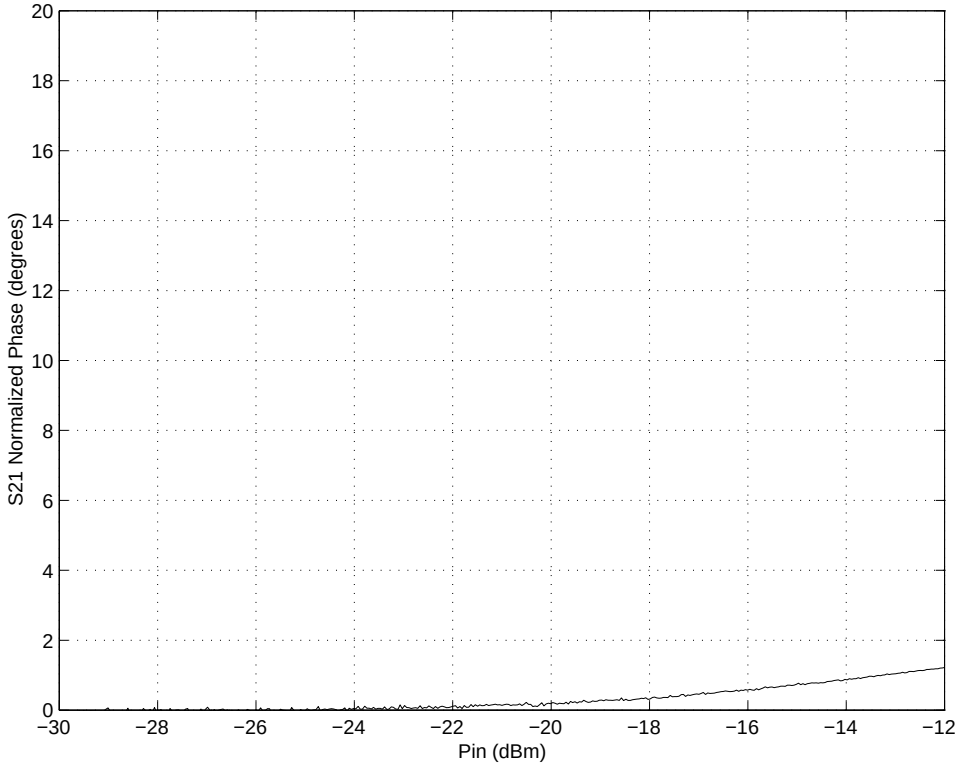

Figure 3.10 HMMC-5040 Power Swept S21 Phase

3.3.3 Combined Amplifier Reference

Table 3.7 Combined Amplifier Conditions

HMMC-5040 Driver	Set Voltage	Measured Voltage	Minimum Measured Voltage at Peak Input	Current with no RF Input	Peak Current at Peak Input
V_D	4.5 V	4.467 V	4.468 V	250 mA	250 mA
V_G	-0.6 V	-0.658 V	-0.658 V	X	X
HMMC-5033 PA					
V_{D1}	3.5 V	3.429 V	3.400 V	196 mA	227 mA
V_{D2}	4.5 V	4.917 V	4.600 V	365 mA	640 mA
V_{G1}	-0.92 V	-0.969 V	-0.993 V	X	X
V_{GG}	NC	X	X	X	X
Case Temperature	94 °F				

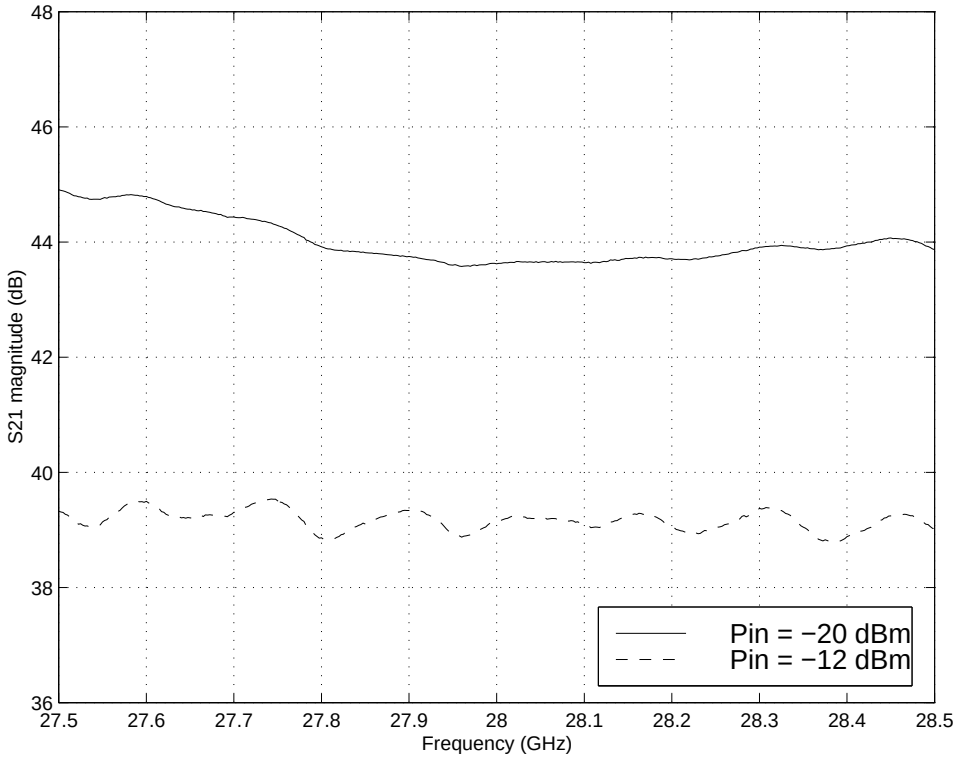

Figure 3.11 Combined Amplifier Frequency Swept S21 Magnitude

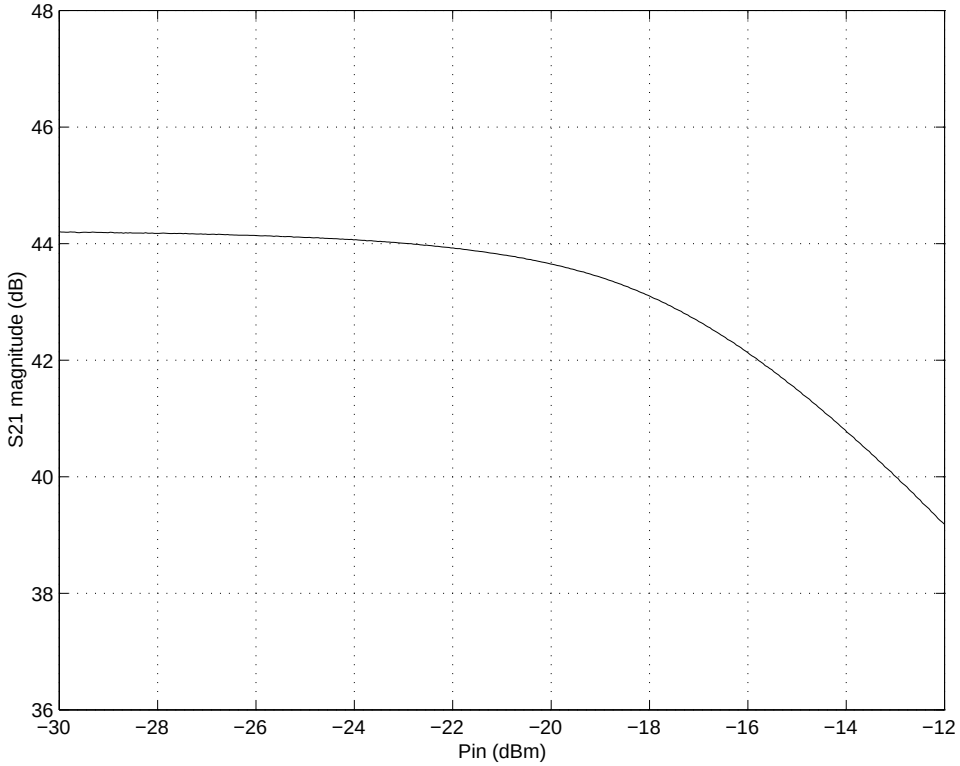

Figure 3.12 Combined Amplifier Power Swept S21 Magnitude

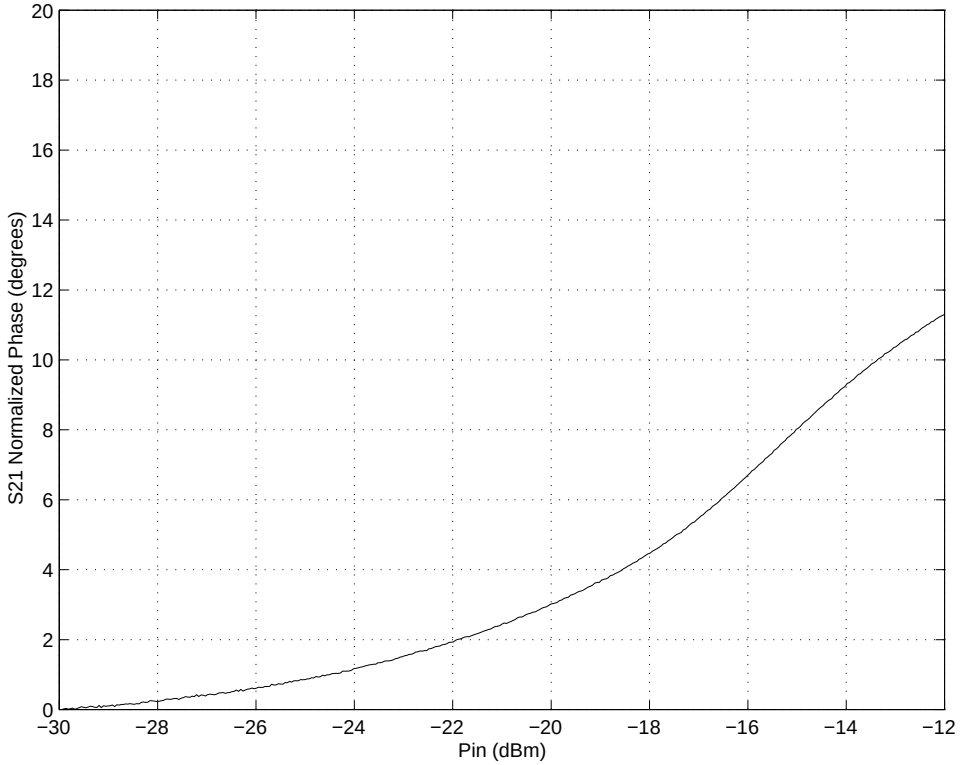

Figure 3.13 Combined Amplifer Power Swept S21 Phase

3.3.4 Combined Amplifier at Different Frequencies

Table 3.8 Combined Amplifier at Different Frequencies Conditions

HMMC-5040 Driver	Set Voltage	Measured Voltage	Minimum Measured Voltage at Peak Input	Current with no RF Input	Peak Current at Peak Input
V_D	4.5 V	4.468 V	4.468 V	250 mA	250 mA
V_G	-0.6 V	-0.658 V	-0.658 V	X	X
HMMC-5033 PA					
V_{D1}	3.5 V	3.429 V	3.400 V	196 mA	227 mA
V_{D2}	5.0 V	4.917 V	4.600 V	365 mA	640 mA
V_{G1}	-0.92 V	-0.969 V	-0.993 V	X	X
V_{GG}	NC	X	X	X	X
Case Temperature	93 °F				

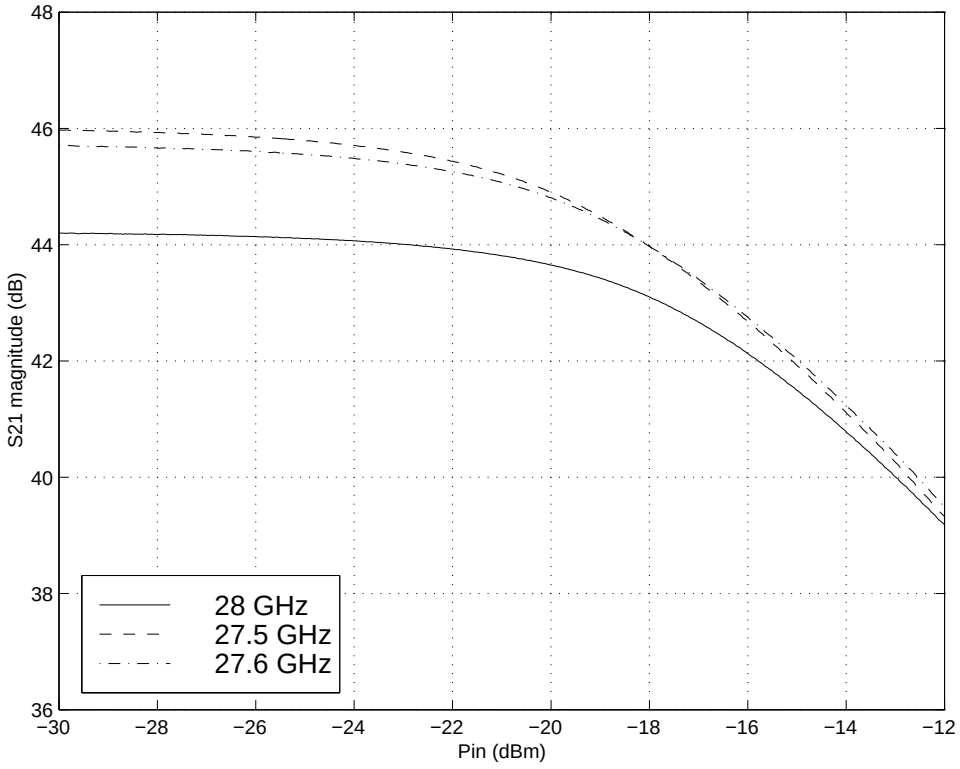

Figure 3.14 Combined Amplifier Power Swept at Different Frequencies S21 Magnitude

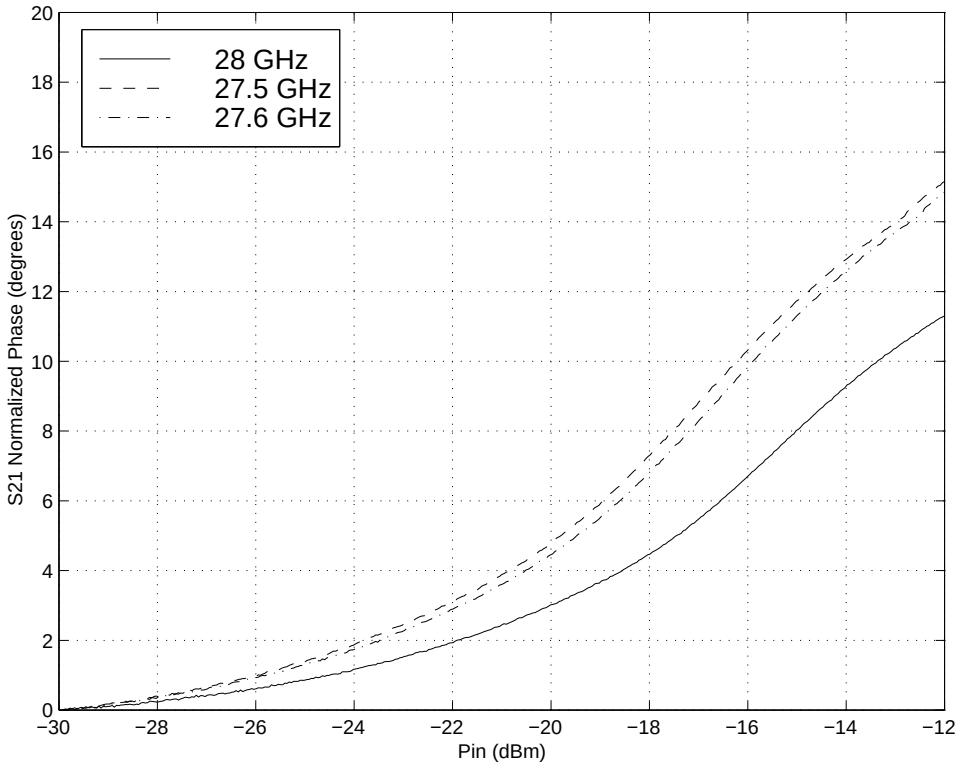

Figure 3.15 Combined Amplifier Power Swept at Different Frequencies S21 Phase

3.3.5 Combined Amplifier with Low Drain Voltage

Table 3.9 Combined Amplifier with Low Drain Voltage Conditions

HMMC-5040 Driver	Set Voltage	Measured Voltage	Minimum Measured Voltage at Peak Input	Current with no RF Input	Peak Current at Peak Input
V_D	4.5 V	4.467 V	4.468 V	250 mA	250 mA
V_G	-0.6 V	-0.658 V	-0.658 V	X	X
HMMC-5033 PA					
V_{D1}	3.15 V	3.087 V	3.084 V	180 mA	210 mA
V_{D2}	4.50 V	4.427 V	4.386 V	320 mA	475 mA
V_{G1}	-0.92 V	-0.964 V	-0.964 V	X	X
V_{GG}	NC	X	X	X	X
Case Temperature	91 °F				

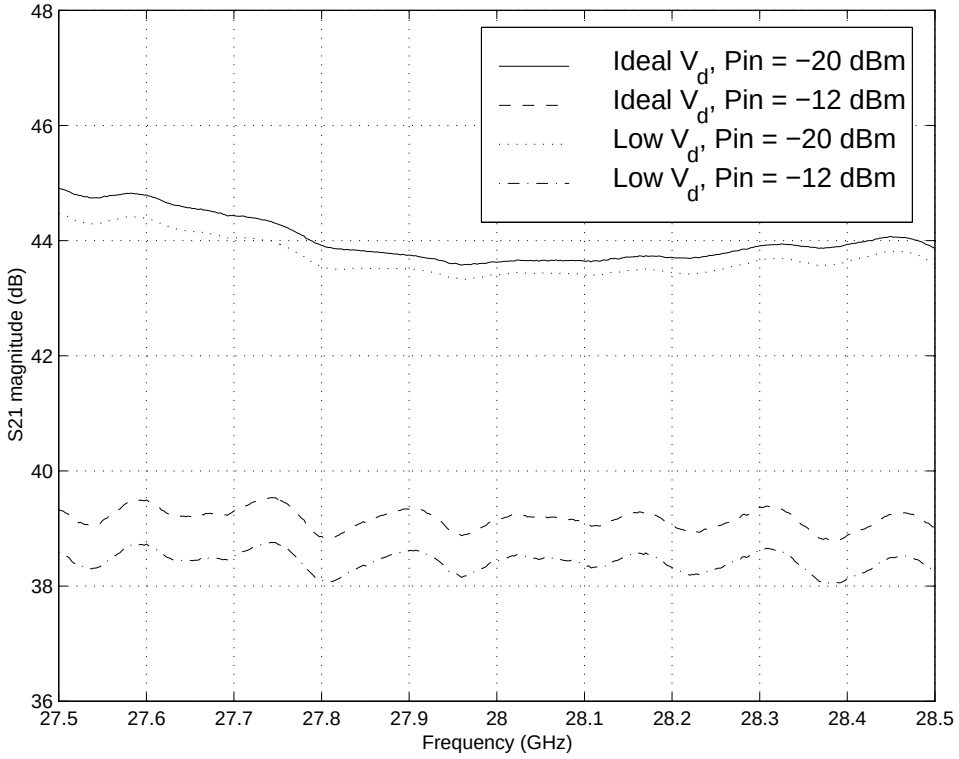

Figure 3.16 Low Drain Voltage Frequency Swept S21 Magnitude

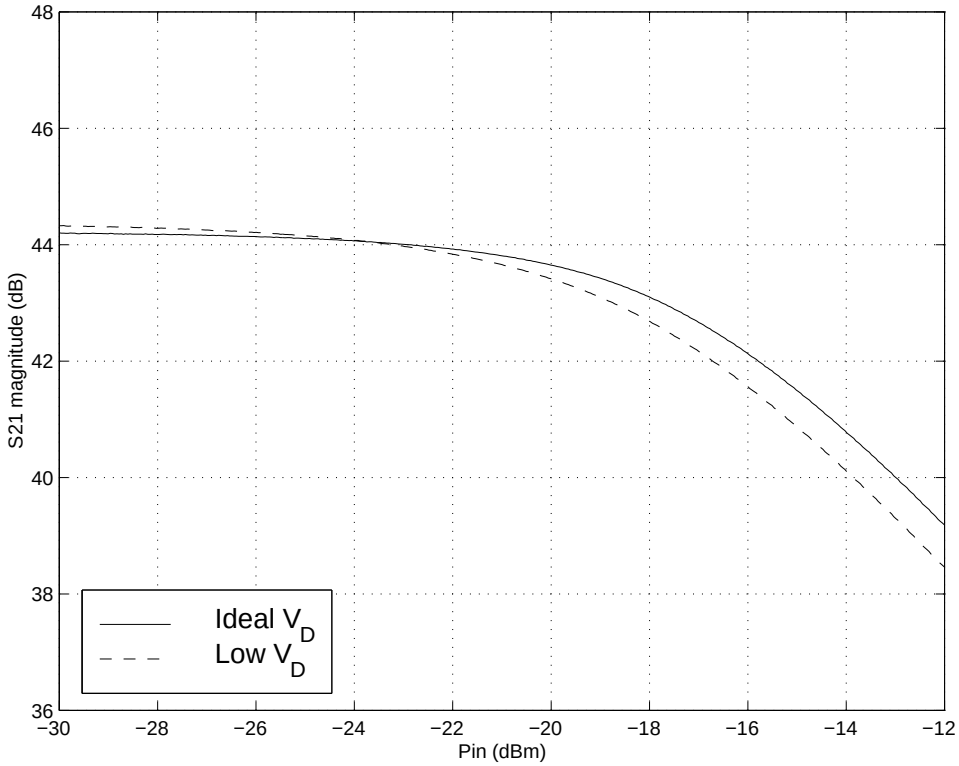

Figure 3.17 Low Drain Voltage Power Swept S21 Magnitude

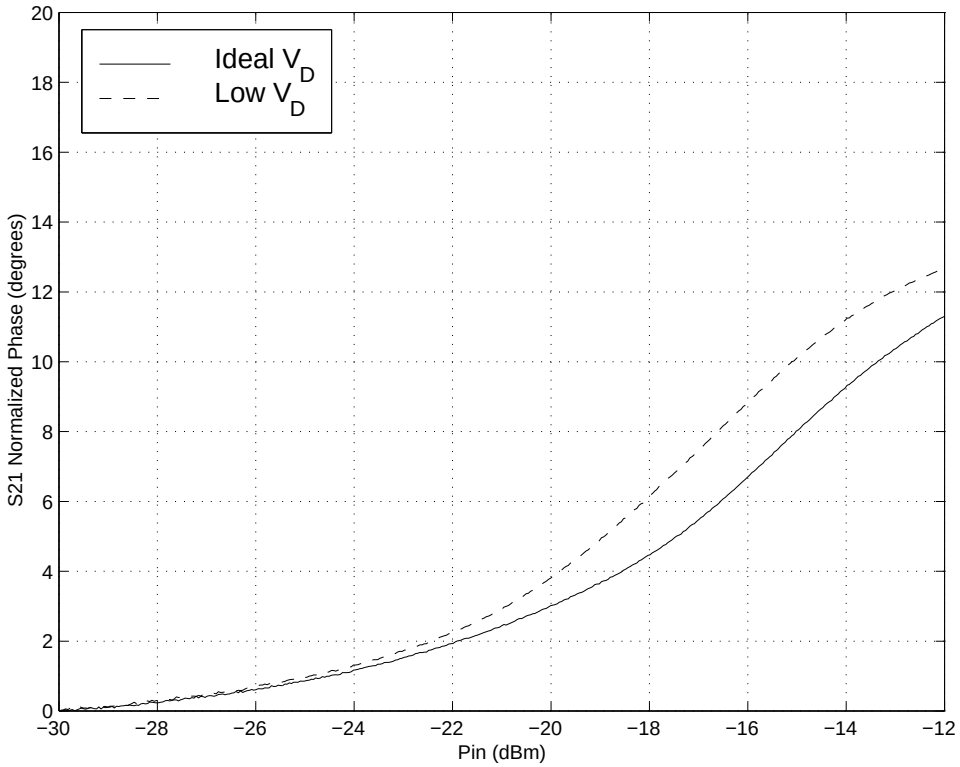

Figure 3.18 Low Drain Voltage Power Swept S21 Phase

3.3.6 Combined Amplifier with Low Drain Current

Table 3.10 Combined Amplifier with Low Drain Current Conditions

HMMC-5040 Driver	Set Voltage	Measured Voltage	Minimum Measured Voltage at Peak Input	Current with no RF Input	Peak Current at Peak Input
V_D	4.5 V	4.467 V	4.468 V	250 mA	250 mA
V_G	-0.6 V	-0.658 V	-0.658 V	X	X
HMMC-5033 PA					
V_{D1}	3.50 V	3.436 V	3.405 V	182 mA	212 mA
V_{D2}	5.00 V	4.925 V	4.867 V	327 mA	627 mA
V_{G1}	-0.96 V	-1.004 V	-1.004 V	X	X
V_{GG}	NC	X	X	X	X
Case Temperature	90 °F				

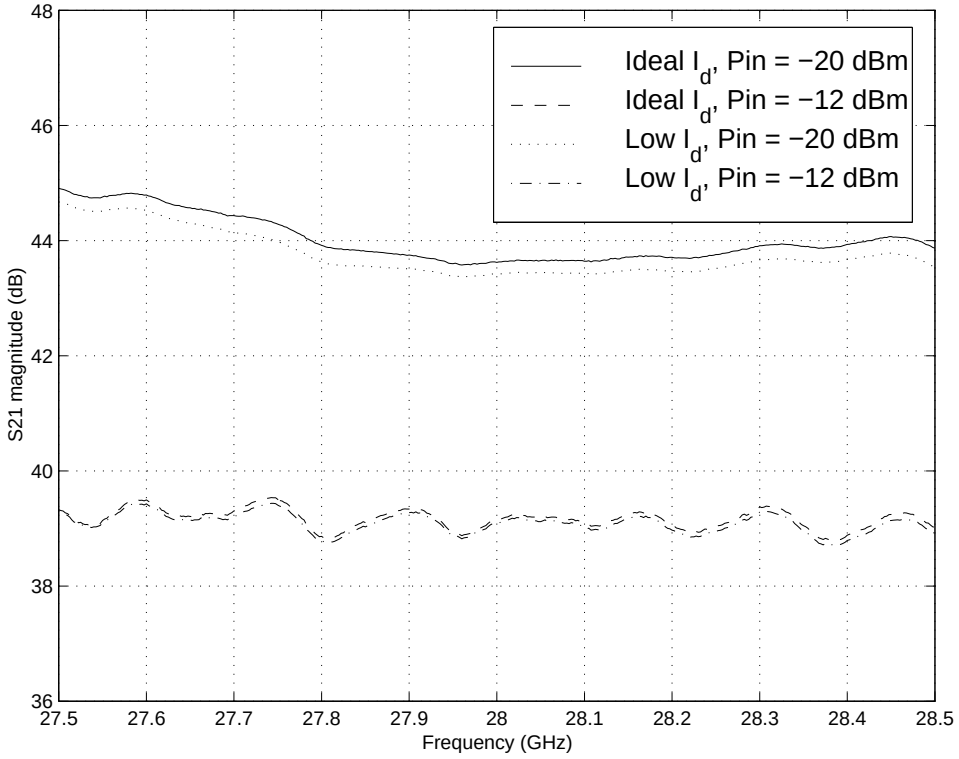

Figure 3.19 Low Drain Current Frequency Swept S21 Magnitude

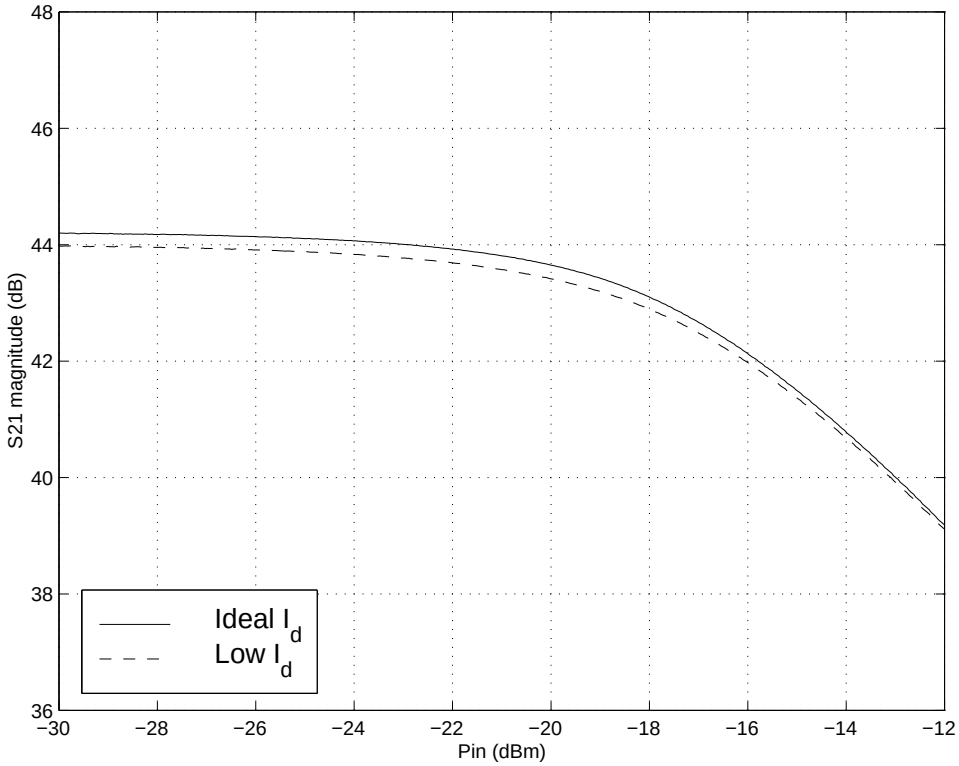

Figure 3.20 Low Drain Current Power Swept S21 Magnitude

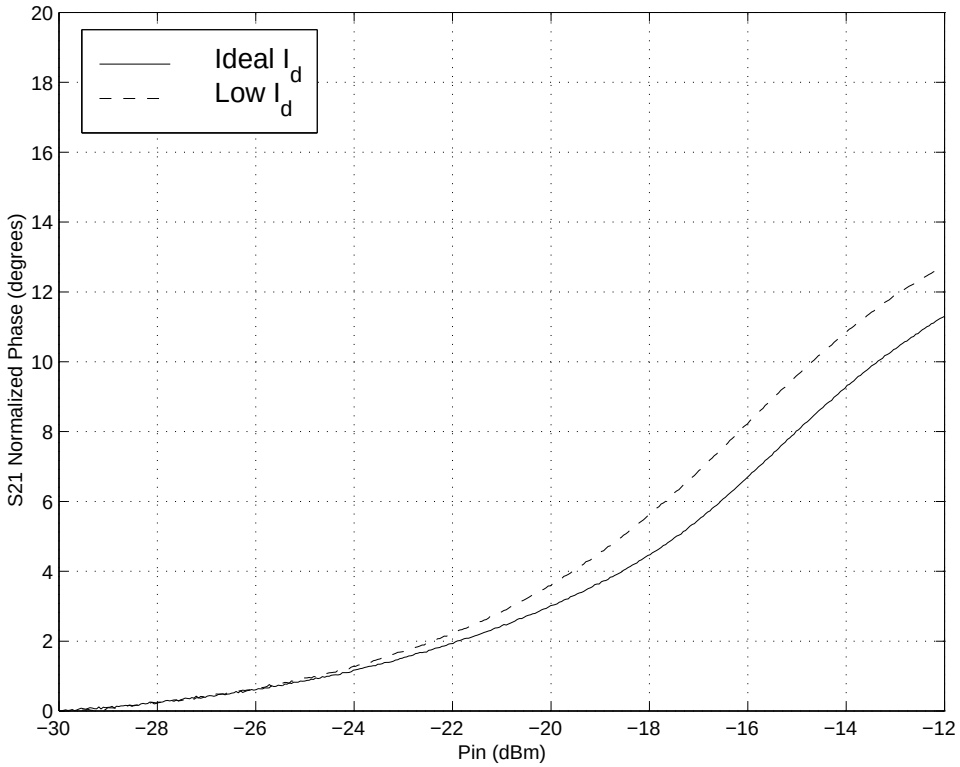

Figure 3.21 Low Drain Current Power Swept S21 Phase

3.3.7 Combined Amplifier with Reduced Temperature

The temperature of the HMMC-5033 case was lowered with Peltier effect devices from the 93°F to 51°F. After the temperature was reduced, it was required to make the gate voltage more negative to keep from exceeding the maximum drain current at the high end of the power swept measurements. These measurements are compared to both the reference and the reduced current cases because of the change in gate voltage.

Table 3.11 Combined Amplifier with Reduced Temperature Conditions

HMMC-5040 Driver	Set Voltage	Measured Voltage	Minimum Measured Voltage at Peak Input	Current with no RF Input	Peak Current at Peak Input
V_D	4.5 V	4.465 V	4.468 V	260 mA	260 mA
V_G	-0.6 V	-0.659 V	-0.659 V	X	X
HMMC-5033 PA					
V_{D1}	3.50 V	3.451 V	3.405 V	147 mA	210 mA
V_{D2}	5.00 V	4.946 V	4.867 V	233 mA	634 mA
V_{G1}	-1.06 V	-1.094 V	-1.094 V	X	X
V_{GG}	NC	X	X	X	X
Case Temperature	51 °F				

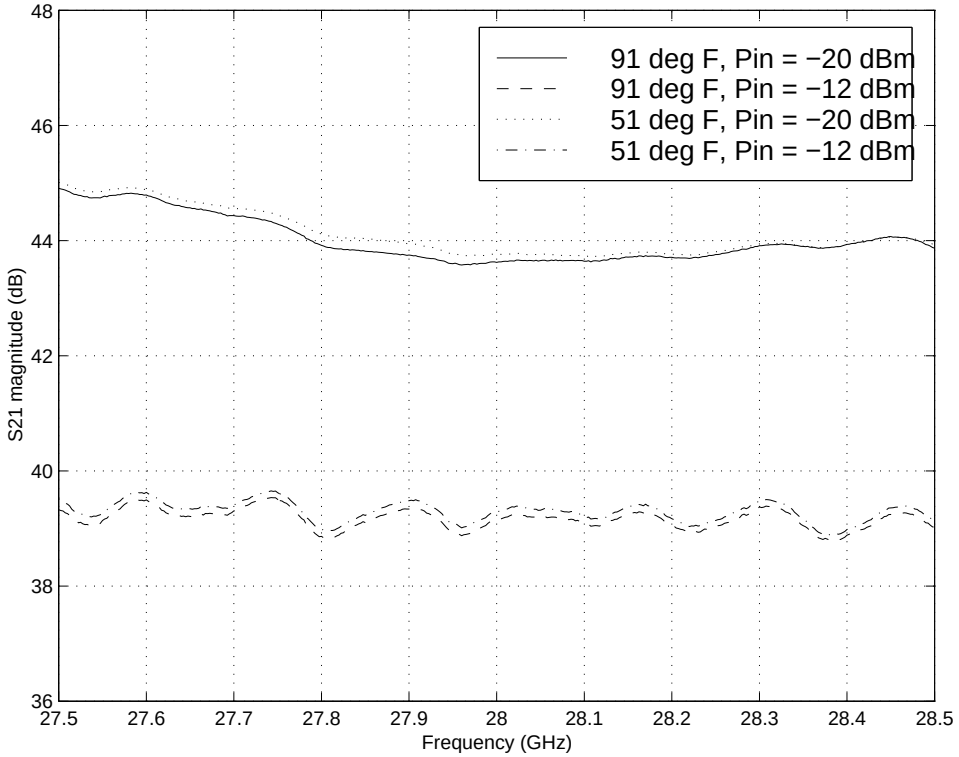

Figure 3.22 Reduced Temperature Frequency Swept S21 Magnitude

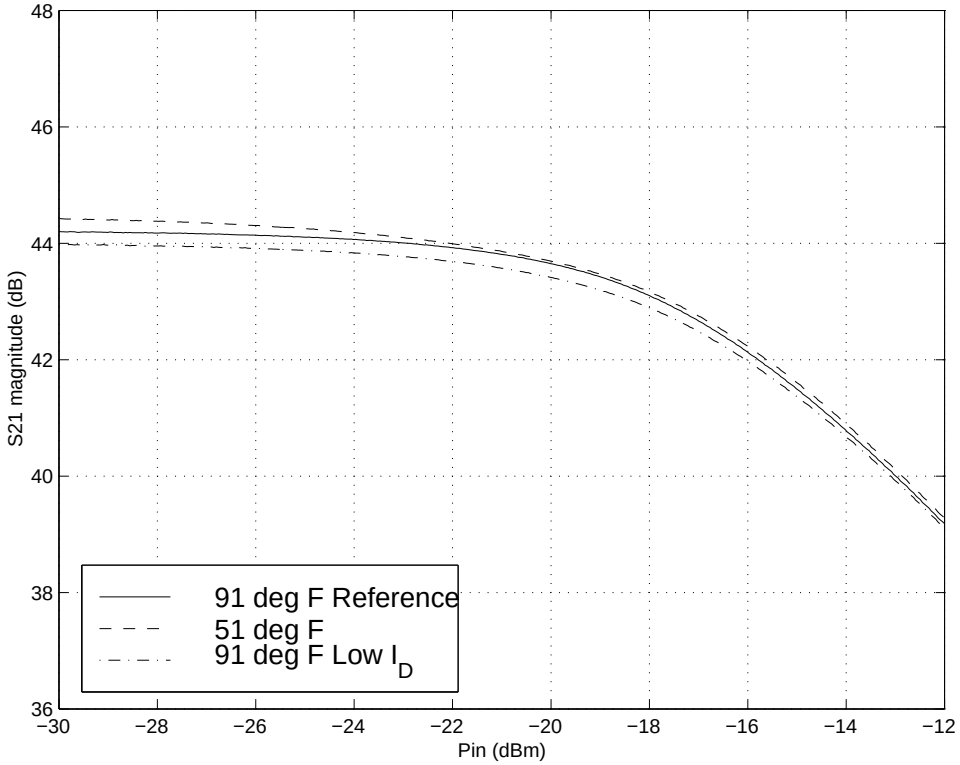

Figure 3.23 Reduced Temperature Power Swept S21 Magnitude

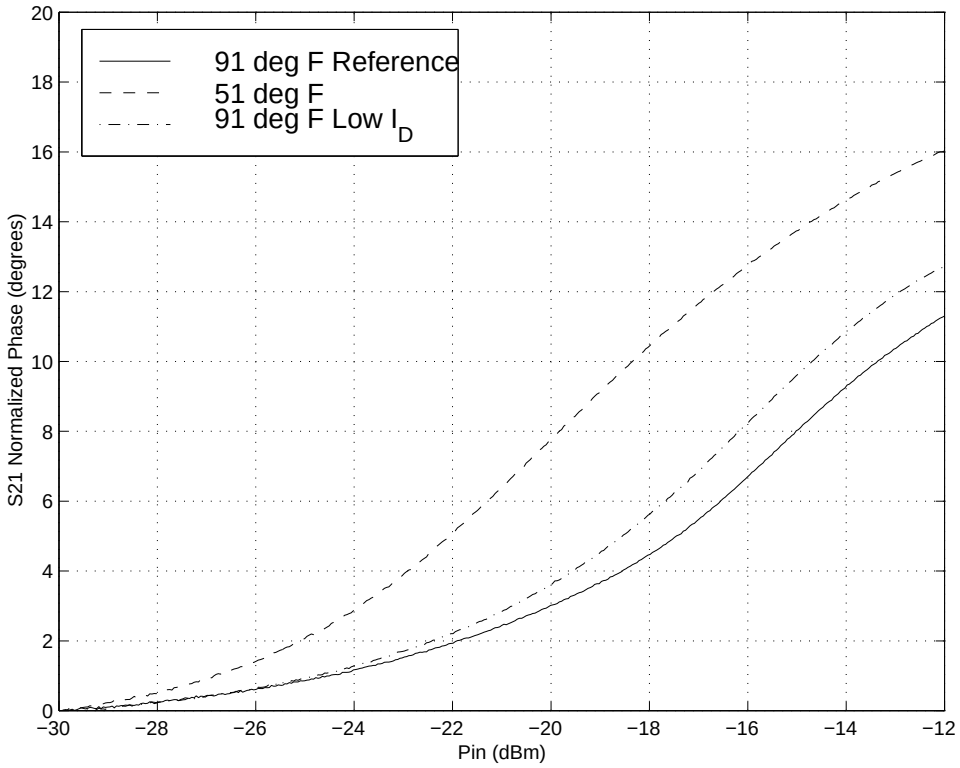

Figure 3.24 Reduced Temperature Power Swept S21 Phase

Chapter 4. Simulation

4.1 Simulation Overview

It is difficult to determine the optimum drive level for an amplifier when using non-constant envelope modulations. An engineer can use the value of the amplifier's -1 dB compression point and rules of thumb for each modulation type to estimate the maximum drive level for an amplifier. However, this does not take into account variances from typical amplitude distortion or phase distortions in the amplifier.

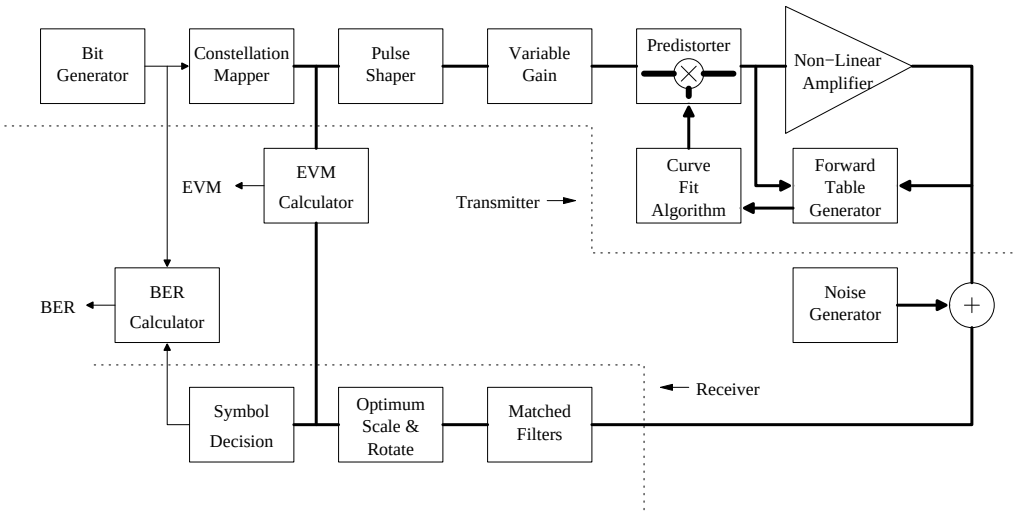

Figure 4.1 Block Diagram of Predistortion Simulator

The developed Matlab simulation determines the optimum drive level for a particular set of conditions. The simulator is capable of simulating QPSK, 16-QAM, 64-QAM, and 256-QAM signals with non-linear distortion. The simulated predistorter is a multistage signal predistorter with a mixture of table lookup and polynomial modeling. The simulation determines the potential gain from this method of predistortion by comparing the error vector magnitude (EVM) of the predistorted system to the EVM of the system without predistortion.

The accuracy and computational complexity are considered for different polynomial order and forward table sizes. The potential for reduction in ACPR and the effect of a

maladjusted predistorter are also considered. The next chapter uses the insight on design decisions gained from these simulations to evaluate the feasibility of a proposed predistorter for a LMDS system.

4.2 Simulation Design

4.2.1 Transmitter

4.2.1.1 Random Sequence Generator

The random sequence generator generates a bit sequence of either one or zero with equal probability. The sequence length is specified when the sequence is generated.

4.2.1.2 Constellation Generator

The constellation generator converts the bit sequence from zeros and ones to a complex valued constellation point. The generator is capable of generating QPSK, 16-QAM, 64-QAM, and 256-QAM signals. Grey coding was used in assigning binary values to each point so errors with adjacent symbols would cause a single bit error. The constellations and decimal values assigned to each symbol are shown in the following figures. The peak power of each constellation is 1W with corresponding peak I and Q voltages of $\sqrt{\frac{1}{2}}$ volt.

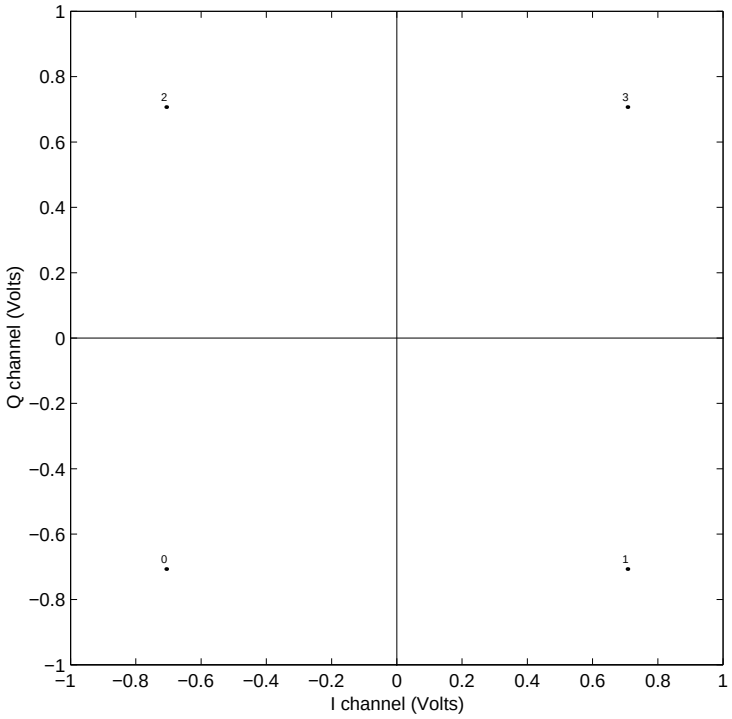

Figure 4.2 QPSK Constellation

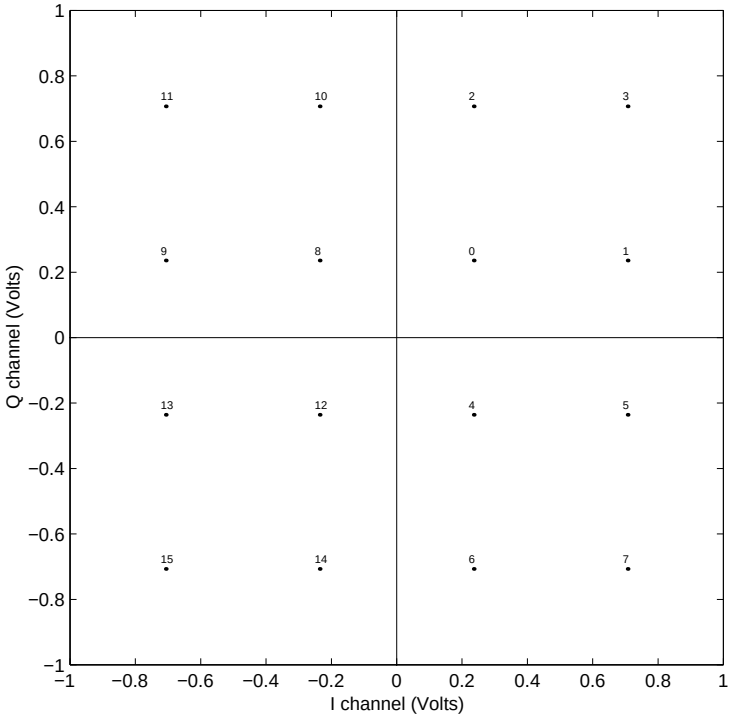

Figure 4.3 16-QAM Constellation

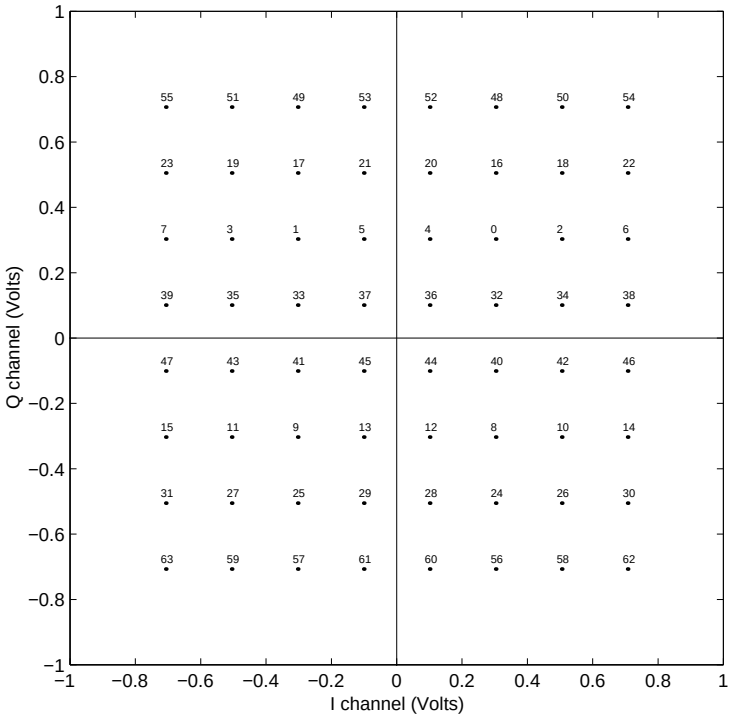

Figure 4.4 64-QAM Constellation

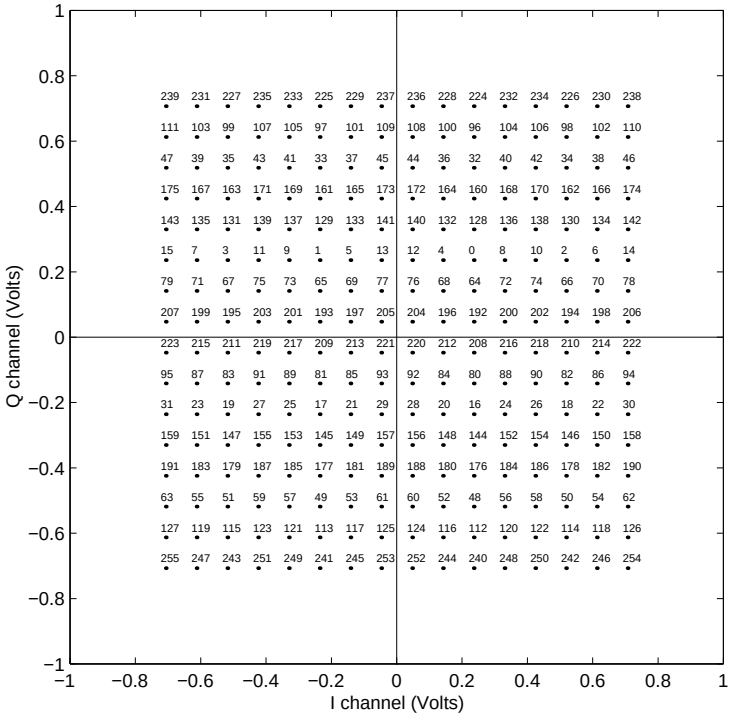

Figure 4.5 256-QAM Constellation

4.2.1.3 Root Raised Cosine Pulse Shaping

The ideal root raised cosine filter has an infinite length and must be truncated when implemented. The delay of 6 symbols was found experimentally by increasing the delay until the error due to the truncated filter was small compared to other errors. An oversampling rate of 8 was used for the simulations; therefore each symbol results in 8 samples. The filter is implemented as a FIR filter with (8 x 6 x 2) + 1 = 97 taps. Each symbol after filtering depends on the values of the six symbols before and the six symbols after the symbol of interest.

The root raised cosine filter rolloff factor affects the shape of the filter. A filter with a rolloff factor of 1 has a gradual cutoff while a filter with a rolloff factor of 0 is an ideal low pass filter. Rolloff factors (r) of 0.15, 0.2, 0.35, and 0.5 are considered in the simulations. The rolloff factors of 0.2 and 0.35 are specified in the DAVIC standard for LMDS systems [32].

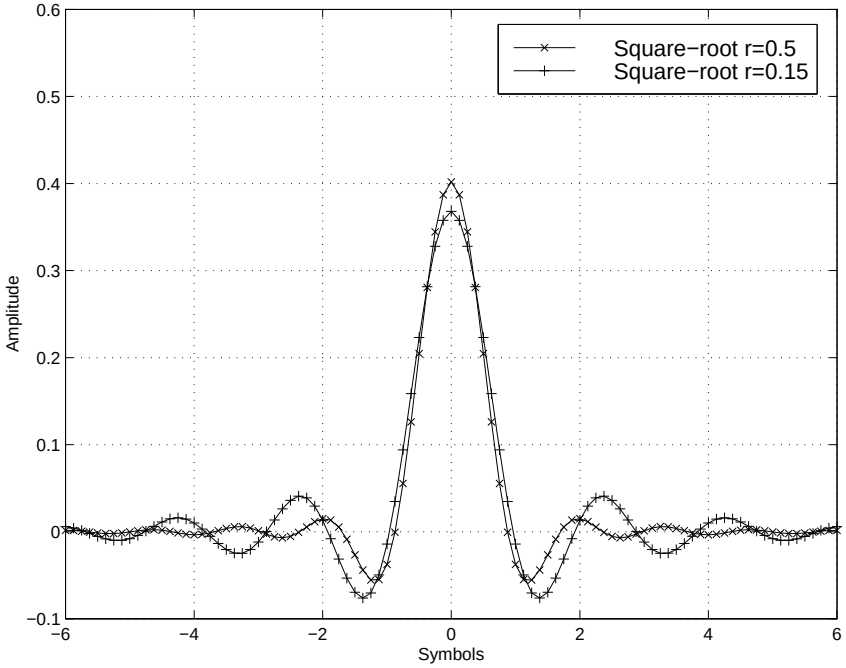

Figure 4.6 Root-Raise Cosine Impulse Response for r=0.5 and r=0.15.

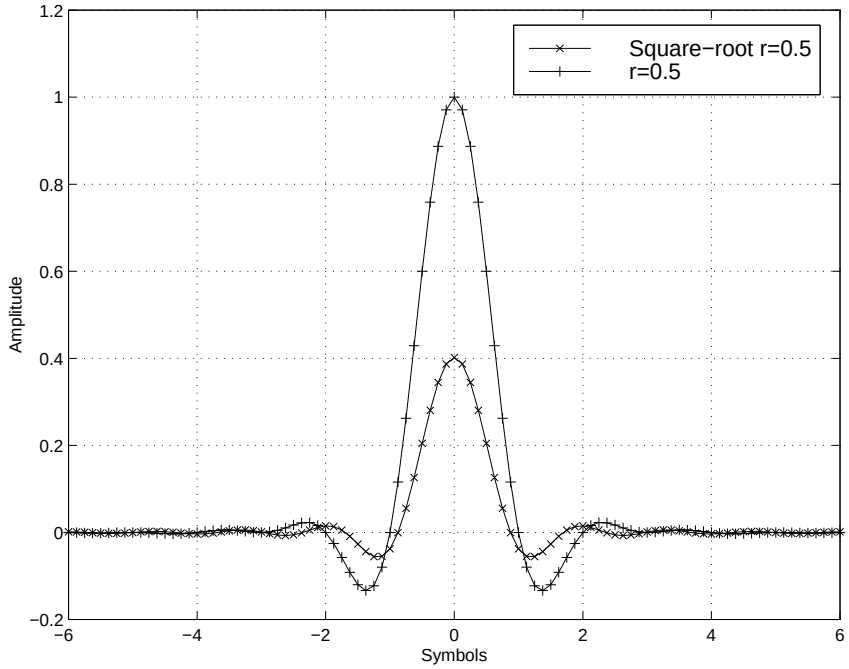

Figure 4.7 Comparison of Root-Raised Cosine Filter and Raised Cosine Filter

4.2.1.4 Adjustable Gain Block

An adjustable gain block is before the predistorter to increase or decrease the input power to the amplifier. The adjustable gain value is the independent variable of later plots that show the point of minimum EVM.

The use of an adjustable gain block was favored over setting a power from the simulated transmitter because differences in the distortion, root-cosine filter parameters, and modulation type make referencing a mean or peak power difficult. The data in the peak-to-average section can be used to determine the peak and average input powers to the amplifier for a specific modulation, rolloff factor, and adjustable gain block setting.

4.2.1.5 Signal Predistorter

The implemented predistorter is a polynomial sample gain predistorter. The predistorter operates on individual samples and multiples the complex result of the predistortion function by the input samples.

The predistortion function can be represented in a polar or rectangular form. The rectangular representation for the function was chosen since the samples are already rectuangular and will most likely be rectangular in an implementation. The rectangular

representation also eliminates the need for complicated polar to rectangular conversions. Both polynomial functions F_I and F_Q are a real function of the input signal power X_m. I_m and Q_m represent the inputs to the predistortion block, and I_p and Q_p represent the outputs of the predistortion block. The coefficients sets *a* and *b* are derived by the polynomial fitting block.

$$X_m = I_m^{\,2} + Q_m^{\,2} \qquad \text{(Eq. 4.1)}$$

$$F_I(X_m) = a_0 + a_1 X_m + a_2 X_m^{\,2} + a_3 X_m^{\,3} \ldots + a_n X_m^{\,n} \qquad \text{(Eq. 4.2)}$$

$$F_Q(X_m) = b_0 + b_1 X_m + b_2 X_m^{\,2} + b_3 X_m^{\,3} \ldots + b_n X_m^{\,n} \qquad \text{(Eq. 4.3)}$$

$$I_p = I_m F_I(X_m) - Q_m F_Q(X_m) \qquad \text{(Eq. 4.4)}$$

$$Q_p = I_m F_Q(X_m) + Q_m F_I(X_m) \qquad \text{(Eq. 4.5)}$$

4.2.1.6 Forward Table

The forward table is created by sending a QPSK, 16-QAM, 64-QAM, or 256-QAM signal through the non-linear distortion model and building a table of the inputs and the outputs of the non-linear amplifier model. The table entries are used by the polynomial fitting routine to determine the inverse of the amplifier characteristics for use in the predistorter. The number of entries in the table is determined by the number of samples in the adaptation sequence. Inputs to the non-linear amplifier model must reach to saturation to fully model the non-linear distortion. Driving the non-linear amplifier model to saturation before any predistorter coefficients are computed will result in distortion of the transmitted signal. In a real system, this only affects the initial adaptation as subsequent adaptations occur with valid coefficients in the predistorter. To aid this adaptation the initial sequence is sent with an adjustable gain block setting of 6 dB for a 16-QAM signal.

4.2.1.7 Least Squares Polynomial Fit

The least squares polynomial fit block uses entries stored in the forward table to generate polynomial coefficients for use in the predistorter. The desired predistorter characteristic is the inverse of the amplifier characteristic.

Several manipulations are made to the values in the forward table before a polynomial fit is performed. First, the data is limited to output powers of 0.0001 above zero and 0.0001 below saturation. Values near zero are removed from the table because small amounts of noise or precision error can create a large change in the measured phase shift. Values near the saturation point of 1 are removed because the table will contain multiple input powers that achieve saturation. The least squares fit will incorrectly attempt to fit to the mean of these points and the resulting curve will not fit well over the useful range.

Second, the values in the forward table were used to generate a secondary table. The amplifier characteristic is calculated by dividing the complex output samples by the complex input samples. The amplifier characteristic is then divided by the magnitude of the gain in a linear region. If this division is not performed, the predistorter removes the gain achieved by the amplifier. The reciprocal of this modified amplifier characteristic becomes the inverse of the amplifier characteristic. The secondary table then consists of the real amplifier output power and a complex multiplier that is the inverse of the amplifier characteristic. This complex multiplier is separated into real and imaginary parts.

Last, polynomial fitting is then done using the polyfit function in Matlab. This is function performs a least squares fit to the secondary table to an order n polynomial. This requires that the QR decomposition be calculated for the table. The function guarantees the minimum squared error between the table and the polynomial function for the specified order.

The resulting polynomial function F_I with the coefficients of $a_0, a_1, a_2,\ldots a_n$ has the amplifier output power as the input and the real portion of the complex inverse of the amplifier gain as the result. A second polynomial function F_Q with the coefficients of b_0,

$b_1, b_2, \ldots b_n$ also has the amplifier output power as the input and the imaginary part of the complex inverse of the amplifier gain as the result.

4.2.1.8 Non-Linear Distortion

The non-linear distortion is based upon the AM-AM and AM-PM distortion characteristics of the measured Agilent HMMC-5040 and HMMC-5033 combined amplifier. The simulation reads the characteristics from a data file saved by an HP network analyzer.

The gain of the measured amplifier was scaled so that 1 was the maximum output power and the amplifier presented unity gain while operating in the linear region. Several special cases were required to extend the model if the input was outside of the measured amplifier characteristics or was not an exact measured value.

If the input to the non-linear block is within the range of measured values then cubic interpolation is used to determine the output magnitude and phase distortion. The resulting response passes through every measured point and an interpolation is made if the input is between two measured points. This is in contrast to the polynomial fit used in the predistorter, which computes a 'best fit' for all data points and does not necessarily pass through the fitted points. The accuracy of cubic interpolation outside the measured points was found to be poor so, further cases were needed.

If the input to the non-linear distortion block is below the measured values, then the gain of the amplifier is linear with a gain equal to the gain at the lowest measured power. Scaling makes this gain unity for the reference amplifier. The phase shift is held equal to the phase shift at the lowest measured power. This is valid if the stored measurements extend into the linear region of the amplifier.

The output of the non-linear distortion is limited to the highest measured output power if the input to the non-linear model is above the highest measured value. The phase distortion is continued with a linear slope that is determined by the point at the highest power and 5% below the highest power. This is valid if the stored measurements extend into the saturation region of the amplifier.

4.2.2 Receiver

4.2.2.1 Noise Generator

The noise generator adds additive white Gaussian noise to the signal before it is received. In a real system, the signal at this point would be a real bandpass signal. Since the simulated signal is baseband, independent noise with half the power of the desired bandpass noise power is added to both the I and Q channels. The bandpass noise power when expressed in decibels is relative to the peak constellation power of 1 W.

4.2.2.2 Scaling and Rotation

This block is analogous to automatic gain control (AGC) and carrier synchronization in a real receiver. The input amplitude to the receiver varies as the adjustable gain block changes the input amplitude to the non-linear amplifier. The varying gain in the non-linear distortion also changes the amplitude at the receiver. The phase distortion in the non-linear distortion model can offset the phase of the constellation. In a real receiver, carrier synchronization will correct a constant phase offset of the constellation. Since the simulation is performed on a baseband signal, carrier synchronization is not needed, but a correction of a constant phase offset is still required.

To correct these problems, scaling and rotation are applied to the symbols at the output of the matched filter and before symbol decision. The average I and Q samples for a particular reference symbol are compared to the ideal values and used to correct each sample from the matched filter output. The reference symbol for every modulation type simulated was the upper right corner point. Multiplying the correction factor to the received symbols rotates and scales the received constellation until the mean of received symbols that should be interpreted as the chosen reference symbol are the same value as the transmitted reference signal.

The complex division of the reference ($I_{\text{ref}} + jQ_{\text{ref}}$) by the mean received signal ($\hat{I}_{\text{ref}} + j\hat{Q}_{\text{ref}}$) for the reference constellation point is used to provide the correction factor. The correction is then multiplied by all the received samples ($\hat{I} + j\hat{Q}$) to obtain scaled and rotated received signal.

$$\hat{I}_{\text{scaled}} + j\hat{Q}_{\text{scaled}} = (\hat{I} + j\hat{Q}) \cdot \frac{I_{\text{ref}} + jQ_{\text{ref}}}{\text{mean}(\hat{I}_{\text{ref}} + j\hat{Q}_{\text{ref}})} \qquad \text{(Eq. 4.6)}$$

Because the reference symbol for all modulations considered is the upper right symbol, non-linear distortions will be the most prominently seen in the constellation points near the zero power. As the simulated amplifier goes into compression, the inner constellation points will move toward the outer points. Similarly, the inner points will show the highest degree of phase distortion.

4.2.2.3 Root Raised Cosine Matched Filters

The two root raised cosine matched filters in the receiver are the second half of the desired raised cosine response. The same length and rolloff factor used in the transmitter pulse shaper is used here. The I and Q signals are separately filtered. Matrix multiplication is used compute the filter output at symbol times. This removes the oversampling and each output then corresponds to a complex mapping of a received symbol.

4.2.2.4 Symbol Decision

The symbol decision routine takes the input I and Q signals and scales the signal so ideal points are at integer values and then the round function is used to determine the closest signal point. The I and Q values are then converted to binary and then finally returned to an array of bits.

4.2.2.5 Error Vector Magnitude

The error vector magnitude (EVM) is used as a measure of signal quality. This measure of performance shows signal degradation before it shows up in bit error measurements. EVM is used because simulations with a high signal to noise ratio require large simulation times to acquire statistically significant BER measurements.

The error vector magnitude is calculated by computing the magnitude of the vector between the received signal ($\hat{I} + j\hat{Q}$) and the transmitted signal ($I + jQ$). The EVM is defined as the error vector voltage as percentage of the symbol with the highest voltage [33]. When expressed in decibels it is referenced to the peak power of 1 W.

$$EVM = \frac{\sqrt{(I-\hat{I})^2 + (Q-\hat{Q})^2}}{\sqrt{I_{peak}{}^2 + Q_{peak}{}^2}} \quad \text{(Eq. 4.7) [33]}$$

If the EVM is shown versus different adjustable gain block levels, the point where EVM is minimum is the optimum amplifier input level and will result in the best performance at the receiver.

4.2.2.6 Bit Error Rate

The bit error rate is calculated on the stream of bits by the following equation.

$$BER = \frac{N_{errors}}{N_{bits}} \quad \text{(Eq. 4.8)}$$

If no bit errors occur during a sequence, a significantly small bit error of 10^{-12} is used to allow plotting on a semi-log graph.

4.3 Simulation Results

4.3.1 Peak-to-Average Ratio

Cavers noticed in [7] that additional backoff was needed for similar performance when the rolloff factor was decreased to 0.2 but did not present a reason. This happens because the peak-to-average ratio increases with a reduction in the rolloff factor. This is a result of increased intersymbol interference (ISI) generated by the root-raised cosine filter. The peak-to-average ratio also increases when the modulation index is increased due to a reduction in the mean power.

The mean voltage of the output from the root raised cosine filter was found to vary only with modulation index. As the rolloff factor was varied from 0.15 to 0.5 the change in the mean between different rolloffs was found to be less than 0.05 dB and therefore insignificant. The mean power input to the adjustable gain block can be determined by the mean powers in the following table. The powers are relative to the peak power output of 1 from the constellation generator.

Table 4.1 Peak-to-Average Ratios for Different Modulations

Modulation	Mean Power Relative to Peak Input Power of 1	Mean Power Relative to QPSK	Peak-to-Average Ratio (r = 0.5)	Peak-to-Average Ratio (r = 0.15)
QPSK	-9.0330 dB	0 dB	3.3495 dB	6.3187 dB
16-QAM	-11.5867 dB	-2.5536 dB	5.9032 dB	8.8724 dB
64-QAM	-12.7123 dB	-3.6793 dB	7.0288 dB	9.9980 dB
256-QAM	-13.2643 dB	-4.2312 dB	7.5808 dB	10.5500 dB

The peak values were determined by filtering a sequence of symbols with the peak power in the constellation by the absolute value of the root cosine coefficients. This guaranteed the contribution from the adjacent points summed and the peak output of this filtering was considered the peak output voltage. The peak output voltage was found to be independent of the modulation index and remains almost constant until the rolloff factor is reduced to below 0.4. The peak output of the filter did not necessarily occur at the times when a symbol was aligned with the center of the filter. The following graph of the peak output power from the root-raised cosine filter is relative to the peak input power of 1 and can be used to determine the peak input power to the adjustable gain block.

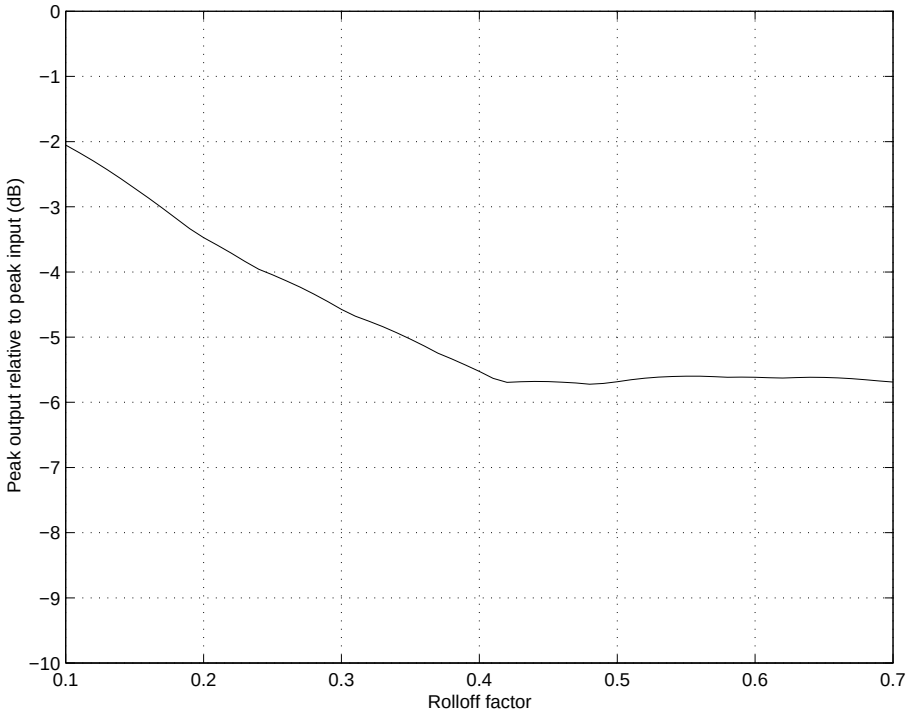

Figure 4.8 Peak Output Power Relative to Peak Input Power vs. Rolloff Factor for a Root-Cosine Filter

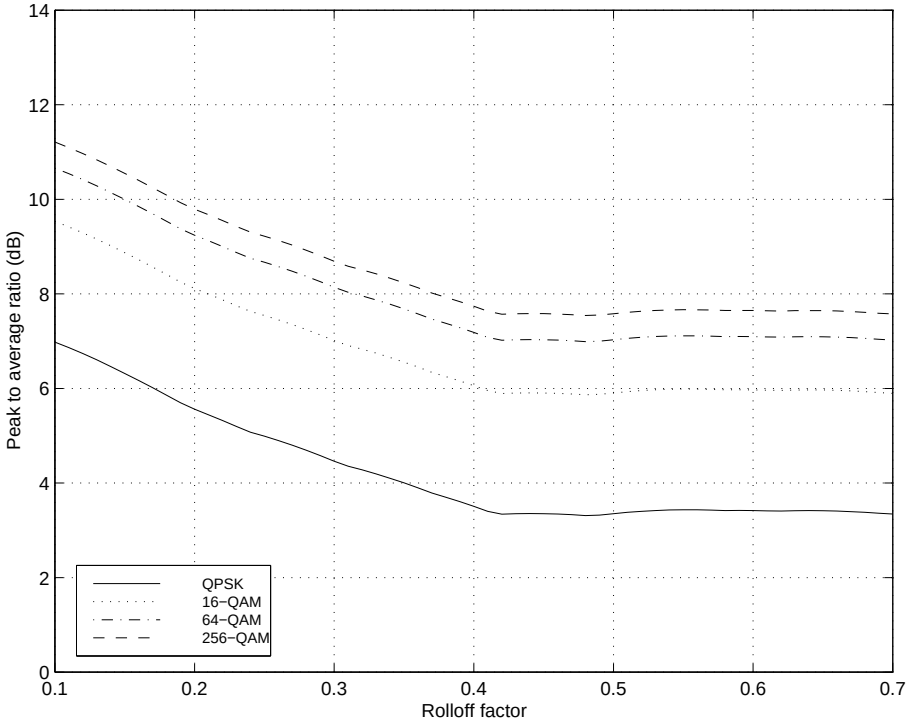

Figure 4.9 Peak-to-Average Power Ratio vs. Root-Cosine Filter Rolloff Factor

Determining the peak-to-average ratio becomes important in determining the average power output possible for a particular modulation and rolloff factor because the amplifier limits the peak amplifier output. Modulations with a higher peak-to-average ratio require further backoff of the input power to the amplifier.

4.3.2 Polynomial Order

A higher polynomial order should result in less error in the polynomial model at the expense of increased computational requirements. This part of the simulation compares the mean squared error to the polynomial order of polynomial function compared to the table that used to derive the function.

The simulations of polynomial order were conducted using 16-QAM training signal with a rolloff factor of 0.5. This generated a forward table size of 20511 entries. The comparison shows that there is no significant benefit gained by increasing the polynomial distorter beyond the eighth order. A table of typical coefficients for an eighth order polynomial fit is also included. The plots compare the eighth order polynomial model to the data stored in the forward table and confirm that the model and the actual response are practically equal.

Table 4.2: Model Error for Different Polynomial Order with Constant Table Size

Polynomial Order	Amplitude MSE	Phase MSE	Mean Squared Error Vector	Real Multiplier (F_I)MSE	Imaginary Multiplier (F_Q)MSE
1	5.6489e-003	4.0394e-004	8.2020e-003	1.6927e-003	6.5092e-003
2	1.0010e-003	1.0365e-004	1.5616e-003	2.9288e-004	1.2687e-003
3	1.5966e-004	1.3091e-005	2.4043e-004	5.9076e-005	1.8135e-004
4	3.1386e-005	2.8239e-007	4.1101e-005	1.5939e-005	2.5162e-005
5	1.0610e-005	3.0139e-007	1.4005e-005	4.3236e-006	9.6811e-006
6	4.8410e-006	1.7216e-007	5.9419e-006	1.5377e-006	4.4043e-006
7	3.5917e-006	1.9780e-007	4.3291e-006	8.1308e-007	3.5160e-006
8	3.3059e-006	1.1501e-007	3.8034e-006	7.7027e-007	3.0331e-006
9	3.2722e-006	1.1573e-007	3.7676e-006	7.5807e-007	3.0095e-006
10	3.2483e-006	1.1393e-007	3.7373e-006	7.5320e-007	2.9841e-006
11	3.2372e-006	1.1385e-007	3.7233e-006	7.4970e-007	2.9736e-006
12	3.2316e-006	1.1445e-007	3.7182e-006	7.4878e-007	2.9694e-006
13	3.2270e-006	1.0891e-007	3.7044e-006	7.4878e-007	2.9556e-006
14	3.2266e-006	1.0834e-007	3.7036e-006	7.4808e-007	2.9556e-006
15	3.2274e-006	1.0559e-007	3.7007e-006	7.4796e-007	2.9527e-006

Table 4.3 Typical Polynomial Coefficients for 8th Order Predistorter

N	a_n	b_n
8	-7.9325	35.3497
7	20.5590	-130.4295
6	-18.0843	200.0525
5	3.6378	-164.0795
4	3.4398	78.3969
3	-2.3786	-21.9845
2	0.4382	3.5822
1	-0.0118	-0.1259
0	-0.7499	0.6624

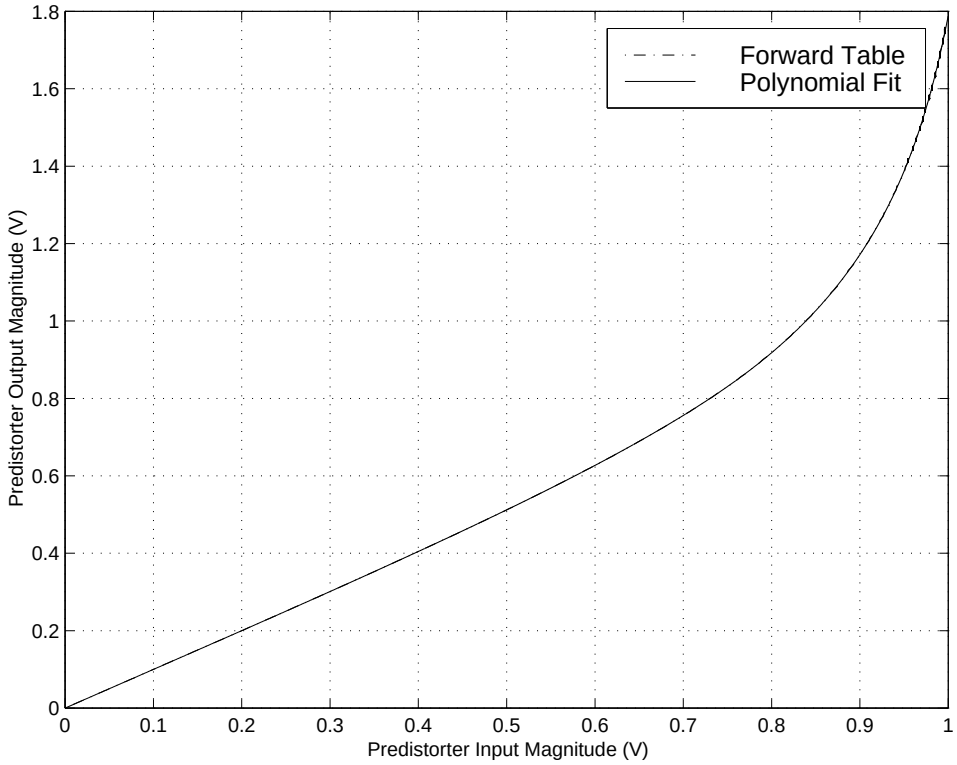

Figure 4.10 Predistorter Output Magnitude vs. Input Magnitude for 8th Order Polynomial

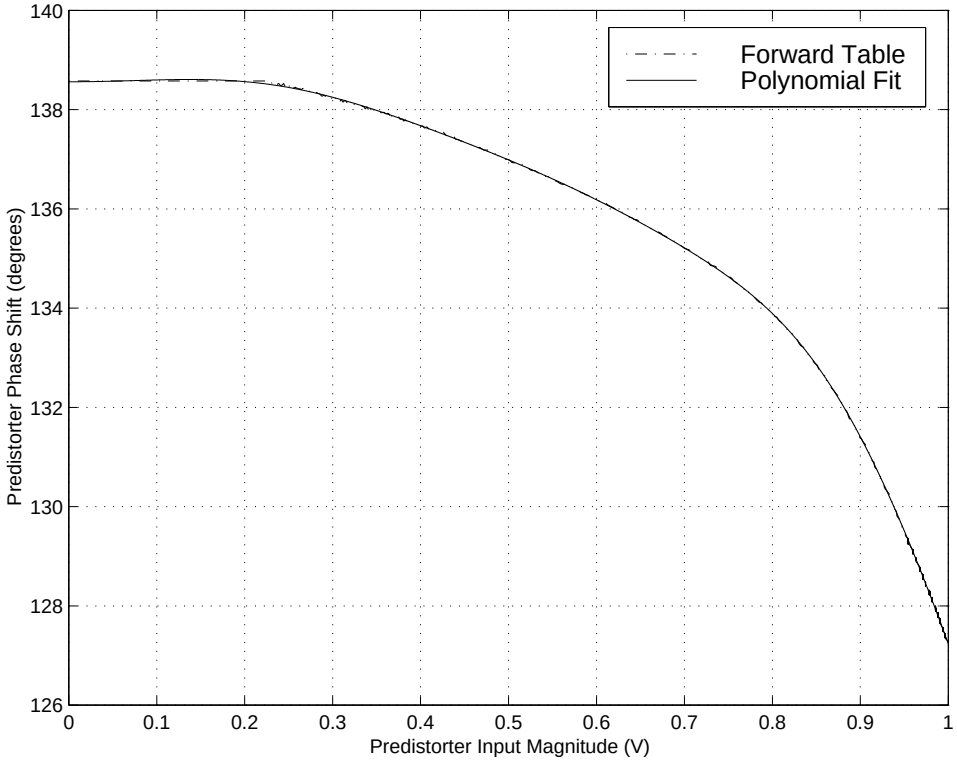

Figure 4.11 Predistorter Output Phase Shift vs. Input Magnitude for 8th Order Polynomial

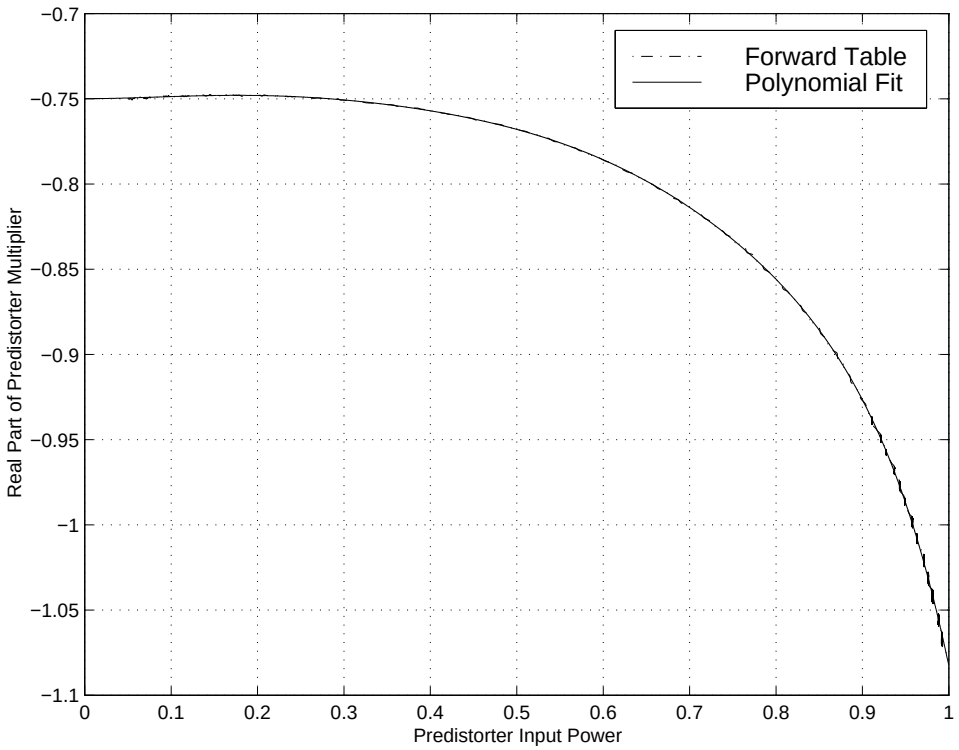

Figure 4.12 Real Part (F_1) of Predistorter Multiplier vs. Input Power for 8th Order Polynomial

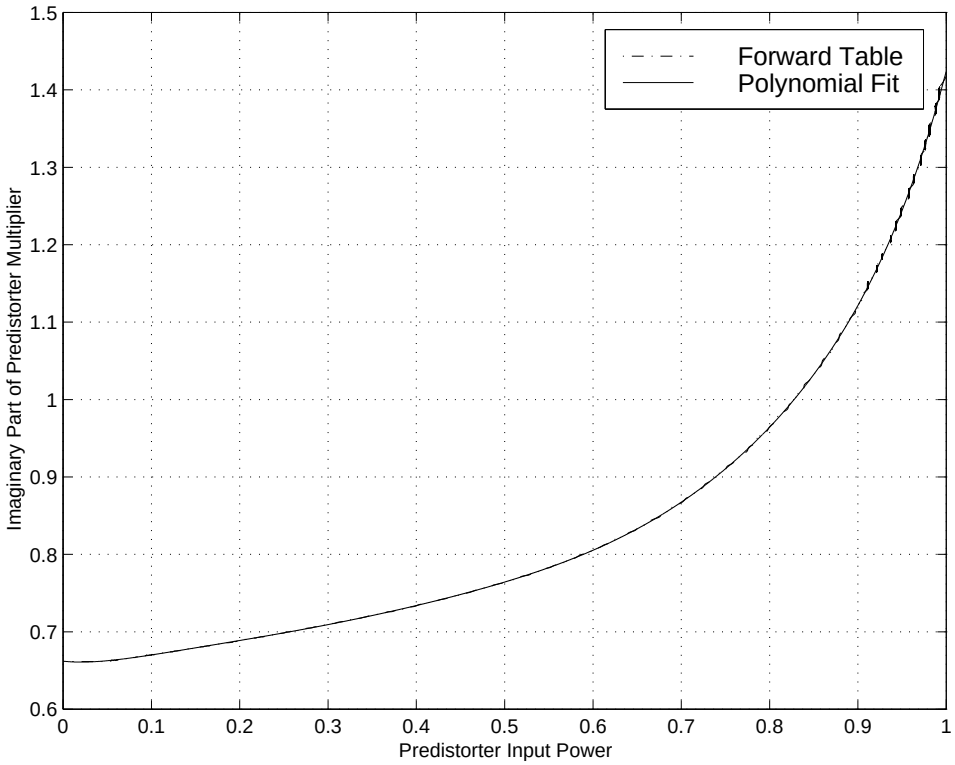

Figure 4.13 Imaginary Part (F_Q) of Predistorter Multiplier vs. Input Power for 8th Order Polynomial

4.3.3 Forward Table Size

The MSE for polynomials derived from a different number of table entries were compared to determine the effect of forward table size on the quality of the curve fit. It was found that there is no hard answer for the required size of the forward table. A good fit requires that the points are located throughout the range between zero power and saturation. Therefore, the number of forward table entries required is dependent on the distribution and the oversampling rate of the modulation. Simulations performed using 16-QAM to build a forward table showed no significant decrease in the MSE of the model after 200 entries in the forward table.

The size if the forward table required is also dependent upon the amount of noise present in the forward table entries. Increasing the size of the table decreases errors in fitting that might be caused by noise.

4.3.4 Dispersion Due to Filtering

The truncation of the root-cosine filter causes a slight dispersion of the constellation points even before the signal passes through the non-linear distortion. The following figures for a 16-QAM signal show that the non-linear distortion noticeably increases the dispersion in the noise-free signal. This is because the non-linear distortion occurs between the root-cosine filters. The memory in the filter spreads the distortion at peak powers across many samples. A data predistorter cannot correct this dispersion however the signal predistorter can reduce this dispersion. The figures were made with an oversampling rate of 8, a rolloff factor of 0.15, a delay of 12 symbols, and an adjustable gain block setting of 6 dB.

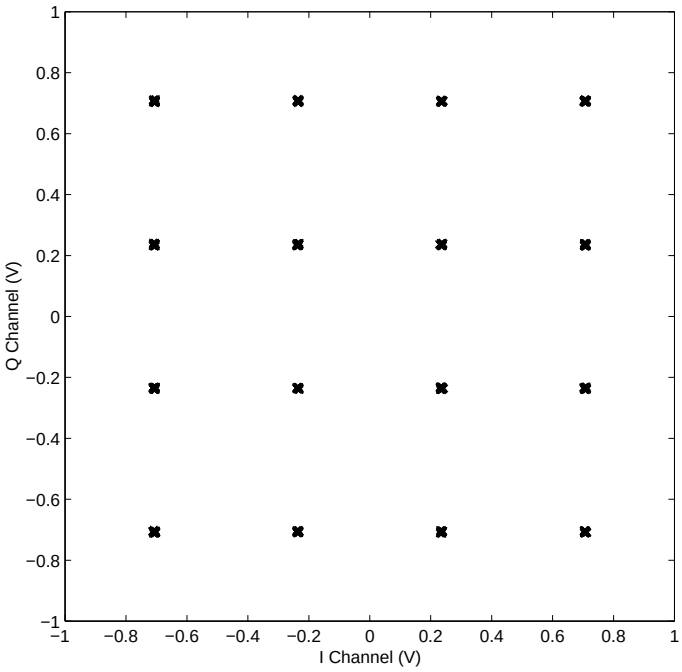

Figure 4.14 16-QAM Constellation before Non-Linear Distortion

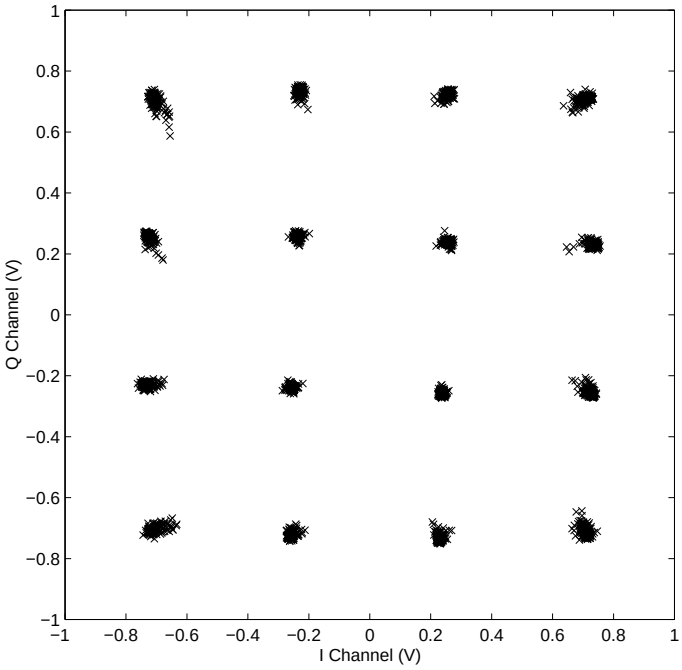

Figure 4.15 16-QAM Constellation after Non-Linear Distortion

4.3.5 Optimum Amplifier Input Power

The object of the EVM simulations was to determine the potential reduction in EVM possible with an implementation of predistortion. These simulations used the measured reference amplifier characteristics for the non-linear distortion.

The optimum amplifier input power is the value that results in the minimum EVM at the receiver. Increasing the amplifier drive level decreases the noise on the received signal but increases the distortion caused by the non-linear distortions present in the amplifier.

The graphs of EVM vs. amplifier input power show three distinct effects. They are the reduction in EVM as transmitter power as increased, a fixed EVM once amplifier distortion becomes dominant, and a EVM floor from other implementation distortions such as truncation of the root raised cosine effect or quantization.

At low input powers, the error vector magnitude of the signal shows improvement as input power to the amplifier is increased. As the input power to the amplifier is increased further, any decrease in the EVM due to an increase in signal power becomes less than the increase in amplifier distortion. This is point of minimum error vector magnitude and any additional increase in the amplifier drive level results in an increase in the EVM.

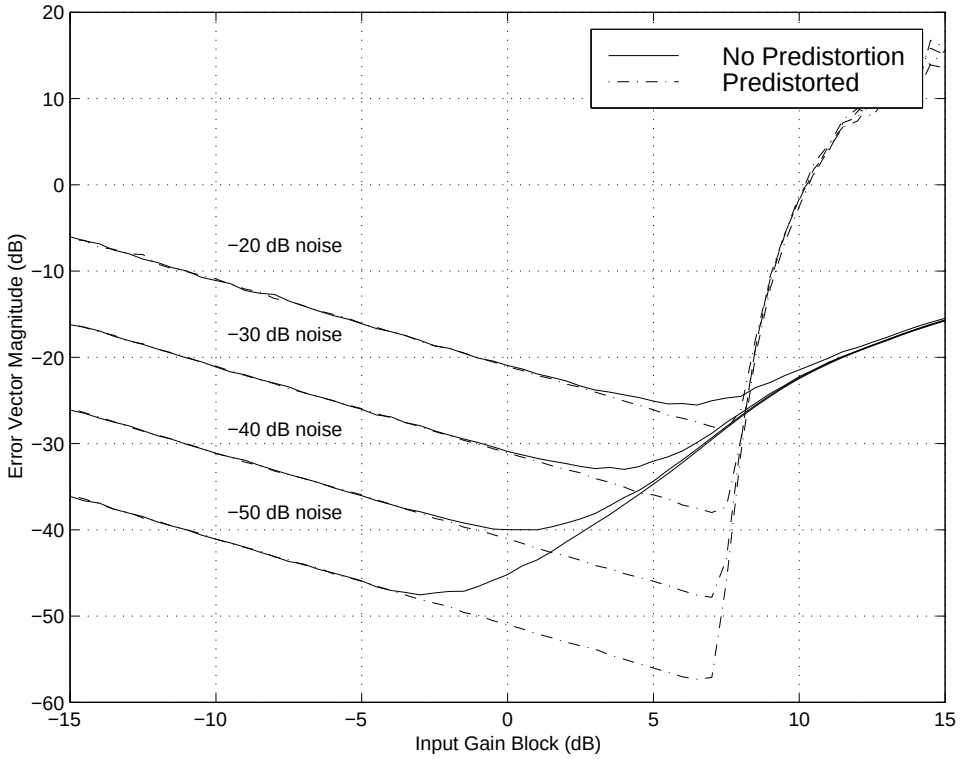

Figure 4.16 EVM for 16-QAM with and without Predistortion for Various Constant Noise Levels

The plot above is for 16-QAM with a rolloff factor of 0.5 and a raised cosine filter delay of 12 symbols. The minimum EVM point is the optimum amplifier input level and will result in the best performance at the receiver. The noise power is referenced to the peak constellation power of 1. The gain from predistortion or the reduction in the minimum EVM is 2.9 dB, 5.0 dB, 7.8 dB, and 9.8 dB for constant noise powers of -20 dB, -30 dB, -40 dB, and -50 dB respectively.

The plots of EVM show that without predistortion optimum amplifier drive level changes with the SNR at the receiver. This is because as the EVM due to noise decreases the total EVM can not decrease lower than the EVM due to the non-linear distortion.

The error vector magnitude due to noise is dependent upon the noise power and input level. The EVM due to amplifier distortion is independent of the noise power and only dependent upon the drive level.

Without predistortion or power control the wireless link should not be optimized for the minimum EVM during clear weather conditions. The link should be optimized for the minimum EVM with a SNR measured at the receiver that is just above the desired minimum performance.

The potential gain from predistortion decreases as the constant noise power decreases if the amplifier input is readjusted for optimum EVM. This is actually the gain of predistortion over continuously varying the amplifier input power to achieve the minimum EVM. If the amplifier input level remains constant, the true gain from the implementation of predistortion remains constant as the link experiences fading. The implementation of predistortion significantly reduces the need for varying the amplifier input power continuously because the point of minimum EVM does not move significantly as the SNR is decreased.

4.3.6 Adjacent Channel Power Ratio

The power spectral densities of the ideal, distorted, predistorted after amplification, and amplified without predistortion waveforms were computed for two drive levels. The simulated power spectral density plot has a symbol rate of 10 Msymbols/second, an oversampling rate of 8, and a sample rate of 80 Msamples/second.

The ACPR of the predistorted signal is slightly less than the ACPR of the amplified signal without predistortion (IQ_a). This difference increases with a reduction in the backoff.

The predistorted signal has only a slightly lower ACPR than the original signal (IQ_m). This confirms that this predistortion method is able to correct much of the out-of-band interference caused by non-linear amplification and that errors in the polynomial modeling were not severe enough to degrade the ACPR. The limiting factors to minimizing out-of-band interference will be quantization and oversampling.

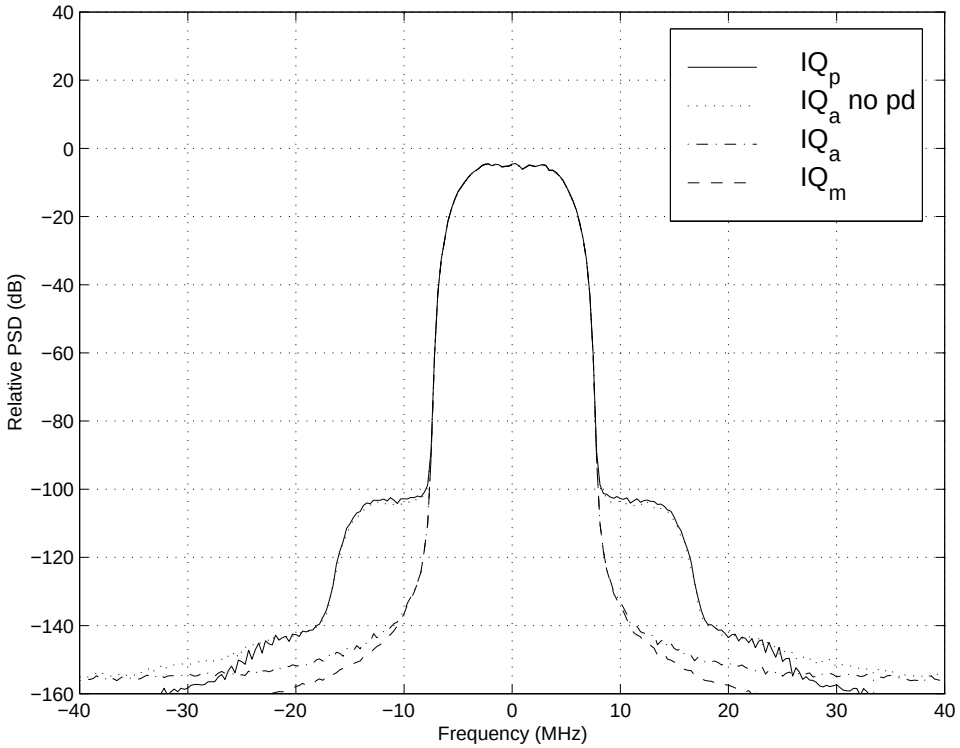

Figure 4.17 Power Spectral Density Plot with Adjustable Gain Block = 0 dB

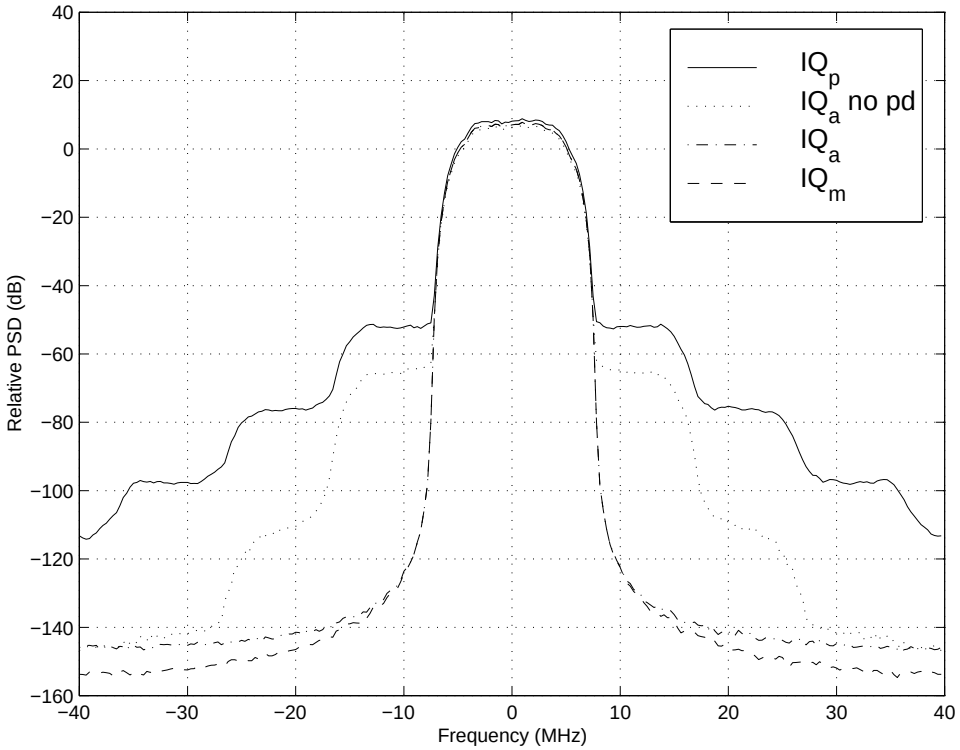

Figure 4.18 Power Spectral Density Plot with Adjustable Gain Block = 6 dB

4.3.7 Computation Complexity

The adaptation computation complexity is a function of both the polynomial order of the model and the number of entries in the forward table. The number of floating point operations was counted by using the `flops` function in Matlab. The counted number of FLOPS is for the two polynomial fits required for adaptation.

Table 4.4 Computational Complexity for Varying Polynomial Order and Varying Forward Table Size

Polynomial Order	FLOPS for 300 entries	FLOPS for 600 entries	FLOPS for 1200 entries	FLOPS for 2400 entries
4	104344	209344	417244	838294
5	142804	286682	569180	1138956
6	184904	374582	747678	1495748
7	237398	473216	949616	1896064
8	293228	586846	1172118	2341680

4.3.8 Maladjusted Predistorter

This part of the simulation uses the measurements of several different amplifier variations from the previous chapter to determine the decrease in performance caused by a predistorter that is adapted to the reference amplifier characteristics.

The simulated amplifier characteristic remained the reference characteristic (Measurement #12) while the predistorter was adapted to one of the measured variations from the previous chapter (Measurements #131, 132, 14, 15, and 17). This results in a non-ideal predistortion characteristic and a change in the EVM curve.

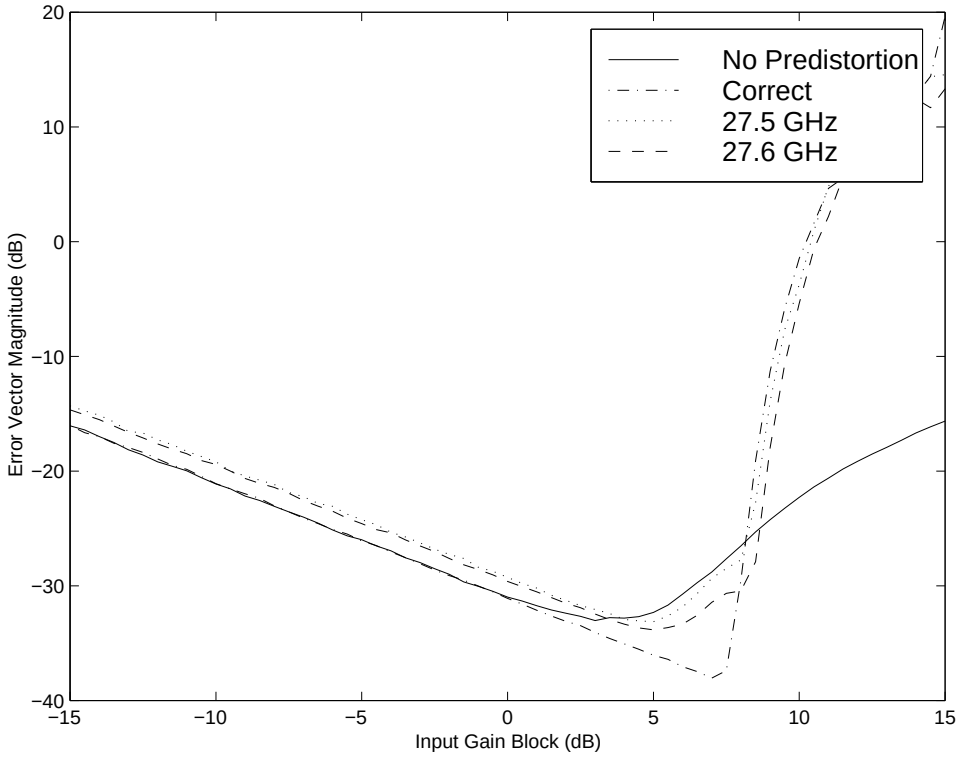

Figure 4.19 Maladjusted Predistorter for Different Frequencies

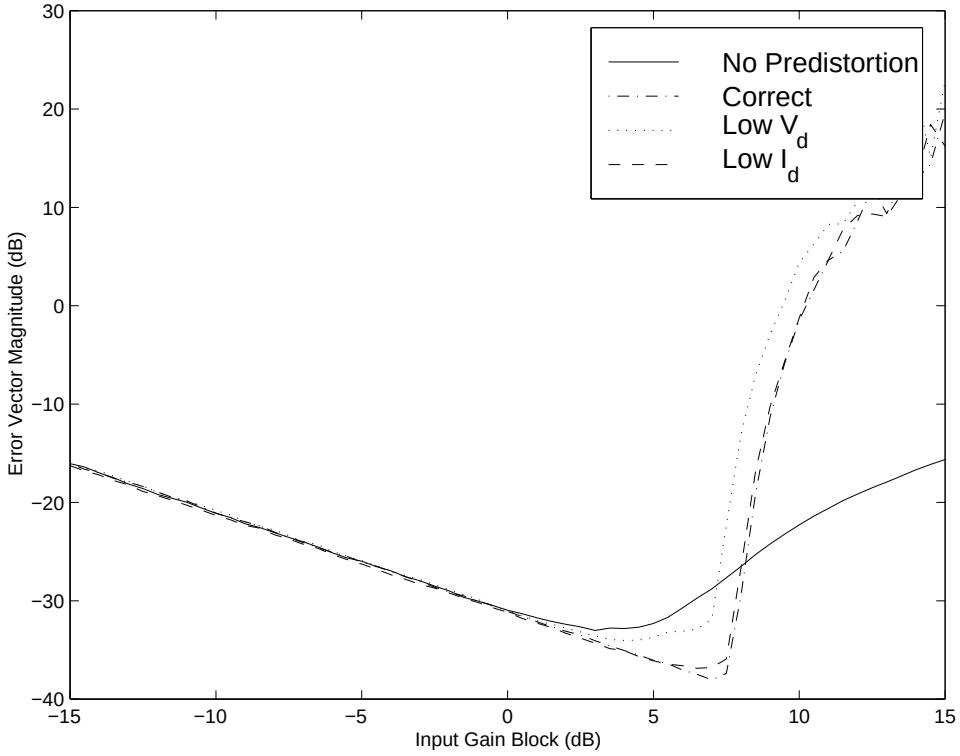

Figure 4.20 Maladjusted Predistorter for Different Bias

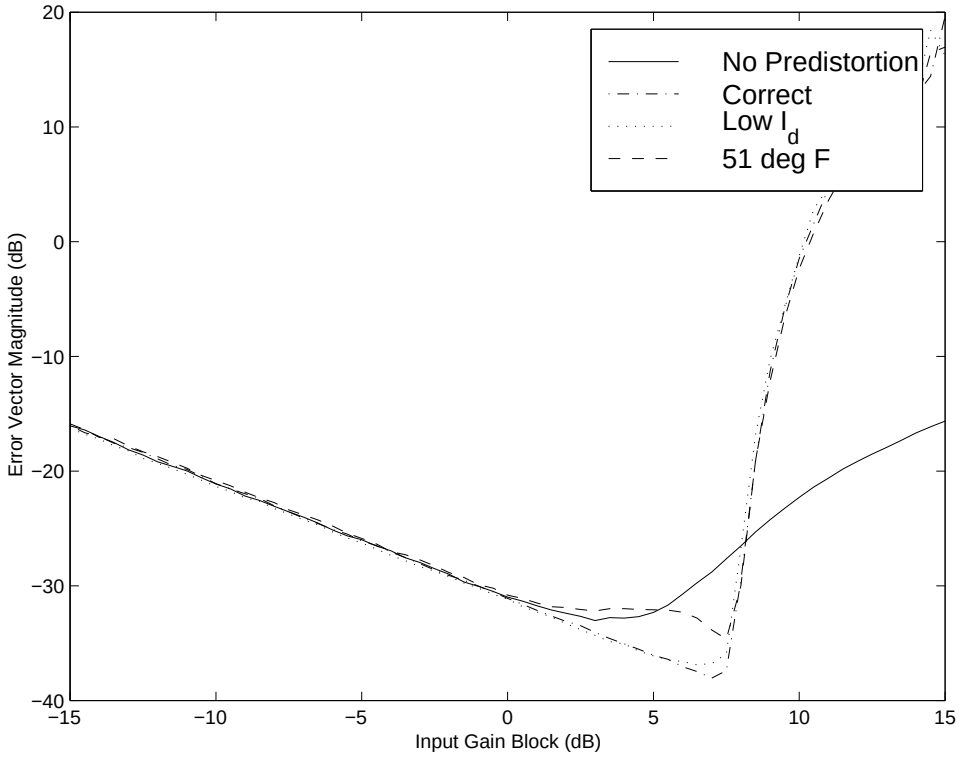

Figure 4.21 Maladjusted Predistorter for Different Temperature

The measurement variations are extreme compared to the computational complexity of the adaptation algorithm. The 10% variations in voltage, 10% variation in current, and the 50°F drop in temperature are all unlikely to occur between adaptations.

Adaptation will be necessary any time the frequency is changed. Temperature is a significant variable in the amplifier characteristics. Variations in temperature can cause a variation in bias and variations in the amplifier characteristics. The variation in current degraded the performance the least.

Chapter 5. Applications to LMDS

5.1 Proposed Multi-stage Implementation for LMDS

The proposed predistortion architecture for LMDS blends simple high-speed digital logic and a digital signal processor. A floating point DSP performs complex operations, such as LMS polynomial curve fitting. DSP speed determines the fastest adaptation rate because the architecture is multi-stage and adaptations occur in blocks. A custom integrated circuit or a FPGA performs the polynomial gain predistortion and generates the forward table. The samples stored in the forward table at the start of adaptation are used to generate polynomial coefficients that are used until the completion of the next adaptation. The results from the previous chapters are used to support suggestions on specifications of the predistortion implementation.

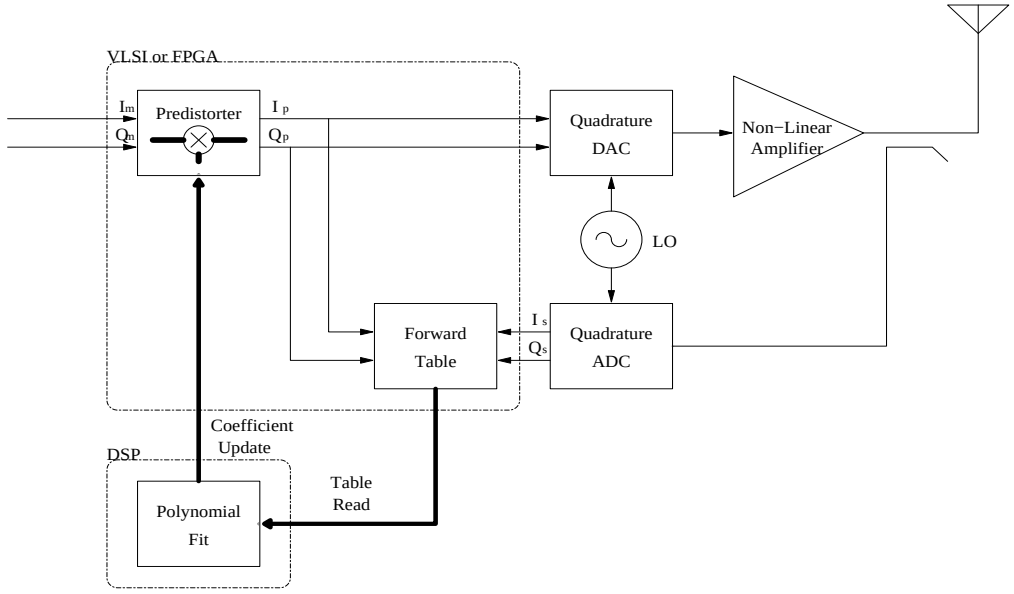

Figure 5.1 Proposed Multi-stage Predistortion System for LMDS

The multi-stage variation was presented in [19] as a method to speed up adaptation. This variation separates the adaptation rate and the symbol rate by adapting the predistorter to a forward model rather than minimizing the error between the input to the predistorter. When the analog delay of waiting for another sample going through digital-to-analog

conversion, upconversion, amplification, downconversion, and analog-to-digital conversion is eliminated, the adaptation speed is limited only by computation speed. This separation can also be used for adaptation in systems where the sample time is less than the computation time required for each sample. This separation also allows a typical digital signal processor along with simple high-speed logic to be used to perform Msymbol/second predistortion.

5.1.1 Quadrature Downconversion

Adaptive predistortion requires a feedback path. Predistortion can be preformed without adaptation, but the simulated error vector magnitude of a maladjusted predistorter shows that adaptation is necessary if predistortion is to achieve its potential benefits.

Multiple frequency conversions are likely necessary to convert a sample of the 28 GHz amplifier output to a digital baseband signal. This makes the downconversion one of the costliest parts of an implementation of adaptive digital predistortion in a LMDS system. Using the same local oscillators as for upconversion to 28 GHz eliminates the need for carrier synchronization in the feedback path. Time division duplex (TDD) systems have a potential advantage because the receiver components are idle while transmitting and could be used to sample the amplifier output.

The delay between the output of the predistorter and the corresponding sample from the power amplifier must be adjusted within $1/64^{th}$ of a symbol period [14]. Since the oversampling rate of 8 only allows adjustment within $1/8^{th}$ of a symbol period and oversampling by 64 is not feasible, another method must be used to keep the error in the delay minimized. The sampling clock of the analog-to-digital conversion of the amplifier output must be delayed by a fraction of the sampling period to be able to adjust within $1/64^{th}$ of a symbol period.

All predistortion implementations are sensitive to imperfections in the sampling of the amplifier output. Utilizing a digital downconversion chip for the final downconversion to baseband can minimize potential phase and magnitude errors. Digital downconversion and upconversion chips are available from a several sources such as Intersil, Graychip, and Analog Devices.

5.1.2 Forward Table

The forward table consists of memory and controlling logic that stores a number of previous digital samples from the output of the predistorter and the output of the amplifier in RAM. The forward table can be implemented with dedicated logic and limited RAM. The logic is suitable for implementation on a custom chip or with a field programmable gate array (FPGA). A forward table of *n* entries contains the previous *n* samples of both signals.

Previous simulations found that forward tables larger than 300 entries did not significantly reduce the mean squared error of the model. However, additional entries could be added to reduce sensitivity to noise. A table size of 2400 entries is used for evaluating computational complexity. Additional memory is required in the forward table to delay the samples from output of the predistorter because the analog group delay of the amplifier is longer than one symbol time.

Table indexing is not an issue since the previous samples are stored. The table of previous samples is also necessary to verify the correct delay between the predistorted samples and the samples of the amplifier output. This delay determination is necessary so that the appropriate predistorter output sample is stored with the appropriate amplifier output sample.

5.1.3 Digital Signal Processor

The digital signal processor's primary task is to convert the information stored in the forward table RAM into the correct polynomial predistorter coefficients to cancel the non-linear effects of the amplifier. An additional task of the DSP is to determine the delay between the digital sample at the output of the predistorter and the digital sample of the amplifier output. After calculating the polynomial coefficients the DSP loads the polynomial coefficients in the polynomial gain predistorter. These coefficients are used until the end of the next adaptation.

The digital signal processor reads the previous samples from the forward table memory and uses them to generate a second table called the predistorter table. The predistorter table contains the complex predistorter multiplier as a function of the input power to the

predistorter block. The values in the predistorter table are obtained by dividing the predistorter output values in the forward table by the amplifier output values in the forward table. This inverse of the amplifier gain is then multiplied by the amplifier gain in a low power linear region to prevent the predistorter from canceling the amplifier gain. The result of these operations is a table of complex multipliers that will correct the measured non-linear distortions in the amplifier. These multipliers are indexed in the predistorter table by the linear gain divided powers of the amplifier output values in the forward table.

A least squares fitting routine is then used to model the predistorter table as a polynomial equation. The least square fit used in the simulation requires a floating point processor to obtain the polynomial coefficients. The number of floating point operations (FLOPs) was estimated in the simulation chapter. Even the worst case of adapting an eighth order polynomial with 2400 forward table entries requires 2,341,680 floating point operations. Under the assumption that the digital signal processor can compute 40 million floating point operations per second (FLOPS), the time required to obtain a polynomial approximation of the table is 0.059 seconds or about $1/17^{th}$ of a second. This delay corresponds to 585,420 symbols in the reference system of 10 Msymbols/second. A few additional operations per table entry are required but are insignificant to the number of operations required to obtain the polynomial coefficients.

The forward table must be filled before the coefficients can be computed. Assuming a forward table of 2400 entries and a symbol rate of 10 Msymbols/second, the forward table can be filled in 240 microseconds. This delay is insignificant compared to the 0.059 seconds that is required to adapt or obtain the coefficients.

The DSP also compares the both sets of samples in the forward table to generate adjustments to the sample clock phase of the amplifier output analog-to-digital converter. This is used to fine adjust the delay between the amplifier output and the predistorter input within the required $1/64^{th}$ of a symbol. Comparing the sign of the slope of both the predistorter output and amplifier output signals is a method that could be used to determine if the delay between the two inputs to the forward table are correct. If the

signs of the slope do not match then the delay would be adjusted in the appropriate direction.

5.1.4 Polynomial Gain Predistorter

The proposed polynomial gain predistorter consists of two parts. The first part implements a complex polynomial as a function of predistorter input power and the second part is a complex multiplier. The polynomial gain predistorter can easily be implemented in either a custom IC or a FPGA since the predistorter design contains only multipliers and adders.

For an *n* order polynomial predistorter there are $2n+6$ real multiplications and $2n+3$ real additions performed for each input sample. The proposed 8^{th} order polynomial predistorter requires 22 multiplications and 19 additions for each sample. This includes conversion of the I and Q voltages samples to a power that requires 2 multiplications and an addition. The complex multiplication of the predistortion vector with in incoming I and Q samples requires 4 multiplications and 2 additions. For the example system with a rate of 10 Msymbols/second with 8X oversampling for a total of 80 Msamples/second, the computational requirement would be 3.28 GFLOPS (billion floating operations per second). The computational needs of this predistorter are quite large when considering implementation in a DSP but the simplicity of the calculations makes a custom IC or FPGA implementation the best solution for the predistorter.

The structures of the multiplier and the polynomial function are shown in the figure 5.2 and figure 5.3. The notation used is the same as used when the signal predistorter is described in the simulation chapter. I and Q are used to represent the real and imaginary parts of a complex signal respectively. The subscript *m* represents the input to the predistorter or the output from the constellation mapper, F_I and F_Q are the real and imaginary outputs of the polynomial function, the subscript *p* represents the predistorted signal, *a* and *b* are the real and imaginary coefficients respectively, and X_m represents the power of the signal input to the predistorter.

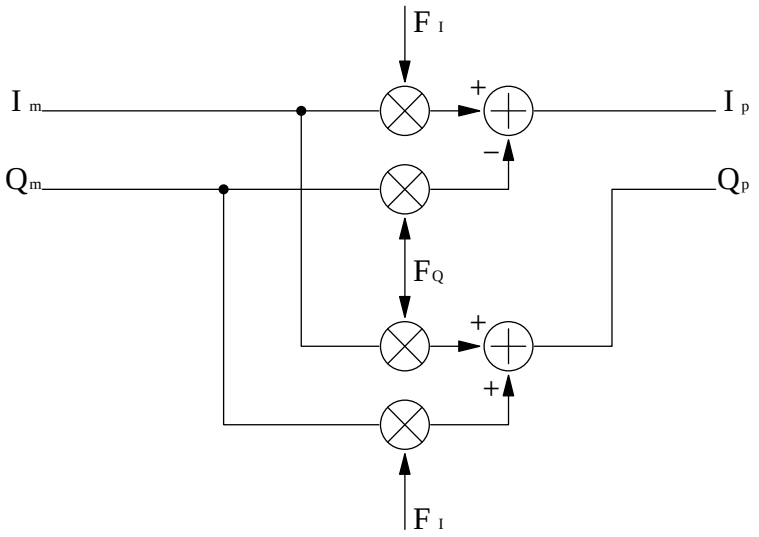

Figure 5.2 Multiplier Portion of the Gain Predistorter Implementation [34]

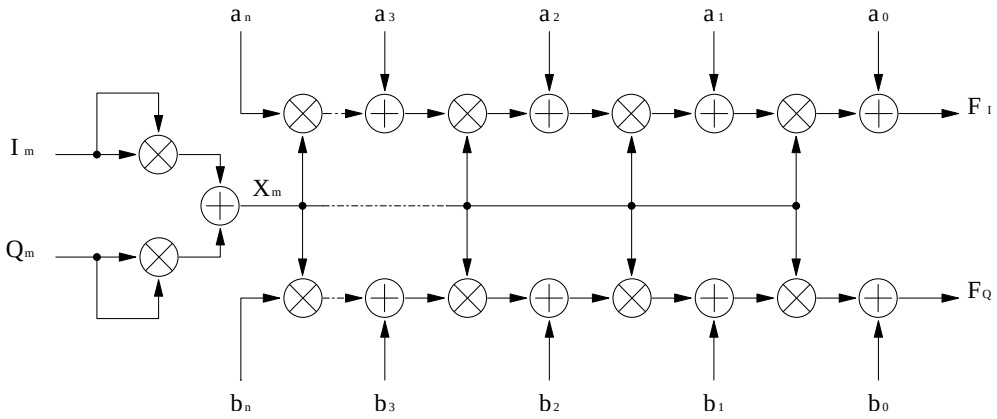

Figure 5.3 Nested Polynomial Implementation [34]

The choice to model the predistortion as real (I) and imaginary (Q) parts and as a function of power rather than amplitude was made to simplify the implementation. When the predistortion is modeled with I and Q signals, the need for polar-to-rectangular or

rectangular-to-polar conversions is eliminated. The use of power rather than amplitude as an input to the function eliminates the need for a square root.

5.1.5 Required Adaptation Rate

The amplifier measurements, simulation of a maladjusted predistorter, and an estimation of the time required to compute polynomial coefficients can be used to determine the feasibility of the proposed adaptive digital predistortion. The changes in the amplifier characteristics for the variations were slight, but the degradation in EVM during the amplifier variations was greater than expected. Daily adaptations to account for amplifier aging are not sufficient and more frequent adaptations than were expected are necessary. Repeated measurements under the same conditions and performed within several minutes yielded similar results. It is therefore reasonable to assume that amplifier characteristics will remain relatively static over the estimated 0.059 seconds required to compute the polynomial coefficients. The measurement variations of 10% decreases in bias voltage, 10% decreases in bias current, and 40°F drops in temperature are unlikely to occur within a few seconds. The reasonable times to achieve these changes are significantly longer than the estimated adaptation time of 0.059 seconds. Therefore, this adaptation rate is sufficient and predistortion by this method is feasible.

5.2 Implications of Predistortion for LMDS

LMDS is typically a bi-directional service. Therefore, different reliabilities or different link margins for the downstream and upstream links have no advantage. Adding predistortion to the base station only could be used to increase the downstream data rate while maintaining similar reliabilities for the downstream and upstream links. The downstream data rate could be increased by an increase in the number of modulation levels or change in forward error correction if used. Addition of predistortion to just the base station transmitter might be useful in cost sensitive applications of predistortion. All subscribers using that particular base station transmitter can benefit from predistortion without the additional cost of predistortion at each subscriber. A higher downstream data rate also better fits the demands of most subscribers.

If predistortion is added to both the base station and subscriber transmitters then the system designer is given more flexibility. The gain from predistortion, like any effective increase in transmitter power, can be used to increase antenna beamwidth, increase link margin, increase maximum distance, increase the data rate for both upstream and downstream links, or any combination.

The following analysis determines the potential impact of a 5 dB or 10 dB increase in the effective transmitter power of a LMDS transmitter. This analysis is valid for any effective increase in the transmitter power from any enhancement and is not limited to predistortion.

The 10 dB increase in link margin allows an increase in the modulation index to the next standard square level. The increase in data rate varies depending on the previous modulation index. If the previous modulation were QPSK the 10 dB increase would allow 16-QAM, which has twice the data rate for the same symbol rate, to show similar performance. If the previous modulation were 16-QAM the 10 dB increase would allow a 64-QAM signal to show similar performance with 1.5 times the data rate of the 16-QAM signal.

The increase in the maximum link distance is rather insignificant at short link distances. The gains are more significant when considering lower reliability links, especially when comparing the amount of outage minutes per year. An increase in effective power can be used to increase the antenna beamwidth proportionally in a single dimension. This may be desirable to reduce the number of transmitters used to cover a given area.

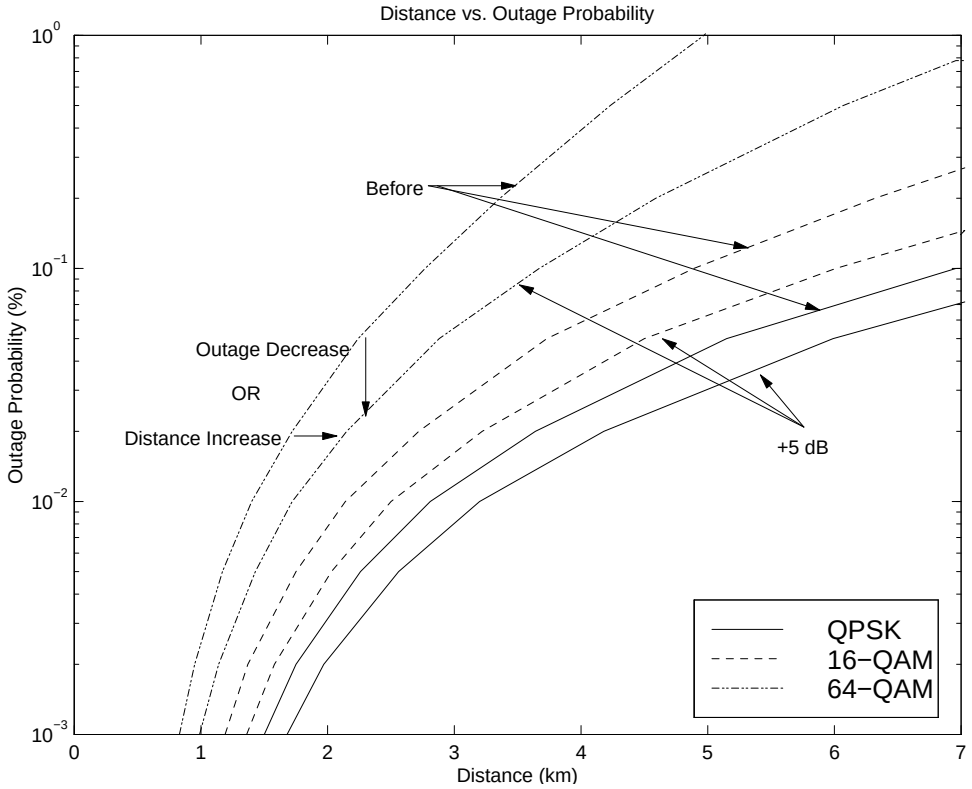

Figure 5.4 Distance vs. Outage Probability for a 5 dB Increase in Transmitter Power

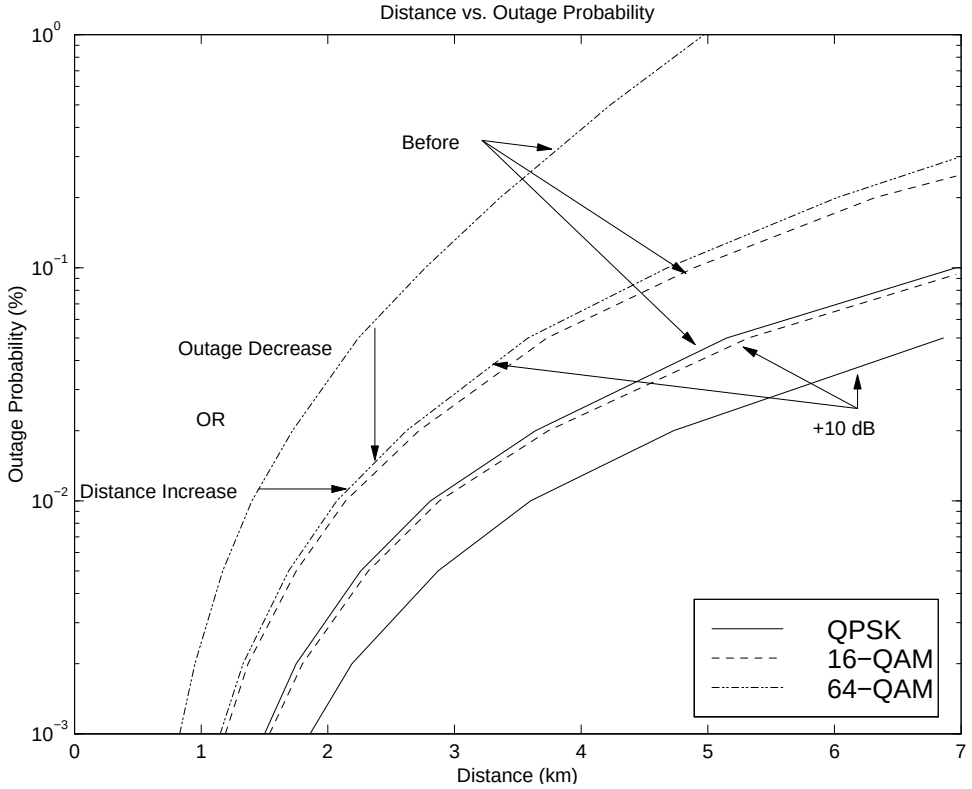

Figure 5.5 Distance vs. Outage Probability for a 10 dB Increase in Transmitter Power

The implementation of predistortion in a LMDS system has other benefits. The addition of adaptive digital predistortion can also be used to identify transmitter degradations before total failure. The forward table or the predistorter coefficients could be downloaded and compared with previous values to detect changes in the power amplifier. These transmitter diagnostics are especially important in point-to-point links where it may be difficult to identify if a link failure is due to a transmitter or the far receiver.

The typical gain for predistortion was defined as the gain between the optimum EVM with predistortion and the optimum EVM without predistortion. The assumption was made that the case without predistortion could be optimized. However the location of the optimum point in unknown to a system without predistortion or EVM feedback from the far receiver. The amplifier input power could be adjusted during the installation but it is likely to require some additional backoff to prevent changing amplifier characteristics or changes in the amplifier input power from degrading the EVM.

5.3 Conclusions

This thesis presented a possible method for adaptive digital predistortion in LMDS systems. Laboratory network analyzer measurements of a 28 GHz amplifier and simulation of a digital communication system was presented to support the feasibility of implementing predistortion in an LMDS system. An emphasis was placed on designing a practical implementation. Predistortion at Msymbol/second rates was found to be feasible by placing complicated adaptation algorithms in a digital signal processor, performing simple high speed tasks with a custom IC or a FPGA, and using a multi-stage predistortion architecture.

Adaptation to changes in the amplifier characteristics is required. The simulation showed that even small changes in amplifier characteristics could nullify the in-band benefits of predistortion.

The implementation of predistortion can increase the effective power of the transmitter by as much as 10 dB. The actual increase is dependent upon level of the non-linear distortion as compared to other distortions such as quantization, noise at the receiver, and the peak-to-average ratio of the signal.

5.3.1 Future Work

The simulated amplifier model was assumed to be mostly memoryless. Two network analyzers would be required to confirm that the amplifier time constants were negligible at frequencies less than the simulated symbol rate. Further work might confirm that this amplifier is memoryless at the modulation rates considered and determine its maximum bandwidth. In addition, the effects of synchronization and equalization in the receiver were not considered during the simulations.

A consideration of the many optimization techniques to estimate the polynomial coefficients from a table of data points is beyond the scope of this work. Other methods might be available that are more appropriate for fixed-point DSPs, are more efficient, or make better use of the parallel architectures of modern DSPs.

Additional insight to implementation challenges could be gained from an actual adaptive digital predistorter implementation. Several imperfections in the system such as quantization, amplitude and phase errors in the quadrature conversions, and error in delay estimation were not considered because these would be dependent upon implementation particulars.

The measurements and simulations show that the non-linear distortion of the amplifier cannot be ignored even in Class A amplifiers. The use of predistortion with Class AB amplifier would enable the use of higher power amplifiers. Predistortion for an OFDM system was not considered here but is of considerable interest because of the higher peak-to-average power ratios of OFDM signals.

References

[1] Harris Corporation, Clearburst Specifications, 2000. Available: http://www.microwave.harris.com/broadband/pdf/169e.pdf.

[2] T. S. Rappaport, *Wireless communications: Principles and Practice*, Prentice Hall, 1996.

[3] L.J. Ippolito et al., *Propagation effects handbook for satellite systems design; a summary of propagation impairments on 10 to 100 GHz satellite links with techniques for system design*, NASA reference publication 1082(03), NASA 1983.

[4] W. Stutzman and *Antenna theory and design*, 2nd ed., Wiley, 1998.

[5] A.S. Sedra and K.C. Smith, *Microelectronic circuits*, Holt, Rinehart, and Winston, 3rd Edition, 1989.

[6] Cheng-Po Liang, Je-Hong Jong, W.E. Stark, J.R.East "Nonlinear amplifier effects in communications systems," *IEEE Transactions on Microwave Theory & Techniques*, vol.47, no.8, Aug. 1999, pp.1461-6.

[7] J.K. Cavers. "The effect of data modulation format on intermodulation power in nonlinear amplifiers," *VTC 1994. 'Creating Tomorrow's Mobile Systems'*, 1994 IEEE 44th Vehicular Technology Conference, Part vol.1, 1994, pp.489-93 vol.1.

[8] W.A. Davis, *Radio & Microwave Engineering*, Class Notes for EE 4605, Virginia Tech, Fall 1998.

[9] H.L. Krauss, C.W. Bostian and F.H. Raab, *Solid State Radio Engineering*, John Wiley and Sons, 1980.

[10] S. Andreoli, H.G. McClure, P. Banelli, S. Cacopardi, "Digital linearizer for RF amplifiers," *IEEE Transactions on Broadcasting*, vol.43, no.1, March 1997, pp.12-19.

[11] A. Lohtia, P.A. Goud, C.G. Englefield, "Power amplifier linearization using cubic spline interpolation," *1993 43rd IEEE Vehicular Technology Conference. Personal Communication -Freedom Through Wireless Technology*, IEEE, 1993, pp.676-9.

[12] W. Bosch and G. Gatti, "Measurement and simulation of memory effects in predistortion linearizers," *IEEE Transactions on Microwave Theory & Techniques*, vol.37, no.12, Dec. 1989, pp.1885-90.

[13] K.G. Gard, H.M. Gutierrez, M.B. Steer. "Characterization of spectral regrowth in microwave amplifiers based on the nonlinear transformation of a complex Gaussian process," *IEEE Transactions on Microwave Theory & Techniques*, vol.47, no.7, pt.1, July 1999, pp.1059-69.

[14] Y. Nagata, "Linear amplification technique for digital mobile communications," *39th IEEE Vehicular Technology Conference*, IEEE. 1989, pp.159-64 vol.1.

[15] B. Sklar, *Digital Communications: Fundamentals and Applications*, Prentice Hall, 1987.

[16] C. Haskins, *Diode Predistortion Linearization for Power Amplifier RFICs in Digital Radios*, Thesis, Virginia Polytechnic Institute and State University, 2000. Available: http://etd.vt.edu.

[17] D.J. Jennings and J.P. McGeehan, "A high-efficiency RF transmitter using VCO-derived synthesis: CALLUM," *IEEE Transactions on Microwave Theory & Techniques*, vol.47, no.6, pt.1, June 1999, pp.715-21.

[18] J.K. Cavers, "A linearizing predistorter with fast adaptation," *40th IEEE Vehicular Technology Conference. On the Move in the 90's*, IEEE, 1990, pp.41-7.

[19] J.T. Stonick, V.L. Stonick, and J.M.F. Moura, "Multi-stage adaptive predistortion of HPA saturation effects for digital television transmission," *1999 IEEE International Conference on Acoustics, Speech, and Signal Processing. Proceedings. ICASSP99*, IEEE. Part vol.5, 1999, pp.2671-4 vol.5.

[20] M. Faulkner, T. Mattsson T, and W. Yates, "Adaptive linearisation using pre-distortion," *40th IEEE Vehicular Technology Conference. On the Move in the 90's*, IEEE. 1990, pp.35-40.

[21] M. Faulkner and M. Johansson, "Adaptive linearization using predistortion-experimental results," *IEEE Transactions on Vehicular Technology*, vol.43, no.2, May 1994, pp.323-32.

[22] J. de Mingo J and A. Valdovinos, "Amplifier linearization using a new digital predistorter for digital mobile radio systems," *1997 IEEE 47th Vehicular Technology Conference. Technology in Motion*, IEEE, Part vol.2, 1997, pp.671-5.

[23] J.K. Cavers JK, "Optimum indexing in predistorting amplifier linearizers," *1997 IEEE 47th Vehicular Technology Conference Technology in Motion*, IEEE. Part vol.2, 1997, pp.676-80 vol.2.

[24] J.T. Stonick, V.L. Stonick, J.M.F. Moura, R.S. Zborowski, "Memoryless polynomial adaptive predistortion (TV transmitters)", *1995 International Conference on Acoustics, Speech, and Signal Processing. Conference Proceedings*, IEEE. Part vol.2, 1995, pp.981-4 vol.2.

[25] F. Szidarovszky and S. Yakowitz, *Principles and procedures of numerical analysis*, New York, Plenum Press, 1978.

[26] R.C. Davis and W. Boyd, "Adaptive Predistorter Technique for Linearizing a Power Amplifier for Digital Data Systems", U.S. Patent 4,291,277, issued 22 Sept. 1982.

[27] M.E. Frerking, *Digital Signal Processing in Communication Systems*, Chapman & Hall, 1994.

[28] B. Taylor, private conversation and e-mail, Agilent Technologies, 2000.

[29] Agilent Technologies, "HMMC-5033 17.7-32 GHz Power Amplifier", [Online Data Sheet], Available: http://www.semiconductor.agilent.com.

[30] Agilent Technologies, "HMMC-5040 20-40 GHz Power Amplifier", [Online Data Sheet], Available: http://www.semiconductor.agilent.com.

[31] Agilent Technologies, “Controlling Test Port Output Power Flatness: PN 8510-16-A”, [Online Product Note] Available: http://www.tm.agilent.com

[32] DAVIC Standard, *Part 8: Lower Layer Protocols and Phsical Interfaces*, Version 1.41, Digital Audio Video Council, 2000. [Online Standard] Available: http://www.davic.org, ftp://ftp.davic.org/davic/pub/Spec1_4_1/141_part08.pdf,

[33] K. Voelker, “Apply error vector measurements in communications design,” *Microwaves & RF*, vol.34, no.17, Dec. 1995, pp.143-4, 146-8, 150, 152.

[34] D.S. Hilborn, S.P. Stapleton, J.K. Cavers, “An adaptive direct conversion transmitter,” *IEEE Transactions on Vehicular Technology*, vol.43, no.2, May 1994, pp.223-33.

[35] Wright A.S., Durtler W.G.,“Experimental performance of an adaptive digital linearized power amplifier (for cellular telephony),” *IEEE Transactions on Vehicular Technology*, vol.41, no.4, Nov. 1992, pp.395-400.

Vita

Daniel Eric Johnson was born in Tennessee on September 22, 1973. After a childhood in Lebanon, TN, he obtained his Bachelor of Science in Electrical Engineering in 1995 from Tennessee Technological University in Cookeville, Tennessee.

After undergraduate studies, he worked for PageNet, the world's largest wireless messaging provider, in Nashville, Tennessee. In 1996, he retuned to Cookeville and worked for a small manufacturer and designer of countersurveillance equipment as an Electrical Engineer.

In the fall of 1998, he left Tennessee to pursue a MSEE at Virginia Polytechnic Institute and State University. His research interests included signal processing and networking for wireless digital communications. As a part of the Center for Wireless Telecommunications, he assisted Virginia Tech's Communication Network Services with the deployment of the Blacksburg LMDS Testbed System. The testbed was one of the first licensed deployments of LMDS technology in the United States.

After completing the requirements for a Master of Science in Electrical Engineering in the summer of 2000, Eric joined Harris Corporation's Government Communications Systems Division in Palm Bay, Florida.